Screw Algebra Based Kinematics Analysis and Its Uses in Reconfiguration Recognition of Mechanisms

Zhang, Xinsheng

Awarding institution:
King's College London

KING'S College LONDON

University of London

Screw Algebra Based Kinematics Analysis and Its Uses in Reconfiguration Recognition of Mechanisms

Xinsheng Zhang

A thesis submitted in fulfilment of the requirements

for the degree of Doctor of Philosophy

King's College London, University of London

Abstract

Reconfigurable mechanisms can change their motion branches or topologies when constraint singularity occurs, and this phenomenon of reconfiguration leads to bifurcation or multi-furcation of mechanisms. Recognising reconfiguration in mechanisms and identifying the corresponding geometrical constraints remain unsolved in the field of mechanism theory and have raised much interest of investigation from 1990s. This dissertation uses the properties of screw algebra and Lie algebra to establish a method of modelling and detecting bifurcation and multi-furcation in reconfigurable mechanisms at singularity configurations. Based on the fundamentals of the screw algebra, this method establishes an algebraic way of modelling the kinematics of mechanisms and the variations of screw systems in which the screws have the same pitch. The screw algebra based method is extended to the scope of Lie group, where this dissertation uses compositional manifolds to explore the feasible finite displacements of reconfigurable mechanisms.

The dissertation starts from investigating the screw dependency based on α- and β-planes generating hyperquadrics in the 5-dimensional projective space. Projective geometry and matrix operation are adopted towards the situation where a non-zero pitch is involved in a screw system. Screw systems are related to hyperquadrics in five-dimensional projective space by constructing projective transformations. Following the screw dependency investigation based on screw algebra, this dissertation examines high-order kinematic analysis of mechanisms by implementing a recursive method of

Lie bracket computation of screws and such a method provides a compact description for kinematic models of mechanisms with integrating the bilinear form representation of kinematic constraints of a derivative queer-square mechanism. This method allows local analysis of mechanisms at any configurations including singularity configurations. Specifically, the research integrates the coefficient matrix of first-order kinematic analysis and the bilinear form matrix of second-order kinematic analysis which makes it possible to identify geometrical constraints when dealing with complex mechanisms. The dissertation then explores the relationship between screw algebra and Lie group. In such a way, the method of identifying finite displacements in reconfigurable mechanisms is investigated. The research explored the traditional PRP kinematic chain producing the planar motion subgroup SE(2) to a relatively generic kinematic chain in which the prismatic-joint direction is not necessary to be perpendicular to the revolute-joint axis, and revealed the equivalent displacement manifold, leading to the discovery of a pseudo-helical motion with a variable pitch of the particular PRP chain.

Throughout the dissertation, the screw algebra based approach of kinematics analysis of mechanisms is proven effective and compact in representing screw-system variations, kinematic constraint modelling of mechanisms at singularity configuration, computational submanifolds analysis of mechanisms, Jabobian matrix construction of reconfigurable mechanisms, and recognition of motion branches using these fundamental theoretical tools. This thesis investigates the properties of screw systems within the context of screw algebra and applies the screw algebra based kinematics to modelling and motion-branch recognising of reconfigurable mechanisms.

Acknowledgement

I would like to express my deepest sense of gratitude to my supervisor Professor Jian S. Dai, for his continuous support and instructions from all aspects of research and life for more than six years. I always feel proud and lucky to have the chance to be a student of Prof. Dai from my MSc period at Tianjin University, China to PhD period at King's. I make sure in such a period following Prof Dai to do research starting from a blank page in mechanisms theory to a PhD student level researcher will bring me unlimited and endless benefits throughout my life.

Prof Dai is one of the world-leading scientists in the fields of mechanisms and robotics, especially in mathematical theories for mechanisms such as screw algebra, screw-system approach, Lie group and Lie algebra, quaternion and dual quaternions, etc. I was so fortunate that I witnessed the whole process from the year of 2011 to 2015 of Prof Dai's writing the two treatises in screw algebra and Lie groups of mechanisms based on his research achievements over the past 30 years. I was the first reader of Prof. Dai's book and during his writing, he taught me so much on learning screw theory and much emphasis was placed on how to be standard, professional, and proficient in doing research and such training supervised by a leading professor really bring me a lot of benefits and fruits. Prof. Dai is so strict and precise in academic stuff that I would say bluntly he changed his books for more than one hundred times to achieve a perfect version for potential readers. I still keep may intermediate version of Prof. Dai's books and those will become my invaluable treasures. In 2013, Prof. Dai offered me an

opportunity to study at King's for my PhD degree. During the period, I was provided many opportunities to attend academic conferences and symposiums, summer schools and high standard lectures. There are many precious memories with Prof. Dai and one of them I would never forget is that I was rescued by Prof. Dai from the deep mire of complicated theories during a very hard time in the first year of my PhD. When he taught Dr Yun Qin about Lie subgroups and revised her dissertation, he always asked me to involve in their discussion and only in this way could I find the research direction of investigating the bifurcation of the 3-PUP parallel mechanism using compositional submanifolds and investigated multi-furcation of the derivative queer-square mechanism using Lie bracket computation and bilinear form representation. Prof. Dai's great support from every aspect means everything to me and I would not have such an amazing journey of my PhD study if without the courage and support from Prof. Dai.

I would thank Dr. Jie Sun who is the closest friend to me and he always offers me a lot of helps in many things in these years. He is a knowledgeable and humorous guy and full of enthusiasm in learning and doing a lot of things. He has a wide range of knowledge in control and we are good partners in the same European project Squirrel in both control and design and maintenance of a metamorphic robotic hand. I would also thank Mr. Xi Kang who is a PhD student at Tianjin University for his selfless helps and many discussions in analysing mechanisms. I really appreciate the friendship with him for many years from my BSc period. I can imagine my career and life will be full of happiness because I will join a spin-off focusing on developing novel robotic grippers and have the opportunity to work together with Prof. Dai, Dr Jie Sun, Mr. Shuangjia Xu and Mr. Xi Kang after my PhD.

I must give my thanks to Dr. Guowu Wei, Dr. Dongming Gan, and Dr Yun Qin for always sharing their research ideas and directions with me and many valuable discussions. I wish to express my gratitude to my close friend and fellow colleagues to Dr Peng Qi, Dr Chen Qiu, Mr. Cheng Peng, Mr. Pablo Lopez-Custodio, Mr Fan Wu, Miss Yaqing Song, Dr Helge Wurdemann, Dr Yohan Noh, Dr Chuang Liu for their friendship and helps.

I would give my sincere thanks to King's Collge London for providing the full scholarship covering my tuition fee and maintenance for three years and to the European Commission 7th Framework Project SQUIRREL "Clearing Clutter Bit by Bit" under Grant No. 610532 for one year maintenance.

At last, I must give my thanks to my parents Mr. Leiyu Zhang and Mrs. Qiufeng Shi, and my wife Yanan Wu who always encourage and support me unconditional with love.

Contents

List of Figures

List of Tables

List of Symbols

$\boldsymbol{\omega}$	The scalar velocities of the kinematic joints in the mechanism
$\boldsymbol{\alpha}$	The angular accelerations of the corresponding revolute joints at the singularity configuration
Δ	The correlation operator
$se(3)$	Lie algebra of the special Euclidean group of 3-dimensional Euclidean space
$se^*(3)$	Projective Lie algebra of the special Euclidean group of 3-dimensional Euclidean space
$\boldsymbol{S}_i$	Screw associated with the *i*th joint
$\boldsymbol{S}_{ij}$	Screw associated with the *j*th joint in the *i*th limb
$\boldsymbol{s}_i$	The direction vector of a screw associated with the *i*th joint
$\boldsymbol{A}_s$	Skew-symmetric matrix constituted by rotation axis $\boldsymbol{s}$
$\boldsymbol{s}_0$	The secondary part of a screw
$\boldsymbol{r}_0$	The position vector of the screw axis with respect to the origin
h	The pitch of a screw
$\mathbb{R}^3$	3-dimensional affine space
$\mathbb{P}^3$	3-dimensional projective space
$\mathbb{P}^n$	*n*-dimensional projective space
$\mathbb{P}^5$	5-dimensional projective space
$\mathbf{V}^n$	*n*-dimensional vector subspaces
$\mathbf{V}^6$	6-dimensional vector space
$\mathbb{S}_n$	Screw system of order n

$\boldsymbol{T}_i$	The twist of associated the *i*th joint
$\boldsymbol{J}$	Jacobian matrix
$\boldsymbol{J}_{\mathrm{h}}$	Hand Jacobian matrix
${}^{i}\mathbf{T}_{j}$	Transformation matrix from the *i*th coordinate frame to the *j*th coordinate frame
$\mathbf{R}(x_i,\varphi_i)$	A 3×3 rotation matrix that represents a rotation about x_i-axis by φ_i
$\boldsymbol{P}_{\mathrm{A}}$	Position vector of point A in the global coordinate frame
${}^{\mathrm{F}}\boldsymbol{P}_{\mathrm{C}i}$	The position vector of point C_i (i = 1, 2 and 3) with respect to global coordinate frame F
$\dot{\boldsymbol{\theta}}_a$	The velocity vector of active joints
$\dot{\theta}_i$	The change rate of the *i*th joint
SE(2)	The special Euclidean group of 2-dimensional Euclidean space
SE(3)	The special Euclidean group of 3-dimensional Euclidean space
O(3)	The orthogonal group of 3-dimensional Euclidean space
SO(3)	The special orthogonal group of 3-dimensional Euclidean space
[$\boldsymbol{r}$×]	Skew-symmetric matrix of vector $\boldsymbol{r}$
$M_4^{(2)}$	The 4-dimensional manifold of degree 2
$\mathcal{M}$	Product submanifold of *SE*(3)
Ω_4	The hyperquadric

Chapter 1 Introduction

1.1 State of the Problem

Reconfigurable mechanisms can change their motion branches or topologies when constraint singularity occurs, and this phenomenon of reconfiguration leads to *bifurcation* or *multi-furcation* of mechanisms. Typical reconfigurable mechanisms include kinematotropic mechanisms and metamorphic mechanisms, the former changes its mobility and kinematics characteristics when bifurcation or multi-furcation happens while the latter even changes its topology and in such a way changes its mobility.

Recognising reconfiguration in mechanisms and identifying the corresponding geometrical constraints remain unsolved in the field of mechanism theory and have raised much interest of investigation from 1990s. This dissertation uses the properties of screw algebra and Lie algebra to establish a method of modelling and detecting bifurcation and multi-furcation in reconfigurable mechanisms at singularity

configurations. Based on screw algebra, this method employs an algebraic way of modelling the kinematics of mechanisms and the variations of screw systems in which the screws have the same pitch. The screw algebra-based method is extended to the scope of Lie groups, where this dissertation uses compositional manifolds to explore the feasible finite displacements of reconfigurable mechanisms.

In screw algebra, when dealing with the correspondence between screws and hyperquadrics in the 5-dimensional projective space, researchers limited to the hyperquadrics as Klein quadric and the screws are of a zero pitch. This dissertation extends it to a relatively general case where screws are of a non-zero constant pitch and works out the corresponding hyperquadrics in the 5-dimensional projective space. The dissertation then investigates the screw dependency based on alpha- and beta-planes generating hyperquadrics in the 5-dimensional projective space and identifies the order of a screw system in which screws are of the same pitch. The fundamentals of screw algebra pave a way of modelling and recognising bifurcation and multi-furcation in mechanisms.

Following the screw dependency investigation based on screw algebra, this dissertation examines high-order kinematic analysis of mechanisms by implementing a recursive method of Lie bracket computation of screws on a derivative queer-square mechanism which has six motion branches. Although multi-furcation of this mechanism was recognised by using screw-system approach in [1], there are two motion states presented in this paper that cannot move through the designated singularity configuration and the essence of the multi-furcation in this mechanism has not been revealed. This dissertation integrates the coefficient matrix of first-order kinematic

analysis and the bilinear form matrix of second-order kinematic analysis which makes it possible to identify geometrical constraints when dealing with such a complex mechanism. This piece of research based on Lie bracket computation of screws produces a method which is effective in determining motion branches of reconfigurable mechanisms.

The dissertation then explores the relationship between screw algebra and Lie group. In such a way, the method of identifying finite displacements in reconfigurable mechanisms is investigated by extending the screw algebra-based method to Lie group based method by using computational manifolds. The research extended the standard PRP kinematic chain producing the planar motion subgroup SE(2) to a relatively generic kinematic chain in which the prismatic-joint direction was not necessary to be perpendicular to the revolute-joint axis, and revealed the equivalent displacement manifold, leading to the discovery of a screw motion with a variable-radius pitch of the skewed PRP chain.

The dissertation presents a parallel mechanism with a reconfigurable base originated from a grasping model using the metamorphic robotic hand [84]. For such a hybrid mechanism with a reconfigurable base, the modelling of velocity and Jacobian matrix analysis is difficult because of its complex structure. This dissertation solves the problem and uses screw algebra-based approach to establish the Jacobian matrix for the complicated mechanism.

In conclusion, this dissertation digs out kinematics properties and variations of screw systems and Lie algebras in the field of screw algebra and explores the map between

Lie algebra and compositional manifolds. A method of recognising reconfigurations and investigating finite displacements in mechanisms is established based on the research in screw algebra. A derivative queer-square mechanism, a 3-PUP parallel mechanism and kinematic chains are used to demonstrate the method of recognising reconfigurations in mechanisms and a parallel mechanism with a reconfigurable mechanism is modelled to demonstrate the method of screw algebra in Jacobian matrix construction.

1.2 Aims and Objectives

The dissertation emphasises the screw algebra-based approach and extends it to the high-order kinematic analysis using Lie bracket of screws, finite displacement representation of mechanism using computational submanifolds, and Jacobian matrix construction for a hybrid mechanism with a reconfigurable base using screw theory. Motion branch recognition of a derivative queer-square mechanism with multi-furcation and a 3-PUP parallel mechanism with bifurcation are investigated using the above methodologies.

The aims and objectives of the dissertation are proposed as and listed follows,

(I) Extend the Klein quadric in the 5-dimensional projective space of zero-pitch screws to a relatively general hyperquadric which corresponds to screws with non-zero constant pitch by using projective transformation and matrix operation in the 5-dimensional projective space.

(II) Recognise the multi-furcation in the derivative queer-square mechanism together with the corresponding geometrical conditions using screw algebra-based approach and reveal the essence of why the multi-furcation happens.

(III) Extract the pseudo-helical motion from a skewed PRP kinematic chain with a tilting angle using the equivalence approach of screw space and then analysis the phenomenon of bifurcation in the 3-PUP parallel mechanism by using compositional submanifolds of SE(3).

(IV) Construct the Jacobian matrix for a hybrid mechanism with a reconfigurable base using screw theory presented in this dissertation.

1.3 Organization of the Thesis

The dissertation is arranged as 10 chapters and the brief introduction of each chapter is presented below.

Chapter 1 introduces the research problems related to recognising motion branches of reconfigurable mechanisms and presents the aims and objectives, and structure of the dissertation.

Chapter 2 presents the background and historical development of the relevant fields, mainly including reconfigurable mechanisms, line geometry and screw theory, Lie algebra and Lie group in mechanisms and high-order kinematic analysis of mechanisms. Basic concepts are illustrated in this chapter.

Chapter 3 introduces the basic concepts of screws and screw systems. The two bilinear forms, the Killing form and Klein form, are presented for representing the pitch of screws and the rule of calculating Lie bracket of two screws is introduced briefly. Following these basic concepts, this chapter compares screw systems with non-zero pitch to hyperquadrics in 5-dimensional projective space bijectively and for the first time proposes a projective transformation on hyperquadrics of screws, revealing the generators of the corresponding hyperquadrics.

Chapter 4 is closely connected to chapter 3 and utilises vector and matrix operations to explore the geometrical relationships of screws in 3-space corresponding to those points lying in an α-plane and a β-plane. Based on the vector and matrix representation and by means of the Shur complement and block diagonalization, this chapter investigates the intersection of the α-planes and β-planes and conventional screw systems of order two are rediscovered.

Chapter 5 introduces a parallel mechanism with a reconfigurable base inspired by object in-hand manipulation with a metamorphic robotic hand. The proposed parallel mechanism is presented with the theory of metamorphosis and its geometric constraint is explored based on the approach of screw algebra. The Jacobian matrix of the mechanism is developed based on screw theory with the velocity analysis of the mechanism derived.

Chapter 6 focuses on establishing kinematic constraints for a derivative queer-square mechanism using an approach with Lie bracket computation in terms of instantaneous screws. The research in this chapter for the first time applies the recursive algorithm

based on Lie bracket to velocity and acceleration analysis of multi-loop mechanisms. By introducing the bilinear form representation, second-order constraints of the mechanism are simplified for identifying motion branches in the next chapter.

Chapter 7 focuses on working out motion branches of the derivative queer-square mechanisms. This chapter is to construct the constraint system of the multi-loop mechanism by integrating the first-order and second-order constraints revealed in the last chapter. Before solving the equation system of constraints, this chapter recognises the geometrical conditions under which the order of the constraint system changes. Solutions to the constraint system of integrating first-order and second-order constraints are solved and given and all motion branches are listed with the corresponding geometrical conditions and prototype validations and with numerical simulations.

Chapter 8 extends the standard PRP kinematic chain generating the planar motion group to a relatively generic case by means of the equivalence of screw spaces as the tangent spaces of compositional submanifolds, in which one of the prismatic joint-direction is not necessarily perpendicular to the revolute-joint axis, leading to the discovery of a pseudo-helical motion with a variable pitch in this kinematic chain. The displacements of such a skewed PRP chain generate a compositional submanifold of the Schoenflies motions subgroup. This chapter investigates for the first time this type of motion and the motion representation of a PRP-Schoenflies parallel mechanism is presented.

Chapter 9 investigates the bifurcated motion in a 3-PUP parallel mechanism by changing the active geometrical constraint in its configuration space. The representation

of motion of the 3-PUP parallel mechanism and its motion branches is derived using computational submanifolds of SE(3) based on the screw-space equivalence in Chapter 7. An experimental test is set up based on a 3D printed prototype of the 3-PUP parallel mechanism to detect the inconspicuous translation of the pseudo-helical motion.

Chapter 10 concludes the dissertation and presents the contributions and future research directions within the related fields.

Chapter 2 Background

2.1 Introduction

This chapter reviews the background which includes the historical development and basic concepts of the relevant fields to the dissertation. The propose and development of reconfigurable mechanisms is going to be introduced firstly in Section 2.2 in which the concept of bifurcation and multi-furcation of mechanisms is to be explained. Existing methods of recognising bifurcation of mechanisms are discussed in this section. Then Section 2.3 reviews the historical development of line geometry and screw theory which is closely connected to the foundation of the dissertation. Line geometry, screw dependency and the application of these theories to the mechanisms analysis is briefly discussed in the scope of 5-dimentional projective space in this section. Following this, Section 2.4 moves to Lie groups from its tangent space of screws and the uses of Lie group-based method will be reviewed. Finally, Section 2.5 discusses the development of the high-order analysis based on screw algebra and its application in bifurcation recognition of mechanisms.

2.2 Development of Reconfigurable Mechanisms and Bifurcation in Mechanisms

In the 1990s, numerous mechanisms came out as they had a common property of reconfiguration which means these mechanisms can change their mobilities or topologies in different ways [2]. The mechanisms with such a property of changing are called reconfigurable mechanisms in mechanisms-theory community. Two typical examples of the reconfigurable mechanisms were the innovative discoveries of kinematotropic mechanisms [3] and metamorphic mechanisms [4]. The difference between kinematotropic and metamorphic mechanisms is that the former change their motion branches and mobility without changing the topologies, while the latter change their topologies leading to the change of mobilities.

In the beginning of the 21st century, more and more research interest has been attracted to this field following the proposal of the kinematotropic and metamorphic mechanisms. In 2002, Lee and Hervé [5] revealed the discontinuously movable mechanisms and explored the bifurcating characteristics of mechanisms using Lie subgroup method. Type synthesis of kinematotropic mechanisms was investigated by Galletti and Fanghella [6] and a large number of single-loop kinematotropic mechanisms were classified with their kinematic and structural properties. Later, the method was extended to the synthesis of multi-loop kinematotropic mechanisms by Galletti and Giannotti [7]. Kong and Gosselin put forward a method of analysis and synthesis of multi-mode mechanisms using the equivalent kinematic tool of virtual chains [8]. Gan, Dai and

Caldwell synthesized the parallel mechanisms with reconfiguration using screw theory [9]. All these types of mechanisms could be classified in the scope of reconfigurable mechanisms.

The ways of achieving morphing was reviewed and characterised in a journal dissertation authored by Aimedee, Gogu, Dai, Bouzgarrou, and Bouton. The ways of morphing include topological morphing and geometrical morphing, the former could be divided into morphing by limiting joint motion range and by using internal forces, while the latter includes morphing by changing relative position of joint axes, by superposing joint axes, by enabling joint axes to be coplanar, and by using the joint-motion switch [10].

The field of reconfigurable mechanisms passed a milestone in 2009, when the first ASME/IEEE conference on reconfigurable mechanisms and robots (ReMAR 2009) was founded and hold by King's College London [11]. From then reconfigurable mechanisms became a cutting edge and important research branch of mechanisms theory. This conference started a triennial academic conference in the field of reconfigurable mechanisms and the conference moved to Tianjin, China in 2012 [12] and to Beijing, China in 2015 [13]. The next conference would be hold by professor Just Herder in Delft University of Technology, Amsterdam.

Reconfigurable mechanisms can switch their motion branches or topologies at a particular singularity configuration, which means the configuration spaces of the mechanisms can be divided into two or more pieces, this phenomenon of switching motion branches in reconfigurable mechanisms is called *bifurcation or multi-furcation*

of mechanisms, depending on how many branches the configuration space is divided into. Bifurcation or multi-furcation happen in reconfigurable mechanisms and this is a necessary condition for a mechanism to be reconfigurable.

For analysis and identification of motion branches, Dongming, Dai and Liao [14], Ketao, Dai and Fang [15] used a screw-system approach to analyse the mobility of reconfigurable mechanisms in different motion branches. Zlatanov explored the constraint singularity of mechanisms and manipulators in their configuration spaces [16]. Kong and Gosselin proposed the method of virtual chains to analyse and synthesise reconfigurable mechanisms [8]. Lerbert [17], Diez-Martínez, Rico and Gallardo [18], Müller [19], López-Custodio, Rico, Cervantes-Sánchez, etc [20] investigated the high-order kinematic properties of reconfigurable mechanisms with open loop and single loop respectively. Though different languages of mathematics were adopted, they all established the high-order kinematic models of mechanisms in the scope of configuration space. Recently, the research in this field was extended to multi-furcation analysis by Qin, Dai and Gogu by using screw-system approach [1]. Kong investigated the structure of configuration space of mechanisms by using dual quaternions representing the kinematic constraints of mechanisms [21].

2.3 Historical Development of Line Geometry and Screw Theory

Dependency of screws has been a basic and essential issue of screw theory ever since Ball's epochal treatise [22], especially when screw theory was applied to constraints

and motion analysis and mobility analysis [23], singularity investigation [24], and type synthesis for parallel mechanisms [25] and compliant mechanisms [26]. It is a neat and effective method specifically for kinematic analysis of overconstrained and reconfigurable parallel mechanisms and origami-inspired mechanisms [4].

As a line in 3-dimensional projective space $\mathbb{P}^3$ can be regarded as a screw with zero pitch, the issue of screws dependency stems originally from and is an extension of the characterization of line varieties. Grassmann's research in 19th century on line varieties was well-known as the earliest study on line geometry. The mathematical foundation to characterization theory of lines was comprehensively laid by Veblen and Young (1918) in their book on projective geometry [27]. A condition that six given lines were linearly dependent were given by Bricard (1927) in terms of the Plücker coordinates of the lines and thus a general and algebraic method to identify the dependency of lines were proposed. The characterization of line varieties was completely revealed by Dandurand (1984) in his work on the rigidity of compound spatial grid [28]. Veblen and Young's work on line geometry and Dandurand's work on characterization in fact provided the method to identify the dependency of lines in $\mathbb{P}^3$ by enumerating all types of line varieties varying from rank one to five. Afterwards, this method was extensively used in the analysis and synthesis of mechanisms, especially in the singularity analysis of parallel mechanism.

Linear dependence of screws is a natural extension of linear dependence of lines [29][30]. Due to the pitch *h* of screws, the dependency identification of screws requires modifying Plücker coordinates to describe screws and devising characterization rules or identification principles. Screw systems were classified by Ball (1900) as the one-

system to the five-system according to the rank of the screw systems and the *Cylindroid* was proposed to study the linear dependence and geometrical properties of two-system [22]. Dimentberg (1965) invented *complex rectangular coordinates* for screws and converted the issue of linear dependence of *screw groups* into matrix algebra issue by using dual numbers and motor algebra [30]. Woo and Freudenstein (1970) released Plücker-like screw coordinates [5] and hence Hunt (1978) provided a general rule to reveal the principle of linear dependence of screws by writing them in a matrix as row vectors [29]. This was a universal method but not usually practical because it requires writing down all the coordinates of screws and then examining the rank of the screw matrix. In early 1990s, Dai proposed a series of propositions with sufficient algebraic demonstration on how to identify the linear dependence of screws according to their geometrical properties in $\mathbb{P}^3$ [32]. K. Hao (1998) developed a concept of free maximal list for screws based on dual numbers and Lie algebra to estimate the rank of screw sets, hence proposed a method for screws classification [33].

In terms of screws dependency, one of the basic issue is characterization and classification of screws. In 1978, Hunt revealed several special screw systems based on some special geometrical cases [29]. Contemporarily, Hervé developed the characterization of screws by classifying the displacements group into Lie subgroups [34]. Gibson and Hunt (1990) explored the representation of screw systems with projective subspaces of 5-dimensional projective space $\mathbb{P}^5$ and developed the classification of screw systems and thus revealed the relationship between screw systems and its reciprocal system [35]. The research on classification of screws was then extended by Rico and Duffy (1992) by using orthogonal space [36], Dai (2001)

using set theory [32], Zlatanov, Sunil and Gosselin (2005) using convex cones [37], and Selig (2014) using Lie group [38], respectively.

In the recent decade, dependency of screws had not stopped attracting researcher's interests. Huang (2002) explored the method for synthesis of lower-mobility parallel mechanism by using the classification of line varieties with respect to various geometrical properties [25]. Dai, Huang, and Lipkin (2004, 2006) investigated the linear dependence of constraint and motion screw systems of parallel mechanisms in an algebraic way by newly bringing set theory, particularly multi-set into screw theory, hence establishing a theory to examine the constraint and motion space and mobility of parallel mechanisms [23]. This theory for motion space and mobility analysis was subsequently adopted to study bifurcation [39] and multi-furcation [1] of metamorphic mechanisms [4]. Su and Hafez (2011) developed the method for flexure synthesis by examining the rank of the relative line varieties in compliant mechanisms [40]. Zlatanov (2012) represented the general three-system by a sphere through the origin, which generalized Ball's circle extracting from the cylindroid to 3-dimensional space [41]. Carricato and Zlatanov (2014) proposed the concepts of persistent screw system to study the special cases of mechanism motion that the end-effector motion space remains invariant with respect to an arbitrary finite rigid displacement [42].

Chapters 3 and 4 of this dissertation are to derive the dependency of screws in $\mathbb{P}^3$ in a manner of algebraic geometry based on α- and β-planes of the hyperquadric in $\mathbb{P}^5$ which corresponds to a set of screws with the same pitch, hence revisiting several Hunt's special screw systems which are extensively used in mechanism analysis. The correspondence between lines in $\mathbb{P}^3$ and points in manifold $M_4^{(2)}$ in $\mathbb{P}^5$ was firstly put

forward by Klein and this manifold is well-known as Klein quadric later. It is the α- and β-planes which are just two families of planes that generate Klein quadric and this viewpoint was revealed by Semple and Roth (1949) [104] with a coordinates transformation being performed to simplify the representation of Klein quadric into normal form. That is to say, Klein quadric can wholly cover the two families of planes named α- and β-planes and conversely, α- and β-planes can fully fill the Klein quadric. After that, Gibson and Hunt (1990) [35] extended the concept of the α- and β-planes of Klein quadric to those of the hyperquadrics corresponding screws with non-zero pitch, by a projective isomorphism that maps screws of a pitch h associated to points in a hyperquadric to those of zero pitch associated to points in Klein quadric. Selig defined α- and β-planes of Klein quadric with matrix form and related them to Hunt's type II screw systems in an algebraic way. However, this research was confined in Klein quadric, not yet having been extended to hyperquadrics of $\mathbb{P}^5$ for screws with non-zero pitch.

2.4 Historical Development of Lie group and Lie Algebra in Mechanisms

Identifying the phenomenon of bifurcation in mechanisms has been of great interest in mechanisms community since 1990s [3][4]. Latest progress in bifurcation recognition has been made by Wei, Chen and Dai using group theory, by Qin, Dai and Gogu on multi-furcation using screw system approach [1] and by Kong using Euler parameter quaternions [44], by Walter, Husty and Pfurner using algebraic equations of Study parameters [45], by Nurahmi, Caro and Wenger et al using algebraic approach with

Study's kinematic mapping of the Euclidean group SE(3) [46] and by López-Custodio et al [47] identifying bifurcation by means of the tangency of generated surfaces. Recently, unified kinematics of a metamorphic parallel mechanism with bifurcation was investigated for singularity analysis and kinematic modelling based screw systems [48]. Multifurcation was discovered in a queer-square mechanism in [1]. A new class of reconfigurable modular parallel robots stemming from the 3-CPS under-actuated topology was proposed with a locking system [49].

To explore the bifurcated motion of a 3-PUP parallel mechanism proposed by Rodriguez-Leal et al [50] and provide a Lie group method for the bifurcation analysis of parallel mechanisms, this dissertation is to extend the traditional PRP kinematic chain that generates SE(2) to a relatively general kinematic chain with a particular pseudo-helical motion embedded. This kinematic chain does not produce SE(2) anymore due to a tilting angle between the revolute-joint axis and the prismatic-joint direction, but generates a submanifold of the special Euclidean group SE(3) in which a pseudo-helical motion with a variable pitch can be extracted. The related concepts of product submanifold and its tangent spaces [51] are to be introduced in this dissertation to reveal the equivalent manifold for the particular chain, laying a foundation for the bifurcated motion analysis of the 3-PUP parallel mechanism.

Lie subgroups of SE(3) with various dimensions are specific cases of submanifolds of SE(3). The kinematic chains that generate the cylindrical subgroup of dimension two were investigated by Mourad and Hervé [52] and by Meng et al [53]. Kinematic generators of the planar motion subgroup SE(2) were investigated by Lee and Hervé [54]. The different mechanical generators of each subgroup of SE(3) were investigated

by Pérez-Soto and Tadeo [55], including the thirty four mechanical generators of the Shoenflies motions subgroup. The kinematic chains generating the pseudo-planar motion subgroup of dimension three and the Schoenflies motion subgroup of dimension four were investigated by Lee and Hervé in [56] and [57] respectively. All subgroups of SE(3) revealed by Hervé [34] have been explored with the corresponding kinematic generators and the connection between Lie subgroups of a rigid body displacement was revealed by Dai [58][59][60] using the Lie adjoint-action approach.

Research has been made in the type synthesis and analysis of parallel manipulators whose limbs and/or desired motion of the moving platform do not generate subgroups of SE(3). In this regard, Li, Huang and Hervé [61] and Meng, Liu and Li [53] applied a group theory approach to perform the synthesis of parallel manipulators with 3R2T motion which is not a subgroup, Kong and Gosselin devised one of the most effective methods for the type synthesis of parallel mechanisms applying the concept of virtual chain [8], Gogu applied a method based on the Jacobian matrix of the limbs in the manipulator [62], Rico et al explored parallel manipulators whose desired motion of the end effector is the composition of two subgroups [63]. In this last case, even though the twist space of kinematic generators cannot form a subalgebra of Lie algebra se(3), it still presents important properties for full-cycle motions. Such phenomenon was investigated by Carricato and Rico [42] and this sort of kinematic generators was coined as persistent screw systems. Tadeo-Chávez et al also investigated these screw systems and called them locally-constant rank screw systems [64]. In a more recent publication, Wu et al [65] studied another kind of submanifolds of SE(3) that, in spite of not being subgroups, present interesting properties, these submanifolds are called symmetric subspaces of SE(3).

A 3-PUP parallel mechanism is an example of parallel manipulator in which the sets of Euclidean displacements of the limbs do not constitute a subgroup of SE(3). The 3-PUP mechanism to be studied in this contribution was firstly put forward by Rodriguez-Leal, Dai and Pennock in [50] with a brief kinematics model. Its bifurcated motion, constraint singularity, and workspace were investigted by Zhang, Dai and Fang [66] and by Gan and Dai [39], using the screw system approach. In their study, the screw system of the parallel mechanism is decomposed into constraint and motion-screw systems of the platform and that of the mechanism and their relationship [32] is revealed. This dissertation solves the problem of describing the motion of these parallel platforms by means of group theory. This method facilitates the analysis of the parallel platform since there is no need to deal with instantaneous constraints or motions as in the previous publications.

2.5 Development of High-Order Kinematic Analysis of Mechanisms

Bifurcation recognition attracts many research interests in last twenty years, from Wohlhart's kinematotropic mechanisms in 1996 [3] and Dai's metamorphic mechanisms in 1999 [4]. Till now there are quite a few methods to identify motion branches in a mechanism, and this is discussed in Section 2.1 of this chapter. However, either relying on kinematics models of mechanisms too much, or not capable of dealing with complicated multi-loop mechanisms, currently we do not have an effective method of predicting the motion branches of reconfigurable mechanisms [10].

The dissertation focuses on the topic of motion branch recognition of mechanisms based on screw algebra and for the first time uses high-order kinematic analysis for predicting motion branches of a multi-loop with even six motion branches. The method proposed in the dissertation integrates the high-order kinematic analysis together with the bilinear form representation of the kinematic constraints of mechanisms for the first time. In 1998, Lerbet investigated the bifurcation of single-loop linkages using analytic geometry and approximated the local properties by computing the tangent cone of a analytic variety which represents the configuration space of a linkage with bifurcation [17]. Diez-Martínez, Rico and Gallardo employed the high-order kinematic analysis to calculate the mobility and connectivity of mechanisms without referring to the change of mobility or topology of mechanisms in 2006 [18] and 2009 [67]. The research used a recursive algorithm based on Lie bracket of instantaneous screws and it is worthy to mention that before using high-order analysis to mobility calculation of mechanism, Rico and Duffy had presented a simple method to perform the acceleration analysis of spatial chains using screw theory in 1996 [68][69] and Rico et al [70] and Gallardo [71] had extended the method to the jerk and jounce analysis of spatial chains.

In 2014, Müller contributed to the high-order kinematic analysis by introducing a closed form expression for the partial derivatives of the joint screws within a kinematic chain and it was stated that the form of the proposed close form expressions was ideal for computer implementations [19]. In 2017, López-Custodio, Rico, Cervantes-Sánchez, Pérez-Soto and Díez-Martínez proposed a compact representation of computation of high-order kinematic analysis [20] and the equations obtained are equivalent to those derived by Lerbet in 1998 [17].

The methods of implementing high-order kinematic analysis have been used for calculating mobility of mechanisms and approximating configuration spaces of mechanisms and identifying bifurcation in open or single-loop mechanisms. However, there is a gap from the method of high-order kinematic analysis to recognising motion branches of complicated multi-loop mechanisms with multi-furcation. This dissertation bridges the gap by introducing bilinear form to represents the constraints obtained by applying high-order kinematic analysis to the mechanisms and by proposing a method of simplifying the constraint system of mechanisms.

2.6 Conclusions

This chapter reviewed the historical development of reconfigurable mechanisms, line geometrical, screw dependency, and Lie group, etc. The basic concepts and connection between these fields were presented mainly with the timeline of development of these relevant research topics. From the reviews in this chapter, screw algebra will be the fundamental mathematical tools and recognition of motion branches together with the corresponding geometrical constraints will the main problem to be solved in this dissertation. Screw algebra will be extended to Lie groups and to Lie bracket computation of screws in this dissertation, however, screw algebra will be the mainline and basic mathematical tools throughout the dissertation.

Chapter 3 Screws in the 5-Dimensional Projective Space

3.1 Introduction

This chapter introduces the basic concepts of screws and screw systems and expresses these geometrical entities in homogeneous coordinates. Then the two bilinear forms, the Killing form and Klein form, are presented for representing the pitch of screws and the rule of calculating Lie bracket of two screws is briefly introduced. Following these basic concepts, this chapter associates screw systems with non-zero pitch to hyperquadrics in 5-dimensional projective space injectively. This chapter for the first time proposes a projective transformation on hyperquadrics of screws, by which the generators of the hyperquadrics can be revealed in an algebraic way of representation.

3.2 Screws and Screw Systems

A screw is the geometrical entity of an instantaneous twist and wrench in kinematics and statics and can be regarded as a line vector in 3-dimensional affine space $\mathbb{R}^3$ together with a pitch h. Hence a screw is in fact an extension of line vector and is usually expressed in the form of 6-dimensional vector as follows

$$\boldsymbol{S} = \begin{pmatrix} \boldsymbol{s} \\ \boldsymbol{s}_0 \end{pmatrix} = \begin{pmatrix} \boldsymbol{s} \\ \boldsymbol{r}_0 \times \boldsymbol{s} + h\boldsymbol{s} \end{pmatrix} \tag{3.1}$$

where the 3-dimensional vector $\boldsymbol{s}$ is the primary part of screw representing the direction vector of screw axis, the 3-dimensional vector $\boldsymbol{s}_0$ is the secondary part constituted of the moment of the screw axis with respect to the origin and the scalar product of the primary part by pitch h, and the 3-dimensional vector $\boldsymbol{r}_0$ represents the position vector of the screw axis with respect to the origin. The geometrical meanings of these vectors and their relationship are further illustrated by Fig. 3.1, in which $\boldsymbol{r}_0 \times \boldsymbol{s} = \boldsymbol{s}_0 - h\boldsymbol{s}$ holds. Similar with an arbitrary 6-dimensional vector, screw can also be represented by six coordinates as

$$\boldsymbol{S} = \left(\xi_0,\ \xi_1,\ \xi_2,\ \xi_3,\ \xi_4,\ \xi_5\right)^{\mathrm{T}} \tag{3.2}$$

which are analogous to Plücker coordinates of lines in $\mathbb{R}^3$, and in fact are homogenous coordinates. Two points in $\mathbb{R}^3$ lying on the screw axis, described by homogeneous coordinates $(x_0, x_1, x_2, x_3)^{\mathrm{T}}$, $(y_0, y_1, y_2, y_3)^{\mathrm{T}}$, together with the pitch h can generate the

above screw coordinates by the means of six Grassmann determinants [72][73] and it has

$$\begin{aligned}
\xi_0 &= \begin{vmatrix} x_0 & x_1 \\ y_0 & y_1 \end{vmatrix}, \quad \xi_1 = \begin{vmatrix} x_0 & x_2 \\ y_0 & y_2 \end{vmatrix}, \quad \xi_2 = \begin{vmatrix} x_0 & x_3 \\ y_0 & y_3 \end{vmatrix} \\
\xi_3 &= \begin{vmatrix} x_2 & x_3 \\ y_2 & y_3 \end{vmatrix} - h \begin{vmatrix} x_0 & x_1 \\ y_0 & y_1 \end{vmatrix}, \\
\xi_4 &= \begin{vmatrix} x_3 & x_1 \\ y_3 & y_1 \end{vmatrix} - h \begin{vmatrix} x_0 & x_2 \\ y_0 & y_2 \end{vmatrix}, \\
\xi_5 &= \begin{vmatrix} x_1 & x_2 \\ y_1 & y_2 \end{vmatrix} - h \begin{vmatrix} x_0 & x_3 \\ y_0 & y_3 \end{vmatrix}
\end{aligned} \tag{3.3}$$

In the above representation of screw, the scalars x_0, y_0 acting as the first coordinates of the points in screw axis are of significance since they determine whether the points stay in 3-dimensional affine space $\mathbb{R}^3$ or not. They are non-zero usually and in this case the points in the screw axis do not lie at infinity and hence lie in $\mathbb{R}^3$, while if x_0, y_0 are equal to zero, the points are at infinity so that the screw axis lie in 3-dimensional projective space $\mathbb{P}^3$ including $\mathbb{R}^3$ and the infinite area.

Naturally, there exists a bijective map between n-dimensional vector subspaces $\mathbf{V}^n$ of six-dimensional vector space $\mathbf{V}^6$ spanned by n linearly independent vectors and screw systems of order n donated as $\mathbb{S}_n$ consist precisely of all linear combinations of the screws $\boldsymbol{S}_i$ as a set of bases of $\mathbb{S}_n$. Simultaneously, an arbitrary screw system of n^{th} order, also called n-system can be defined as

$$\mathbb{S}_n = \left\{ \boldsymbol{S} \,\middle|\, \boldsymbol{S} = \sum_{i=1}^{n} \lambda_i \boldsymbol{S}_i,\ \lambda_i \in \mathbf{R},\ \boldsymbol{S}_i \in \mathbf{V}^6 \right\} \tag{3.4}$$

At the moment screw can be seen as an element of 6-dimensional vector space $\mathbf{V}^6$ and expressed by six homogenous coordinates generated by Grassmann determinants together with pitch h as Equation (3.3). Screw system of n^{th} order n can be viewed as n-dimensional vector subspace of $\mathbf{V}^6$.

3.3 Bilinear Forms and Lie Bracket of Screws

In an alternative way screw $\boldsymbol{S}$ can be thought of as an element of projective Lie algebra $se^*(3)$, on which there are two symmetric bilinear forms. The first one is the *Klein form*, which is also known as *mutual moment* of line vectors and *reciprocal product* of screws, and can be given by

$$Kl(\boldsymbol{S}_1, \boldsymbol{S}_2) = \xi_0\xi_3' + \xi_1\xi_4' + \xi_2\xi_5' + \xi_3\xi_0' + \xi_4\xi_1' + \xi_5\xi_2' \tag{3.5}$$

where $\boldsymbol{S}_1,\ \boldsymbol{S}_2 \in se^*(3)$, and $(\xi_0, \xi_1, \xi_2, \xi_3, \xi_4, \xi_5)$, $(\xi_0', \xi_1', \xi_2', \xi_3', \xi_4', \xi_5')$ are homogenous coordinates of $\boldsymbol{S}_1$, $\boldsymbol{S}_2$ respectively. The other symmetric bilinear form is the *Killing form* which can be presented in the form of

$$Ki(\boldsymbol{S}_1, \boldsymbol{S}_2) = \xi_0\xi_0' + \xi_1\xi_1' + \xi_2\xi_2' \tag{3.6}$$

Through the above two symmetric bilinear forms on *se**(3), the pitch of screw $\boldsymbol{S}$ can be defined as the following form

$$h = \frac{1}{2}\frac{Kl(\boldsymbol{S},\boldsymbol{S})}{Ki(\boldsymbol{S},\boldsymbol{S})} \tag{3.7}$$

From definition of screws, any screw in the 3-dimensional projective space satisfies the above quadratic constraint constructed by the two symmetric bilinear forms on *se**(3), thus this quadratic constraint will be used to define hyperquadrics corresponding to screws in the next section.

Given two screws $\boldsymbol{S}_1$ ($\boldsymbol{s}_1$, $\boldsymbol{s}_{10}$) and $\boldsymbol{S}_2$ ($\boldsymbol{s}_2$, $\boldsymbol{s}_{20}$), the Lie bracket or Lie product of the two screws can be expressed as follows

$$\left[\boldsymbol{S}_1, \boldsymbol{S}_2\right] = \begin{pmatrix} \boldsymbol{s}_1 \times \boldsymbol{s}_{20} \\ \boldsymbol{s}_1 \times \boldsymbol{s}_{20} + \boldsymbol{s}_{10} \times \boldsymbol{s}_2 \end{pmatrix} \tag{3.8}$$

in which the anti-commutativity property holds for the equation.

3.4 Hyperquadric of Screws

Particularly, when pitch *h* vanishes, line vectors are obtained from screws and the quadratic constraint in the above equation degenerates such that another quadratic constraint constructed by Klein form can be obtained, thus defining a manifold $M_4^{(2)}$ in $\mathbb{P}^5$ as

$$M_4^{(2)} \equiv Kl(\boldsymbol{S}, \boldsymbol{S}) = 0 \tag{3.9}$$

This 4-dimensional manifold $M_4^{(2)}$ is of degree 2 and was put forward firstly by Klein and known as *Klein quadric* [74] or *quadric primal* [75]. Any line in $\mathbb{P}^3$, including the lines at infinity, can be represented by a point lying in $M_4^{(2)}$ in $\mathbb{P}^5$. Indeed, the Klein quadric provides an elegant way to represent lines in $\mathbb{P}^3$ with points in $\mathbb{P}^5$, and this make it possible to explore the projective properties of the $M_4^{(2)}$ in $\mathbb{P}^5$ and then convert the properties into theorems and propositions in line geometry.

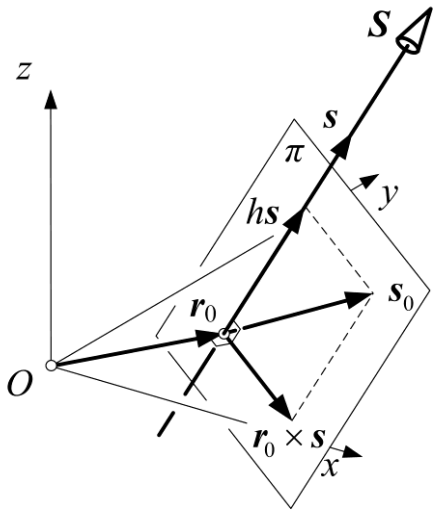

Figure 3.1 The geometrical meanings of the relative vectors of a screw

For instance, the Klein quadric is generated by two distinct families of planes named α-planes and β-planes [38]; hence considering the one-to-one correspondence between the projective subspace of $\mathbb{P}^5$ and line varieties in $\mathbb{P}^3$, a line pencil in $\mathbb{P}^3$ of rank 3 where lines share a common point can be obtained from the α-plane, and a plane of lines of rank 3 in which lines lie in a specified plane can be obtained from the β-plane. The α-planes and β-planes as the generators of Klein quadric $M_4^{(2)}$, and their correspondence with line varieties in $\mathbb{P}^3$ have been investigated in geometrical method by [76][77] and proved in algebraic way by [38]. In this dissertation the concept of α-planes and β-planes of Klein quadric associated with line vectors and the related results in line geometry are to be extended to those of hyperquadric corresponding to screws and five screw systems with particular geometrical properties are hence obtained in a manner of algebraic geometry.

From the above, all the projective points corresponding to line vectors in $\mathbb{P}^3$ constitute the Klein quadric in $\mathbb{P}^5$ which can be represented by Equation (3.9). Analogously, all the corresponding points of screws in $\mathbb{P}^3$ with the same but non-zero pitch can also form a hyperquadric in $\mathbb{P}^5$. The hyperquadric can be defined by the quadratic constraint for screws with the same pitch and represented as

$$\Omega_4 \equiv Kl(\boldsymbol{S}, \boldsymbol{S}) - 2h \cdot Ki(\boldsymbol{S}, \boldsymbol{S}) = 0 \tag{3.10}$$

This is in fact a quadratic form on $se^*(3)$ and was defined as *pitch hyperquadric* in [35].

In the above equation, if $h = 0$, i.e. $Kl(\boldsymbol{S}, \boldsymbol{S}) = 0$, the hyperquadric Ω_4 degenerates into Klein quadric $M_4^{(2)}$ given by Equation (3.9). If h is a variable parameter in the real number field, a pencil of non-degenerate hyperquadrics can be obtained. Otherwise, if h tends to infinity, i.e. the primary part of screw $\boldsymbol{s}$ equals $\mathbf{0}$ leading to $Ki(\boldsymbol{S}, \boldsymbol{S}) = 0$, then the hyperquadric degenerates into a plane in $\mathbb{P}^5$ which is common to the pencil of hyperquadrics and Klein quadric. In fact, the space of $\mathbb{P}^5$ is fully filled by the pencil of hyperquadrics [35].

The hyperquadric of screws can also be expressed by other forms of representations. Using the coordinates for screws in Equation (3.2) and considering Equations (3.1) and (3.3), the above Equation (3.10) can be rewritten as

$$\Omega_4 \equiv \xi_0\xi_3 + \xi_1\xi_4 + \xi_2\xi_5 - h\left(\xi_0^2 + \xi_1^2 + \xi_2^2\right) = 0 \tag{3.11}$$

Combining Equations (3.2) with Equation (3.3), it has $\boldsymbol{s} = (\xi_0, \xi_1, \xi_2)$ and $\boldsymbol{s}_0 = (\xi_3, \xi_4, \xi_5)$, hence the vector representation of the above hyperquadric is acquired as

$$\Omega_4 \equiv \boldsymbol{s}^{\mathrm{T}}\left(\boldsymbol{s}_0 - h\boldsymbol{s}\right) = 0 \tag{3.12}$$

where the vector $(\boldsymbol{s}_0 - h\boldsymbol{s})$ represents the position of the axes of the screws of pitch h which equals $\boldsymbol{r}_0 \times \boldsymbol{s}$ and this is indicated by the parallelogram in Fig. 3.1. Rewriting Equation (3.12) into the matrix form, we can get the matrix representation of the hyperquadric Ω_4 and it is

$$\Omega_4 \equiv \boldsymbol{S}^{\mathrm{T}}\mathbf{A}\boldsymbol{S} = \boldsymbol{S}^{\mathrm{T}}\begin{bmatrix} -h\mathbf{I} & \frac{1}{2}\mathbf{I} \\ \frac{1}{2}\mathbf{I} & \mathbf{0} \end{bmatrix}\boldsymbol{S} = 0 \tag{3.13}$$

where 3×3 matrix **I** are identity matrix, screw $\boldsymbol{S}$ is the six homogenous coordinates in Eq. (2), and the 6×6 symmetric partitioned matrix **A** can uniquely identify a hyperquadric Ω_4.

Hence, the hyperquadric Ω_4 of screws with the same pitch h has been defined by a quadratic form on $se^*(3)$ and been expressed by coordinate representation as Equation (3.2), vector representation as Equation (3.12), and matrix representation as Equation (3.13).

3.5 Projective Transformations

From the above section, the hyperquadric Ω_4 of screws can be regarded as the extension of Klein quadric $M_4^{(2)}$ of line vectors. Further, this section is to reveal that the concept of α-planes and β-planes of $M_4^{(2)}$ can also be extended to those of Ω_4 through a projective transformation.

For an arbitrary hyperquadric in n-dimensional projective space $\mathbb{P}^n$, there exists a projectively equivalent hyperquadric of the normal form (Otto Schreier, 1961) [78]

$$\Omega_{n-1} \equiv \xi_0^2 + \xi_1^2 + \cdots + \xi_k^2 - \xi_k^2 - \cdots - \xi_n^2 = 0,\ k \in \mathbb{Z},\ 0 \le k \le n \tag{3.14}$$

To obtain the normal form of the hyperquadric Ω_4, a projective transformation $\mathbf{T}$ is performed on the coordinate system $\boldsymbol{S}$ as follows

$$\boldsymbol{S}' = \begin{pmatrix} \boldsymbol{x} \\ \boldsymbol{y} \end{pmatrix} = \mathbf{T} \begin{pmatrix} \boldsymbol{s} \\ \boldsymbol{s}_0 \end{pmatrix} = \mathbf{T}\boldsymbol{S} \tag{3.15}$$

where $\mathbf{T}$ is a 6×6 matrix indicating the projective transformation and screw $\boldsymbol{S}'$ gives the resultant coordinate system of $\mathbb{P}^5$ as

$$\boldsymbol{S}' = \begin{pmatrix} \boldsymbol{x} \\ \boldsymbol{y} \end{pmatrix} = \left(x_1,\ x_2,\ x_3,\ y_1,\ y_2,\ y_3 \right)^{\mathrm{T}} \tag{3.16}$$

To construct the projective transformation that changes the hyperquadric Ω_4 into normal form as Equation (3.14), it is natural to perform a coordinate transformation that makes Equation (3.12) adaptable to the *difference of two squares formula*, thus the following substitution of coordinates is given as

$$\begin{cases} \boldsymbol{s} = \boldsymbol{x} + \boldsymbol{y} \\ \boldsymbol{s}_0 - h\boldsymbol{s} = \boldsymbol{x} - \boldsymbol{y} \end{cases} \tag{3.17}$$

Based on the algebraic relationship between $\boldsymbol{x}$, $\boldsymbol{y}$ and $\boldsymbol{s}$, $\boldsymbol{s}_0$ given by the above equation and by their geometrical relationship in plane π in Fig. 3.1, two vector parallelograms can be established as EGFH and GHQP as indicated in Fig. 3.2. The former

parallelogram EGFH is the geometrical expression of the Eq. (3.14), while the latter parallelogram GHQP is nothing but the copy of the parallelogram in Figure 3.1. In Figure 3.2, the vectors $\boldsymbol{s}$, $\boldsymbol{s}_0$ in colour red form the initial coordinate system $\boldsymbol{S}$, while the vectors $\boldsymbol{x}$, $\boldsymbol{y}$ in colour blue constitute the resultant coordinate system $\boldsymbol{S}'$.

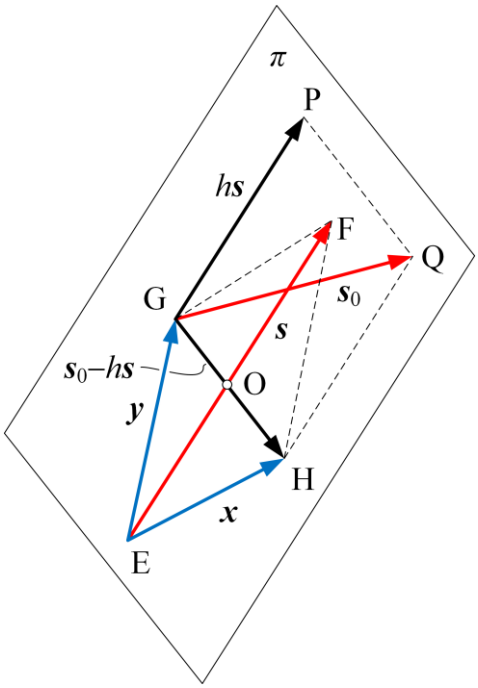

Figure 3.2 The geometrical relationship between coordinate system **S** and **S'**

In vector polygon EOGQH in Figure 3.2, vector $\boldsymbol{x}$ can be represented and calculated as follows

$$\begin{aligned} \overrightarrow{\mathrm{EH}} &= \overrightarrow{\mathrm{EO}} + \overrightarrow{\mathrm{OG}} + \overrightarrow{\mathrm{GQ}} + \overrightarrow{\mathrm{QH}} \\ \boldsymbol{x} &= \frac{1}{2}\boldsymbol{s} - \frac{1}{2}\left(\boldsymbol{s}_0 - h\boldsymbol{s}\right) + \boldsymbol{s}_0 - h\boldsymbol{s} \\ &= \frac{1}{2}\left(1-h\right)\boldsymbol{s} + \frac{1}{2}\boldsymbol{s}_0 \end{aligned} \tag{3.18}$$

Similarly, vector $\boldsymbol{y}$ can be solved through vector polygon EOHQG as

$$\begin{aligned}\overrightarrow{\mathrm{EG}} &= \overrightarrow{\mathrm{EO}} + \overrightarrow{\mathrm{OH}} + \overrightarrow{\mathrm{HQ}} + \overrightarrow{\mathrm{QG}} \\ \boldsymbol{y} &= \frac{1}{2}\boldsymbol{s} + \frac{1}{2}\left(\boldsymbol{s}_0 - h\boldsymbol{s}\right) + h\boldsymbol{s} - \boldsymbol{s}_0 \\ &= \frac{1}{2}\left(1+h\right)\boldsymbol{s} - \frac{1}{2}\boldsymbol{s}_0\end{aligned} \tag{3.19}$$

Based on Equation (3.15) combining Equation (3.18) with Equation (3.19) and writing them in matrix form, the projective transformation **T** can thus be revealed as

$$\boldsymbol{S}' = \begin{pmatrix}\boldsymbol{x} \\ \boldsymbol{y}\end{pmatrix} = \begin{bmatrix}\frac{1}{2}\left(1-h\right)\mathbf{I} & \frac{1}{2}\mathbf{I} \\ \frac{1}{2}\left(1+h\right)\mathbf{I} & -\frac{1}{2}\mathbf{I}\end{bmatrix}\begin{pmatrix}\boldsymbol{s} \\ \boldsymbol{s}_0\end{pmatrix} = \mathbf{T}\boldsymbol{S} \tag{3.20}$$

Hence, perform the projective transformation onto the matrix representation **A** of Ω_4 given by Equation (3.13), and then it has

$$\begin{aligned}\boldsymbol{S}^{\mathrm{T}}\boldsymbol{A}\boldsymbol{S} &= \left(\mathbf{T}^{-1}\boldsymbol{S}'\right)^{\mathrm{T}}\mathbf{A}\left(\mathbf{T}^{-1}\boldsymbol{S}'\right) \\ &= \left(\boldsymbol{S}'\right)^{\mathrm{T}}\left(\mathbf{T}^{-\mathrm{T}}\mathbf{A}\mathbf{T}^{-1}\right)\boldsymbol{S}' \\ &= \left(\boldsymbol{S}'\right)^{\mathrm{T}}\mathbf{A}'\boldsymbol{S}'\end{aligned} \tag{3.21}$$

The above coordinate transformation in fact gives the relationship between matrix **A** and $\mathbf{A}'$ as

$$\mathbf{A}' = \mathbf{T}^{-\mathrm{T}}\mathbf{A}\mathbf{T}^{-1} \tag{3.22}$$

which gives a congruent transformation between matrix **A** and **A**′.

3.6 *α*- and *β*-Planes of a Hyperquadric in the 5-Dimensional Projective Space

Substituting matrix **T** given by Equation (3.20) into Equation (3.22) and writing the result into coordinate representation analogous with Equation (3.11), the normal form of Ω_4 can be obtained as

$$\Omega_4 \equiv x_1^2 + x_2^2 + x_3^2 - y_1^2 - y_2^2 - y_3^2 = 0 \tag{3.23}$$

Alternatively, the above normal form of Ω_4 can be directly calculated by substituting Equation (3.17) into Equation (3.12), and the result is written as

$$\Omega_4 \equiv \boldsymbol{x}^{\mathrm{T}}\boldsymbol{x} - \boldsymbol{y}^{\mathrm{T}}\boldsymbol{y} = 0 \tag{3.24}$$

This coincides with the result given by Equation (3.23) which was obtained through projective transformation matrix **T**. The former method by means of establishing a projective transformation is more complicated compared with the direct way to obtain the normal form of Ω_4, but revealing the intrinsic geometrical relationship between ***x***, ***y***

and $\boldsymbol{s}$, $\boldsymbol{s}_0$ is of meanings in deriving the special screw systems through α-planes and β-planes in the next chapter.

In algebraic geometry, an arbitrary projective plane in $\mathbb{P}^5$ can be thought of as the intersection of three hyperplanes and thus can be expressed by three linear equations in the form of matrix as

$$\boldsymbol{x} = \mathbf{B}\boldsymbol{y} \tag{3.25}$$

where $\mathbf{B}$ is a 3×3 non-singular matrix and can be regarded as the matrix representation of plane in $\mathbb{P}^5$. To explore the properties with the normal form of Ω_4, the coordinates given by Equation (3.16) that have undergone the projective transformation is adopted in the above equation. Substituting the above equation into Equation (3.25), it has

$$\Omega_4 \equiv \boldsymbol{y}^{\mathrm{T}}(\mathbf{B}^{\mathrm{T}}\mathbf{B} - \mathbf{I})\boldsymbol{y} = 0 \tag{3.26}$$

In this equation indicating the intersection of the plane expressed by Equation (3.25) with Ω_4, if the coefficient matrix $\mathbf{B}$ is an element of orthogonal group $O(3)$, i.e. $\mathbf{B}^{\mathrm{T}}\mathbf{B}=\mathbf{I}$, the plane given by Equation (3.25) does lie entirely in Ω_4. Since the elements of $O(3)$ can be classified into two types with respect to the determinant of the elements, the Ω_4 in $\mathbb{P}^5$ is hence generated by two families of planes. The planes identified by elements of $O(3)$ whose determinant satisfies $\det(\mathbf{B}) = +1$ are α-planes, while the other planes identified by $\det(\mathbf{B}) = -1$ are β-planes.

3.7 Conclusions

In this chapter, basic concepts of screw theory and Lie bracket were introduced in the algebraic language. A projective transformation was for the first time proposed for the hyperquadrics of screws with non-zero pitch in the 5-dimensional projective space. Using this method, any hyperquadrics corresponding to screw systems with a constant pitch can be represented in a matrix form, by which it can be attained that the hyperquadrics were generated by two bundles of planes as α-planes and β-planes. This chapter lays the foundation of recognising the dependency of screws for the next chapter and basic concepts and operations will be used in the following part of the dissertation, especially Chapter 5 the Lie bracket computation and bilinear form representation of constraints and Chapter 7 the tangent spaces of compositional submanifolds of mechanisms.

Chapter 4 Screw Systems and Recognition of the Geometrical Conditions

4.1 Introduction

Following chapter 3, this chapter is to use vector and matrix operation to explore the geometrical relationships of screws in 3-space corresponding to those points lying in an α-plane and a β-plane, leading to the representation of two conventional screw systems of order three. Based on the vector and matrix representation and by means of the Shur complement and block diagonalization, this chapter investigates the intersection of the α-planes and β-planes and conventional screw systems of order two are rediscovered. All the derivations and the equations of vectors and matrices are going to be validated numerically by constructing the related matrix representations and implementing the projective transformations in the last section of this chapter.

4.2 Three-Systems as α-Planes

A screw system of order n, also named n-system, is an n-dimensional vector subspace, hence it corresponds to an $(n-1)$-dimensional projective subspace. The α-planes and β-planes of Ω_4 can be obtained by applying three linear constraints onto 5-dimensional projective space, due to which the α-planes and β-planes of Ω_4 are of dimension 2. Hence, there exist 3-systems corresponding to the α-planes and β-planes of Ω_4 and 2-systems corresponding to lines as the intersection of the α-planes and β-planes if they do have intersection. In what follows the geometrical properties of the corresponding screw systems are to be revealed and several propositions regarding the dependency of screw varieties are further put forward.

To obtain the geometrical properties of 3-systems corresponding to the α-planes and β-planes, it is natural to explore the relationship between the direction vectors of the screws $\boldsymbol{s}$ and the moment of the screw axes about the origin $\boldsymbol{s}_0 - h\boldsymbol{s}$. In the vector triangle OHF in Fig. 2, it has

$$\begin{aligned} \overrightarrow{\mathrm{OH}} &= \overrightarrow{\mathrm{OF}} + \overrightarrow{\mathrm{FH}} \\ \frac{1}{2}(\boldsymbol{s}_0 - h\boldsymbol{s}) &= \frac{1}{2}\boldsymbol{s} - \boldsymbol{y} \end{aligned} \tag{4.1}$$

Similarly, in the vector triangle GOF, the following equation holds

$$\begin{aligned} \overrightarrow{\mathrm{GO}} &= \overrightarrow{\mathrm{GF}} + \overrightarrow{\mathrm{FO}} \\ \frac{1}{2}\left(\boldsymbol{s}_0 - h\boldsymbol{s}\right) &= \boldsymbol{x} - \frac{1}{2}\boldsymbol{s} \end{aligned} \tag{4.2}$$

Combining Equations (3.25), (4.1), and (4.2), eliminating vector $\boldsymbol{x}$, $\boldsymbol{y}$, the following equation can be obtained

$$\left(\mathbf{B}+\mathbf{I}\right)\left(\boldsymbol{s}_0 - h\boldsymbol{s}\right) = \left(\mathbf{B}-\mathbf{I}\right)\boldsymbol{s} \tag{4.3}$$

The α-planes and the β-planes correspond to two kinds of three-systems. To explore the geometrical properties of the screws with the same pitch h of the 3-systems, the relationship between the vectors $\boldsymbol{x}$, $\boldsymbol{y}$ in the resultant coordinate system $\boldsymbol{S}'$ and the dual vectors $\boldsymbol{s}$, $\boldsymbol{s}_0$ of screws can be derived by rewriting and performing the projective transformation in Equation (3.22) as follows

$$\begin{pmatrix} \boldsymbol{x} \\ \boldsymbol{y} \end{pmatrix} = \begin{bmatrix} \left(1-h\right)\boldsymbol{I} & \boldsymbol{I} \\ \left(1+h\right)\boldsymbol{I} & -\boldsymbol{I} \end{bmatrix} \begin{pmatrix} \boldsymbol{s} \\ \boldsymbol{s}_0 \end{pmatrix} \tag{4.4}$$

Hence, the projective planes presented by matrix $\boldsymbol{B}$ in Equation (3.25) become

$$\left(1-h\right)\boldsymbol{s} + \boldsymbol{s}_0 = \boldsymbol{B}\left(\left(1+h\right)\boldsymbol{s} - \boldsymbol{s}_0\right) \tag{4.5}$$

To explore the geometrical properties of the corresponding 3-systems, we rewrite the above equation as follows

$$(\boldsymbol{B}+\boldsymbol{I})(\boldsymbol{s}_0-h\boldsymbol{s})=(\boldsymbol{B}-\boldsymbol{I})\boldsymbol{s} \tag{4.6}$$

where the vector $\boldsymbol{s}$ represents the orientation of the axis of the screws in the corresponding three-systems and the vector ($\boldsymbol{s}_0 - h\boldsymbol{s}$) represents the position of the axis of the screws.

Consequently, there are two cases to consider. As for α-planes, it has det($\boldsymbol{B}$) = +1 so that $\boldsymbol{B}$ belongs to special orthogonal group $SO(3)$, then the 3×3 matrix ($\boldsymbol{B} + \boldsymbol{I}$) is usually non-singular, hence the above equation can be written as

$$\boldsymbol{s}_0-h\boldsymbol{s}=\left(\boldsymbol{B}+\boldsymbol{I}\right)^{-1}\left(\boldsymbol{B}-\boldsymbol{I}\right)\boldsymbol{s} \tag{4.7}$$

It can be proved that the matrix $(\boldsymbol{B} + \boldsymbol{I})^{-1}(\boldsymbol{B} - \boldsymbol{I})$ is skew-symmetric (Bottema and Roth, 1979) [79], and this gives *Cayley formula* [80]. The above equation can be rewritten as follows

$$\boldsymbol{s}_0-h\boldsymbol{s}=\left[\boldsymbol{r}\times\right]\boldsymbol{s} \tag{4.8}$$

where matrix [$\boldsymbol{r}$ ×] represents the 3×3 skew-symmetric matrix $(\boldsymbol{B} + \boldsymbol{I})^{-1}(\boldsymbol{B} - \boldsymbol{I})$ in Equation (4.7) and it has

$$[\boldsymbol{r}\times] = (\boldsymbol{B}+\boldsymbol{I})^{-1}(\boldsymbol{B}-\boldsymbol{I}) \tag{4.9}$$

In Equation (4.8), vector ($\boldsymbol{s}_0 - h\boldsymbol{s}$) presents specifically the moment with respect to the origin of the axes of the screws belonging to the corresponding three-system identified by the matrix $\boldsymbol{B}$ satisfying $\det(\boldsymbol{B}) = +1$. The position vector $\boldsymbol{r}$ determined by skew-symmetric matrix [$\boldsymbol{r}$ ×] in Equation (4.9) represents a constant point in $\mathbb{R}^3$. Consequently, all the screws whose axes pass through the constant point $\boldsymbol{r}$ constitute the solutions to Equation (4.7). Moreover, as the projective points corresponding to these n screws lie exactly in the α-planes identified by the matrix $\boldsymbol{B}$ and the screws whose axes pass through the constant point $\boldsymbol{r}$ form a screw system of 3rd order. Now we can conclude that three or less than three screws with the same pitch, whose axes intersect at a point in $\mathbb{R}^3$ are linearly independent while more than three screws with the same pitch whose axes intersect at a point in $\mathbb{R}^3$ are linearly dependent. The following corollary can be extracted from the above.

Corollary 1. *If the axes of n screws with the pitch h intersect at a constant point in* $\mathbb{R}^3$*, all the corresponding projective points lie entirely in an α-plane of the related hyperquadric* $\boldsymbol{Q}_h$ *in* $\mathbb{P}^5$*, thus these n screws constitute a screw system of* 3rd *order. Therefore, if* $n \leq 3$*, n screws with this geometrical property whose axes have a common point are linearly independent*; *if* $n > 3$*, these n screws are linearly dependent.*

Now consider the singular case for matrix ($\boldsymbol{B}$+$\boldsymbol{I}$). Owing to the singularity, matrix ($\boldsymbol{B}$+$\boldsymbol{I}$) has at least one zero eigenvalue, meaning its algebraic multiplicity of zero $\kappa(0)$ is not less than 1. For α-planes, matrix $\boldsymbol{B}$ represents a rotation action with respect to an axis through the origin due to the fact that matrix $\boldsymbol{B}$ belongs to $SO(3)$. Hence matrix B can be expressed by Euler-Rodrigues formula as follows

$$\boldsymbol{B} = \boldsymbol{I} + \sin\theta \boldsymbol{A}_s + (1-\cos\theta)\boldsymbol{A}_s\boldsymbol{A}_s \tag{4.10}$$

where $\boldsymbol{A}_s$ is a skew-symmetric matrix constituted by rotation axis $\boldsymbol{s}$ = (s_x, s_y, s_z) and it has $\boldsymbol{A}_s = [\boldsymbol{s}\times]$, θ is amplitude of the rotation and $\boldsymbol{I}$ is 3×3 identity matrix. When θ equals π, matrix ($\boldsymbol{B}$+$\boldsymbol{I}$) can be derived as

$$\boldsymbol{B} + \boldsymbol{I} = 2(\boldsymbol{A}_s\boldsymbol{A}_s + \boldsymbol{I}) \tag{4.11}$$

which can be expanded as follows

$$\begin{aligned} \boldsymbol{B} + \boldsymbol{I} &= 2\left(\begin{bmatrix} 0 & -s_z & s_y \\ s_z & 0 & -s_x \\ -s_y & s_x & 0 \end{bmatrix}\begin{bmatrix} 0 & -s_z & s_y \\ s_z & 0 & -s_x \\ -s_y & s_x & 0 \end{bmatrix} + \begin{bmatrix} 1 & 0 & 0 \\ 0 & 1 & 0 \\ 0 & 0 & 1 \end{bmatrix}\right) \\ &= 2\left(\begin{bmatrix} -s_y^2 - s_z^2 & s_x s_y & s_x s_z \\ s_y s_x & -s_z^2 - s_x^2 & s_y s_z \\ s_z s_x & s_z s_y & -s_x^2 - s_y^2 \end{bmatrix} + \begin{bmatrix} 1 & 0 & 0 \\ 0 & 1 & 0 \\ 0 & 0 & 1 \end{bmatrix}\right) \end{aligned} \tag{4.12}$$

Considering the condition that $\boldsymbol{s}$ is a unit vector as $s_x^2 + s_y^2 + s_z^2 = 1$, the above equation becomes

$$\boldsymbol{B} + \boldsymbol{I} = 2\begin{bmatrix} s_x^2 & s_x s_y & s_x s_z \\ s_y s_x & s_y^2 & s_y s_z \\ s_z s_x & s_z s_y & s_z^2 \end{bmatrix} \tag{4.13}$$

Applying elementary operations to the matrix on the right-hand side of the above equation by multiplying the three rows by $s_y s_z$, $s_z s_x$, $s_x s_y$, respectively, then subtract the first row from the second row and from the third row respectively, it has

$$\begin{bmatrix} s_x^2 & s_x s_y & s_x s_z \\ s_y s_x & s_y^2 & s_y s_z \\ s_z s_x & s_z s_y & s_z^2 \end{bmatrix} \rightarrow \begin{bmatrix} s_x^2 s_y s_z & s_x s_y^2 s_z & s_x s_y s_z^2 \\ s_x^2 s_y s_z & s_x s_y^2 s_z & s_x s_y s_z^2 \\ s_x^2 s_y s_z & s_x s_y^2 s_z & s_x s_y s_z^2 \end{bmatrix} \rightarrow \begin{bmatrix} s_x^2 s_y s_z & s_x s_y^2 s_z & s_x s_y s_z^2 \\ 0 & 0 & 0 \\ 0 & 0 & 0 \end{bmatrix} \quad (4.14)$$

It can be concluded from the above equation that matrix ($\boldsymbol{B}+\boldsymbol{I}$) is singular due to rank ($\boldsymbol{B}+\boldsymbol{I}$) = 1 when matrix $\boldsymbol{B}$ represents a rotation by π. In this case, based on ($\boldsymbol{s}_0 - h\boldsymbol{s}$) = [$\boldsymbol{r}_0\times$] $\boldsymbol{s}$, it has

$$\left(\left(\boldsymbol{B}+\boldsymbol{I}\right)\left[\boldsymbol{r}_0\times\right]-\left(\boldsymbol{B}-\boldsymbol{I}\right)\right)\boldsymbol{s}=\boldsymbol{0} \quad (4.15)$$

where [$\boldsymbol{r}_0\times$] is the skew-symmetric matrix constituted by the position vector of the axes of the corresponding screws. Due to the singularity of matrix ($\boldsymbol{B}+\boldsymbol{I}$) in the above equation, thus the position vector $\boldsymbol{r}_0$ includes at least one element with infinite quantity to balance the equation, meaning all the corresponding screw axes intersect at a point at infinity. The screw axes intersecting at infinity can be interpreted as a bundle of parallel screw axes. The above contents about the singular case can be concluded by the following corollary.

Corollary 2. *If the axes of n screws with the pitch h are parallel in* $\mathbb{R}^3$, *all the corresponding projective points lie entirely in an α-plane of the related hyperquadric*

$\boldsymbol{Q}_h$ in $\mathbb{P}^5$, thus these n screws constitute a screw system of 3rd *order. Therefore, if* $n \leq 3$, *n screws with this geometrical property whose axes are parallel are linearly independent*; *if* $n > 3$, *these n screws are linearly dependent*.

4.3 Three-Systems as β-Planes

Consider the β-planes of the hyperquadrics $\boldsymbol{Q}_h$, then the matrix $\boldsymbol{B}$ satisfies $\det(\boldsymbol{B}) = -1$. Hence, the 3×3 matrix $(\boldsymbol{B} - \boldsymbol{I})$ is usually non-singular, so that Equation (4.6) can be written as

$$\boldsymbol{s} = \left(\boldsymbol{B} - \boldsymbol{I}\right)^{-1}\left(\boldsymbol{B} + \boldsymbol{I}\right)\left(\boldsymbol{s}_0 - h\boldsymbol{s}\right) \tag{4.16}$$

The matrix $(\boldsymbol{B} - \boldsymbol{I})^{-1}(\boldsymbol{B} + \boldsymbol{I})$ is also skew-symmetric and then the above equation can be presented as follows

$$\boldsymbol{s} = \boldsymbol{r}' \times \left(\boldsymbol{s}_0 - h\boldsymbol{s}\right) \tag{4.17}$$

where the vector $\boldsymbol{r}'$ is a three-dimensional vector determined by the 3×3 skew-symmetric matrix $(\boldsymbol{B} - \boldsymbol{I})^{-1}(\boldsymbol{B} + \boldsymbol{I})$ and thus it has

$$\boldsymbol{r}' = \left(\boldsymbol{B} - \boldsymbol{I}\right)^{-1}\left(\boldsymbol{B} + \boldsymbol{I}\right) \tag{4.18}$$

Taking the scalar products of the constant vector $\boldsymbol{r}'$ on both sides of Equation (4.17) yields

$$\boldsymbol{r}' \cdot \boldsymbol{s} = 0 \tag{4.19}$$

The above equation represents all the lines which are perpendicular to the vector $\boldsymbol{r}'$. Considering the vector representation of screw, we have $\boldsymbol{s}_0 - h\boldsymbol{s} = \boldsymbol{r}_0 \times \boldsymbol{s}$. Substituting this into Equation (4.17) and applying the vector triple product identity, it gives

$$\boldsymbol{r}' \cdot \boldsymbol{r}_0 = -1 \tag{4.20}$$

The solutions to Equation (4.17) can be extracted from Equations (4.19) and (4.20) as all the screws with pitch h whose axes lie on a plane in $\mathbb{R}^3$. Further, the n screws constitute a three-system because the corresponding projective points are lying on a β-plane identified by the matrix $\boldsymbol{B}$ satisfying $\det(\boldsymbol{B}) = -1$. Hence, it can be derived that three or less than three screws whose axes lie on a plane in $\mathbb{R}^3$ are linearly independent whilst more than three screws whose axes lie on a plane in $\mathbb{R}^3$ are linearly dependent and this gives the following corollary.

Corollary 3. *If the axes of n screws with the pitch h lie on a common plane in* $\mathbb{R}^3$*, all the corresponding projective points lie entirely in a β-plane of the related hyperquadric* $\boldsymbol{Q}_h$ *in* $\mathbb{P}^5$*, thus these n screws constitute a screw system of third order. Therefore, if* $n \leq 3$*, these n screws with this geometrical property whose axes lie on a common plane are linearly independent*; *if* $n > 3$*, these n screws are linearly dependent.*

4.4 Intersection of α-Planes and β-Planes

In $\mathbb{P}^5$, two projective planes generally do not intersect besides several special cases for α-planes and β-planes. For two arbitrary projective planes in $\mathbb{P}^5$, they can be represented by 3×3 matrices $\boldsymbol{B}_1$ and $\boldsymbol{B}_2$ respectively. Thus, their intersection can be expressed in the form of linear equations system immediately as follows

$$\begin{bmatrix} \boldsymbol{I} & -\boldsymbol{B}_1 \\ \boldsymbol{I} & -\boldsymbol{B}_2 \end{bmatrix} \begin{pmatrix} \boldsymbol{x} \\ \boldsymbol{y} \end{pmatrix} = \boldsymbol{0} \tag{4.21}$$

Consequently, we can examine the rank of the 6×6 matrix in the above equation to identify the dimension of the intersection of two arbitrary projective planes, including α-planes and β-planes.

4.4.1 Shur Complement and Block Diagonalization

By applying the Aitken block-diagonalization formula, the 6×6 coefficient matrix in Equation (4.21) can be decomposed as

$$\begin{bmatrix} \boldsymbol{I} & -\boldsymbol{B}_1 \\ \boldsymbol{I} & -\boldsymbol{B}_2 \end{bmatrix} = \begin{bmatrix} \boldsymbol{I} & \boldsymbol{0} \\ \boldsymbol{I} & \boldsymbol{I} \end{bmatrix} \begin{bmatrix} \boldsymbol{I} & \boldsymbol{0} \\ \boldsymbol{0} & \boldsymbol{B}_1 - \boldsymbol{B}_2 \end{bmatrix} \begin{bmatrix} \boldsymbol{I} & -\boldsymbol{B}_1 \\ \boldsymbol{0} & \boldsymbol{I} \end{bmatrix} \tag{4.22}$$

which gives the *block diagonalization form* of the coefficient matrix and the 3×3 block $\boldsymbol{B}_1-\boldsymbol{B}_2$ is called *Shur complement* of the coefficient matrix.

From the above decomposition and the resultant block diagonalization form, we can directly obtain the rank formula as follows

$$\operatorname{rank}\left(\begin{bmatrix} \boldsymbol{I} & -\boldsymbol{B}_1 \\ \boldsymbol{I} & -\boldsymbol{B}_2 \end{bmatrix}\right) = \operatorname{rank}\left(\begin{bmatrix} \boldsymbol{I} & \boldsymbol{0} \\ \boldsymbol{0} & \boldsymbol{B}_1-\boldsymbol{B}_2 \end{bmatrix}\right) = \operatorname{rank}(\boldsymbol{I}) + \operatorname{rank}(\boldsymbol{B}_1-\boldsymbol{B}_2) \qquad (4.23)$$

Hence, given two arbitrary projective planes represented by matrices $\boldsymbol{B}_1, \boldsymbol{B}_2$, the dimension of their intersection of two arbitrary projective planes is determined by the rank of the Shur component of the coefficient matrix. By means of the rank formula in Equation (4.23), if the Shur component $\boldsymbol{B}_1-\boldsymbol{B}_2$ is of full rank, the rank of the coefficient matrix equals 6 and thus provides 6 effective linear constraints for the intersection of the two projective planes. Considering the relationship between vector subspaces and projective subspaces given by chapter 3, the two projective planes represented by matrices $\boldsymbol{B}_1$, $\boldsymbol{B}_2$ respectively do not intersect. If the rank of the Shur component $\boldsymbol{B}_1-\boldsymbol{B}_2$ equals to 2, the number of the effective constraints provided by the coefficient matrix is 5. Hence, the dimension of the corresponding vector subspace of the intersection of the two projective planes is 1 in this case and the related projective subspace of the intersection equals 0. Thus, it can be concluded that two projective planes intersect at a projective point when the rank of the corresponding Shur component is 2. In like manner, it can be derived that two projective planes intersected at a projective line if

the rank of the corresponding Shur component equal 1. Concatenating the above derivation gives the following proposition.

Proposition 3. *Consider two arbitrary projective planes in* $\mathbb{P}^5$ *represented by* 3×3 *matrices* $\boldsymbol{B}_1$, $\boldsymbol{B}_2$ *respectively*. *Their intersection is determined by the Shur component* $\boldsymbol{B}_1-\boldsymbol{B}_2$ *of the related coefficient matrix given by Eq.* (46). *The two projective planes do not intersect if the Shur component is of full rank*. *Otherwise, they intersect at a projective point or a projective line if the rank of the Shur component equals* 2 *or* 1.

4.4.2 Intersection of α-Planes and β-Planes

For α-planes and β-planes, matrices $\boldsymbol{B}_1$ and $\boldsymbol{B}_2$ belong to orthogonal group $O(3)$ with the condition $\det(\boldsymbol{B}_1)=+1$ and $\det(\boldsymbol{B}_2)=-1$. In analyzing the rank of the Shur component $\boldsymbol{B}_1-\boldsymbol{B}_2$, an efficient way is to premultiply the Shur component by the full-rank matrix $\boldsymbol{B}_2^{\mathrm{T}}$ and this operation satisfies the following equation as

$$\operatorname{rank}\left(\boldsymbol{B}_1-\boldsymbol{B}_2\right)=\operatorname{rank}\left(\boldsymbol{B}_2^{\mathrm{T}}\left(\boldsymbol{B}_1-\boldsymbol{B}_2\right)\right)=\operatorname{rank}\left(\boldsymbol{B}_2^{\mathrm{T}}\boldsymbol{B}_1-\boldsymbol{I}\right) \tag{4.24}$$

where the matrix $\boldsymbol{B}_2^{\mathrm{T}}\boldsymbol{B}_1$ certainly satisfies the condition $\det\left(\boldsymbol{B}_2^{\mathrm{T}}\boldsymbol{B}_1\right)=-1$ and is an element of $O(3)$ as

$$\left(\boldsymbol{B}_2^{\mathrm{T}}\boldsymbol{B}_1\right)^{\mathrm{T}}\left(\boldsymbol{B}_2^{\mathrm{T}}\boldsymbol{B}_1\right)=\boldsymbol{B}_1^{\mathrm{T}}\left(\boldsymbol{B}_2\boldsymbol{B}_2^{\mathrm{T}}\right)\boldsymbol{B}_1=\boldsymbol{I} \tag{4.25}$$

In fact $\operatorname{rank}\left(\boldsymbol{B}_2^{\mathrm{T}}\boldsymbol{B}_1-\boldsymbol{I}\right)$ in Equation (4.24) determines the dimension of the eigenspace related to the eigenvalue 1 of matrix $\boldsymbol{B}_2^{\mathrm{T}}\boldsymbol{B}_1$ because the eigenspace is given by the null space of matrix $\boldsymbol{B}_2^{\mathrm{T}}\boldsymbol{B}_1-\boldsymbol{I}$. This can be illustrated by the following equation

$$\left(\boldsymbol{B}_2^{\mathrm{T}}\boldsymbol{B}_1-1\cdot\boldsymbol{I}\right)\boldsymbol{x}=\boldsymbol{0} \tag{4.26}$$

in which scalar 1 is the eigenvalue of $\boldsymbol{B}_2^{\mathrm{T}}\boldsymbol{B}_1$, vector $\boldsymbol{x}$ is the null space of matrix and can be regarded as the related eigenvectors constituting the eigenspace. Thus, the relationship between $\operatorname{rank}\left(\boldsymbol{B}_2^{\mathrm{T}}\boldsymbol{B}_1-\boldsymbol{I}\right)$ and the geometric multiplicity of the eigenvalue 1 of matrix $\boldsymbol{B}_2^{\mathrm{T}}\boldsymbol{B}_1$ can be given as follows

$$\operatorname{rank}\left(\boldsymbol{B}_2^{\mathrm{T}}\boldsymbol{B}_1-\boldsymbol{I}\right)+\gamma(1)=3 \tag{4.27}$$

where the scalar $\gamma(1)$ is the geometric multiplicity of the eigenvalue 1 of matrix $\boldsymbol{B}_2^{\mathrm{T}}\boldsymbol{B}_1$, presenting the dimension of the associated eigenspace, and 3 represents the row number of matrix $\boldsymbol{B}_2^{\mathrm{T}}\boldsymbol{B}_1$. Therefore, $\operatorname{rank}\left(\boldsymbol{B}_2^{\mathrm{T}}\boldsymbol{B}_1-\boldsymbol{I}\right)$ can be obtained directly through the geometric multiplicity γ of the eigenvalue 1 of matrix $\boldsymbol{B}_2^{\mathrm{T}}\boldsymbol{B}_1$, Thus, it is necessary to explore the characteristics of the orthogonal matrix $\boldsymbol{B}_2^{\mathrm{T}}\boldsymbol{B}_1$.

Every element of $O(3)$ whose determinant equals −1 is congruent and similar to a orthogonal matrix presenting a rotation about a line combined with reflection in the

orthogonal plane. Hence, performing the congruence and similarity transformation, the matrix $\boldsymbol{B}_2^{\mathrm{T}}\boldsymbol{B}_1$ can be rewritten as

$$\boldsymbol{B}_2^{\mathrm{T}}\boldsymbol{B}_1 = \boldsymbol{R}^{\mathrm{T}}\boldsymbol{C}\boldsymbol{R} = \boldsymbol{R}^{\mathrm{T}}\begin{bmatrix} -1 & 0 & 0 \\ 0 & \cos\varphi & -\sin\varphi \\ 0 & \sin\varphi & \cos\varphi \end{bmatrix}\boldsymbol{R} \tag{4.28}$$

where matrix $\boldsymbol{R}$ is an element of $O(3)$ and matrix $\boldsymbol{C}$ is the similarity and congruence matrix of $\boldsymbol{B}_2^{\mathrm{T}}\boldsymbol{B}_1$. Since congruent and similar matrices share eigenvalues and geometric multiplicities, the geometric multiplicity of the congruence and similarity matrix $\boldsymbol{C}$ can be used to obtain the rank of matrix $\boldsymbol{B}_2^{\mathrm{T}}\boldsymbol{B}_1 - \boldsymbol{I}$, and further to find the rank of the Shur component $\boldsymbol{B}_1$–$\boldsymbol{B}_2$.

For the congruence and similarity matrix $\boldsymbol{C}$, it is not complicated to find its three eigenvalues in complex field as

$$-1,\ e^{+j\varphi},\ e^{-j\varphi} \tag{4.29}$$

Thus, the geometric multiplicity of the eigenvalue 1 is generally 0. Specially, if $\varphi = 0$, the three eigenvalues become –1, 1, 1 and the geometric multiplicity of the eigenvalue 1 can be obtained as $\gamma(1)=2$. In such case, the rank of the Shur component $\boldsymbol{B}_1$–$\boldsymbol{B}_2$ is equal to 1 according to Equation (4.27), hence it has $\mathrm{rank}\left(\boldsymbol{B}_2^{\mathrm{T}}\boldsymbol{B}_1 - \boldsymbol{I}\right) = 1$.

Consequently, α-plane and β-plane generally do not intersect with each other for the geometric multiplicity of the eigenvalue 1 of the matrix $\boldsymbol{B}_2^{\mathrm{T}}\boldsymbol{B}_1$ is 0 in most cases. Meanwhile, in some special cases, α-plane and β-plane do intersect at a projective line when the corresponding geometric multiplicity equals 2.

4.5 Two-Systems as the Intersection of *A*-Planes and *B*-Planes

Consider the case in which an α-plane and a β-plane intersect at a projective line. The corresponding vector subspace of the projective line is of dimension 2, thus the intersection of α-plane and β-plane as a projective line in $\mathbb{P}^5$ can be represented by four linear equations in matrix form as follows

$$\left[\begin{array}{ccc:ccc} a_1 & b_1 & c_1 & d_1 & e_1 & f_1 \\ a_2 & b_2 & c_2 & d_2 & e_2 & f_2 \\ a_3 & b_3 & c_3 & d_3 & e_3 & f_3 \\ \hdashline a_4 & b_4 & c_4 & d_4 & e_4 & f_4 \end{array}\right] \left(\begin{array}{c} x_1 \\ x_2 \\ x_3 \\ \hdashline y_1 \\ y_2 \\ y_3 \end{array}\right) = \mathbf{0} \tag{4.30}$$

Therefore, the projective line as the intersection of the α-plane and the β-plane can be interpreted as the intersection of the α-plane with a general hyperplane as well as the intersection of the β-plane with another hyperplane. Consequently, the following system of linear equations in the form of partitioned matrix holds for the projective line

$$\begin{bmatrix} \boldsymbol{I} & \boldsymbol{B}_i \\ \boldsymbol{e}_i^{\mathrm{T}} & \boldsymbol{f}_i^{\mathrm{T}} \end{bmatrix} \begin{pmatrix} \boldsymbol{x} \\ \boldsymbol{y} \end{pmatrix} = \boldsymbol{0} \quad i = 1, 2 \tag{4.31}$$

in which matrices $\boldsymbol{B}_i$ are 3×3 orthogonal matrices as elements of $O(3)$ representing the α-plane and the β-plane, $\boldsymbol{e}_i^{\mathrm{T}}$ and $\boldsymbol{f}_i^{\mathrm{T}}$ are 3-dimensional vectors acting as the coefficients of the general hyperplanes.

Hence, the projective line as the intersection of the α-plane and β-plane corresponds to a two-system with particular geometrical properties. Let $\delta(0)$ denote the algebraic multiplicity of zero eigenvalue of a matrix. Compared with the geometric multiplicity $\gamma(1)$ which played a vital role in obtaining the rank of matrix, algebraic multiplicity is always acting as the determinant of invertibility of matrix. On one hand, the projective line can be regarded as the subspace of the α-plane presented by matrix $\boldsymbol{B}_1$. On the other hand, the projective line can also be regarded as subspace of the β-plane presented by matrix $\boldsymbol{B}_2$, i.e., Equations (4.19) and (4.20) are tenable for the projective line. Concatenating the mentioned equations gives

$$\begin{cases} \boldsymbol{s}_0 - h\boldsymbol{s} = \boldsymbol{r} \times \boldsymbol{s} \\ \boldsymbol{r}' \cdot \boldsymbol{s} = \boldsymbol{0} \\ \boldsymbol{r}' \cdot \boldsymbol{r}_0 = -1 \\ \delta(0) = 0 \end{cases} \tag{4.32}$$

in which $\delta(0) = 0$ for matrix $\boldsymbol{B}_1 + \boldsymbol{I}$ indicates its nonsingularity, vector $\boldsymbol{r}$ and $\boldsymbol{r}'$ are two constant position vectors, vector $\boldsymbol{r}_0$, $\boldsymbol{s}$ and $\boldsymbol{s}_0 - h\boldsymbol{s}$ are three variable vectors describing the

geometrical characteristics of the screws of the corresponding two-system and present the position vectors, direction vectors and moment of the direction vectors of the screws, respectively. From the geometrical meanings of Equation (4.32), it can be obtained that all the screws with the same pitch whose axes pass through the constant point $\boldsymbol{r}$ and also lie on a plane determined by vector $\boldsymbol{r}'$ constitute the solutions to Equation (4.32) on the condition that $\boldsymbol{r}' \cdot \boldsymbol{r} = -1$ which means the point $\boldsymbol{r}$ also lies on the plane. That is, the projective line in $\mathbb{P}^5$ as the intersection of α-plane and β-plane corresponds to a planar pencil of screws with the same pitch in $\mathbb{R}^3$, of which the centre and the plane is determined by the α-plane and the β-plane respectively. This planar pencil of screws forms a two-system. Further, we can conclude that more than two screws with the same pitch in a planar pencil of screws are linearly dependent while two of less than two screws with the same pitch in a planar pencil of screws are linearly independent. Hence, the corollary on linear dependence of screws with the same pitch can be obtained as follows.

Corollary 4. *If the axes of n screws form a planar pencil of lines in* $\mathbb{R}^3$*, all the corresponding projective points lie entirely in a projective line in* $\mathbb{P}^5$*, thus these n screws constitute a screw system of* 2^{nd} *order. Therefore, if* $n > 2$*, n screws with this geometrical property whose axes have a common point and lie on a common plane are linearly dependent*; *if* $n \leq 2$*, these n screws are linearly independent.*

If matrix $\boldsymbol{B}_1+\boldsymbol{I}$ is singular, concatenate Equations (4.19), (4.20) and (4.15)gives the following geometrical constraints on the projective line as the intersection of α-plane and β-plane

$$\begin{cases} \left(\left(\boldsymbol{B}_1+\boldsymbol{I}\right)\left[\boldsymbol{r}_0\times\right]-\left(\boldsymbol{B}_1-\boldsymbol{I}\right)\right)\boldsymbol{s}=\boldsymbol{0} \\ \boldsymbol{r}'\cdot\boldsymbol{s}=\boldsymbol{0} \\ \boldsymbol{r}'\cdot\boldsymbol{r}_0=-1 \\ \delta(0)\neq 0 \end{cases} \tag{4.33}$$

where the notations are of the same geometrical meanings as those in Equation (4.32). It can be seen that a cluster of screws with the same pitch whose axes are parallel and coplanar constitutes the solutions to the above equation. In like manner, the following corollary on linear dependence of screws with the same pitch can be obtained.

Corollary 5. *If the axes of n screws with the pitch h are parallel and coplanar in* $\mathbb{R}^3$*, all the corresponding projective points lie entirely in a projective line in* $\mathbb{P}^5$*, hence these n screws constitute a screw system of* 2^{rd} *order. Therefore, if n* > 2*, n screws with this geometrical property whose axe are parallel and coplanar are linearly dependent*; *if n* ≤ 2*, these n screws are linearly independent*.

4.6 Constructing the Matrices for α-plane, β-plane, and Their Intersection Through Given Screws with Geometrical Properties

The above derivations and principle can be illustrated and verified by the following numerical example, which presents a method for constructing the matrices for projective subspaces such as α-plane, β-plane, and their intersection by utilizing several clusters of screws designated with specific geometrical properties. To validate the

derivation in this chapter sufficiently, a converse procedure from several given three-systems and two-systems to the corresponding α-plane, β-plane, and their intersection is adopted. This procedure is just the contrary to the derivation in this chapter and chapter 3.

This example contains three parts. The first part is to obtain the matrix representation of α-plane through a bundle of screws with the same pitch whose axes have a common point in $\mathbb{R}^3$. In this part the projective transformation is implemented and a 9×9 coefficient matrix is constructed. In like manner, the second part is to obtain the matrix representation of β-plane through a plane of screws with the same pitch. Then matrix representation of the intersection of the α-plane in the first part with the β-plane in the second part is calculated through a given planar pencil of screws with the same pitch. The matrix representation is given in Equation (4.31) and this calculation is performed by taking the intersection of the α-plane with the β-plane as the intersection of a general hyperplane with the α-plane or the β-plane. Finally, it can be seen that the matrices for the α-plane and the β-plane are the elements of orthogonal group $O(3)$ and the matrix for the projective line as the intersection of the α-plane and the β-plane is of the form in Equation (4.31). Thus, the derivations in this chapter and chapter 3 in respect of the interrelationship of screw system with projective subspace and the issue of linear dependence of screws are completely verified.

4.6.1 Constructing the Matrix for the α-Plane Through a Bundle of Screws with the Same Pitch

Given a bundle of screws with the same pitch. Suppose the direction vectors of the screws are arbitrarily chosen as

$$\begin{aligned} \boldsymbol{s}_1 &= \begin{pmatrix} -0.500 & 0.600 & 0.500 \end{pmatrix}^{\mathrm{T}} \\ \boldsymbol{s}_2 &= \begin{pmatrix} 0.500 & -0.700 & 0.600 \end{pmatrix}^{\mathrm{T}} \\ \boldsymbol{s}_3 &= \begin{pmatrix} 0.600 & 0.500 & -0.800 \end{pmatrix}^{\mathrm{T}} \\ \boldsymbol{s}_4 &= \begin{pmatrix} 0.700 & -0.600 & -0.700 \end{pmatrix}^{\mathrm{T}} \end{aligned} \tag{4.34}$$

Suppose all the screws are located at

$$\boldsymbol{r} = \begin{pmatrix} 0.600 & 0.500 & 0.800 \end{pmatrix}^{\mathrm{T}} \tag{4.35}$$

The pitch of the screws is given as h=0.500. According to the dual vector representation in Equation (3.1), the 6-dimensional homogenous coordinates of the screws can be written as

$$
\begin{aligned}
\boldsymbol{S}_1 &= \begin{pmatrix} \boldsymbol{s}_1 \\ \boldsymbol{s}_{10} \end{pmatrix} = \begin{pmatrix} \boldsymbol{s}_1 \\ \boldsymbol{r} \times \boldsymbol{s}_1 + h\boldsymbol{s}_1 \end{pmatrix} = \begin{pmatrix} -0.500 & 0.600 & 0.500 & -0.480 & -0.400 & 0.860 \end{pmatrix}^{\mathrm{T}} \\
\boldsymbol{S}_2 &= \begin{pmatrix} \boldsymbol{s}_2 \\ \boldsymbol{s}_{20} \end{pmatrix} = \begin{pmatrix} \boldsymbol{s}_2 \\ \boldsymbol{r} \times \boldsymbol{s}_2 + h\boldsymbol{s}_2 \end{pmatrix} = \begin{pmatrix} 0.500 & -0.700 & 0.600 & 1.110 & -0.310 & -0.370 \end{pmatrix}^{\mathrm{T}} \\
\boldsymbol{S}_3 &= \begin{pmatrix} \boldsymbol{s}_3 \\ \boldsymbol{s}_{30} \end{pmatrix} = \begin{pmatrix} \boldsymbol{s}_3 \\ \boldsymbol{r} \times \boldsymbol{s}_3 + h\boldsymbol{s}_3 \end{pmatrix} = \begin{pmatrix} 0.600 & 0.500 & -0.800 & -0.500 & 1.210 & -0.400 \end{pmatrix}^{\mathrm{T}} \\
\boldsymbol{S}_4 &= \begin{pmatrix} \boldsymbol{s}_4 \\ \boldsymbol{s}_{40} \end{pmatrix} = \begin{pmatrix} \boldsymbol{s}_4 \\ \boldsymbol{r} \times \boldsymbol{s}_4 + h\boldsymbol{s}_4 \end{pmatrix} = \begin{pmatrix} 0.700 & -0.600 & -0.700 & 0.480 & 0.680 & -1.060 \end{pmatrix}^{\mathrm{T}}
\end{aligned}
\tag{4.36}
$$

With the above conditions, the projective transformation can be constructed and implemented to the bundle of screws. Hence, the coordinates of these screws in the coordinate system $\boldsymbol{S}'$ can be calculated as follows

$$
\begin{aligned}
\boldsymbol{S}_1' &= \boldsymbol{T}\,\boldsymbol{S}_1 = \begin{pmatrix} -0.730 & -0.100 & 1.110 & -0.270 & 1.300 & -0.110 \end{pmatrix}^{\mathrm{T}} \\
\boldsymbol{S}_2' &= \boldsymbol{T}\,\boldsymbol{S}_2 = \begin{pmatrix} 1.360 & -0.660 & -0.070 & -0.360 & -0.740 & 1.270 \end{pmatrix}^{\mathrm{T}} \\
\boldsymbol{S}_3' &= \boldsymbol{T}\,\boldsymbol{S}_3 = \begin{pmatrix} -0.200 & 1.460 & -0.800 & 1.400 & -0.460 & -0.800 \end{pmatrix}^{\mathrm{T}} \\
\boldsymbol{S}_4' &= \boldsymbol{T}\,\boldsymbol{S}_4 = \begin{pmatrix} 0.830 & 0.380 & -1.410 & 0.570 & -1.580 & 0.010 \end{pmatrix}^{\mathrm{T}}
\end{aligned}
\tag{4.37}
$$

where matrix $\boldsymbol{T}$ represents the projective transformation with the effect of changing the coordinate system of screws to achieve the normal form of the hyperquadric. It can be seen that after applying the projective transformation the equation of the hyperquadric is satisfied for $\boldsymbol{S}_1'$, $\boldsymbol{S}_2'$, $\boldsymbol{S}_3'$, and $\boldsymbol{S}_4'$, thus the corresponding projective points of these screws are all lying in the hyperquadric. Therefore, the effectiveness of the projective transformation constructed in this dissertation is verified.

This chapter claimed that a bundle of screws in $\mathbb{R}^3$ corresponds an α-plane in $\mathbb{P}^5$. This it to be verified if we can solve Equation (3.25) with the entries of matrix $\boldsymbol{B}$ as the unknowns and then confirm that matrix $\boldsymbol{B}$ is an orthogonal matrix as an element of $O(3)$ with $\det(\boldsymbol{B}) = +1$. Accordingly, choosing three screws arbitrarily, for instance, $\boldsymbol{S}_1'$, $\boldsymbol{S}_2'$, and $\boldsymbol{S}_4'$, substituting them into Equation (3.25)and rewriting it, the following system of linear equations is constructed as

$$\begin{bmatrix} \boldsymbol{s}_{10}' & \mathbf{0} & \mathbf{0} & \boldsymbol{s}_{20}' & \mathbf{0} & \mathbf{0} & \boldsymbol{s}_{40}' & \mathbf{0} & \mathbf{0} \\ \mathbf{0} & \boldsymbol{s}_{10}' & \mathbf{0} & \mathbf{0} & \boldsymbol{s}_{20}' & \mathbf{0} & \mathbf{0} & \boldsymbol{s}_{40}' & \mathbf{0} \\ \mathbf{0} & \mathbf{0} & \boldsymbol{s}_{10}' & \mathbf{0} & \mathbf{0} & \boldsymbol{s}_{20}' & \mathbf{0} & \mathbf{0} & \boldsymbol{s}_{40}' \end{bmatrix}^{\mathrm{T}} \begin{pmatrix} \boldsymbol{b}_1 \\ \boldsymbol{b}_2 \\ \boldsymbol{b}_3 \end{pmatrix} = \begin{pmatrix} \boldsymbol{s}_1' \\ \boldsymbol{s}_2' \\ \boldsymbol{s}_4' \end{pmatrix} \tag{4.38}$$

where vectors $\boldsymbol{s}_{i0}', \boldsymbol{s}_i'$ are the secondary parts and primary parts of $\boldsymbol{S}_1'$, $\boldsymbol{S}_2'$, and $\boldsymbol{S}_4'$ respectively, $\boldsymbol{b}_1, \boldsymbol{b}_2$ and $\boldsymbol{b}_3$ are three-dimensional vectors presenting the column spaces of matrix $\boldsymbol{B}$. Solving the system of linear equations, we immediately obtain the numerical form of matrix $\boldsymbol{B}$ as

$$\boldsymbol{B} = \begin{bmatrix} 0.209 & -0.444 & 0.871 \\ 0.978 & 0.111 & -0.178 \\ -0.018 & 0.889 & 0.458 \end{bmatrix} \tag{4.39}$$

Therefore, it can be verified that matrix $\boldsymbol{B}$ presenting the α-plane corresponding to the bundle of screws with the same pitch satisfies the following two conditions

$$\begin{aligned} \boldsymbol{B}^{\mathrm{T}}\boldsymbol{B} &= \boldsymbol{I} \\ \det(\boldsymbol{B}) &= +1 \end{aligned} \tag{4.40}$$

Obviously, matrix $\boldsymbol{B}$ belongs to $O(3)$ with the condition $\det(\boldsymbol{B}) = +1$. Thus it has been validated that the corresponding projective points of a bundle of screws with the same pitch constitutes an α-plane in $\mathbb{P}^5$, and the bundle of screws forms a three-system. The proposition on the linear dependence of a bundle of screws whose axes have a common point in $\mathbb{R}^3$ proposed in corollary 1 is thus verified.

Further, substituting the numerical form of matrix **B** into Equation (4.9), the skew-symmetric matrix of the position vector of the bundle of screws can be calculated as

$$[\boldsymbol{r}\times] = \begin{bmatrix} 0 & -0.800 & 0.500 \\ 0.800 & 0 & -0.600 \\ -0.500 & 0.600 & 0 \end{bmatrix} \tag{4.41}$$

This result is precisely coincident with Equation (4.35) thus the corollary 1 has been verified.

From this chapter, a cluster of parallel screws with the same pitch also corresponds to an α-plane in $\mathbb{P}^5$. In a similar way, corollary 2 regarding a cluster of parallel screws with the same pitch can be verified.

4.6.2 Constructing the Matrix for the β-Plane Through a Plane of Screws with the Same Pitch

In the second section of the example, to construct the matrix for the β-plane presented, a plane of screws with the same pitch is given with the direction vectors being designated as

$$\begin{aligned}
\boldsymbol{s}_1 &= \begin{pmatrix} -0.300 & 0.500 & -0.300 \end{pmatrix}^{\mathrm{T}} \\
\boldsymbol{s}_2 &= \begin{pmatrix} -0.700 & 0.200 & 0.460 \end{pmatrix}^{\mathrm{T}} \\
\boldsymbol{s}_3 &= \begin{pmatrix} 0.500 & -0.600 & 0.220 \end{pmatrix}^{\mathrm{T}} \\
\boldsymbol{s}_4 &= \begin{pmatrix} 0.800 & -0.500 & -0.200 \end{pmatrix}^{\mathrm{T}}
\end{aligned} \tag{4.42}$$

A position vector $\boldsymbol{r}_0$ to locate the plane π of the screws is given as follows

$$\boldsymbol{r}_0 = \begin{pmatrix} -0.500 & -0.600 & -0.500 \end{pmatrix}^{\mathrm{T}} \tag{4.43}$$

The direction vectors and the position vector satisfy the condition $\boldsymbol{s}_i \cdot \boldsymbol{r}_0 = 0$, which makes the screws lie in a series of parallel planes. Additionally, this position vector $\boldsymbol{r}_0$ is designated beforehand to make vector $\boldsymbol{r}$ in Equation (4.35) and vector $\boldsymbol{r}_0$ in the above equation satisfy the condition $\boldsymbol{r} \cdot \boldsymbol{r}_0 = -1$ given. All the points in $\mathbb{R}^3$ identified by a position vector whose dot product with position vector $\boldsymbol{r}_0$ equals -1 are lying in a certain plane. Thus the condition $\boldsymbol{r} \cdot \boldsymbol{r}_0 = -1$ is to locate point $\boldsymbol{r}$ given by Equation (4.35) in the plane π in Figure 3.2 and four position vectors are chosen to locate the screws in the plane π as follows

$$\begin{aligned}
\boldsymbol{r}_1' &= \begin{pmatrix} 0.400 & 1.000 & 0.400 \end{pmatrix}^{\mathrm{T}} \\
\boldsymbol{r}_2' &= \begin{pmatrix} 0.400 & 0.500 & 1.000 \end{pmatrix}^{\mathrm{T}} \\
\boldsymbol{r}_3' &= \begin{pmatrix} 1.000 & 0.000 & 1.000 \end{pmatrix}^{\mathrm{T}} \\
\boldsymbol{r}_4' &= \begin{pmatrix} 1.000 & 0.000 & 1.000 \end{pmatrix}^{\mathrm{T}}
\end{aligned} \tag{4.44}$$

and the direction vectors of the screws can be arbitrarily chosen as

$$\begin{aligned}
\boldsymbol{s}_1 &= \begin{pmatrix} -0.300 & 0.500 & -0.300 \end{pmatrix}^{\mathrm{T}} \\
\boldsymbol{s}_2 &= \begin{pmatrix} -0.700 & 0.200 & 0.460 \end{pmatrix}^{\mathrm{T}} \\
\boldsymbol{s}_3 &= \begin{pmatrix} 0.500 & -0.600 & 0.220 \end{pmatrix}^{\mathrm{T}} \\
\boldsymbol{s}_4 &= \begin{pmatrix} 0.800 & -0.500 & -0.200 \end{pmatrix}^{\mathrm{T}}
\end{aligned} \tag{4.45}$$

The pitch of the screws is also given as $h = 0.500$.

From the above known conditions, the 6-dimensional homogenous coordinates of the plane of screws can be obtained. Then the coordinates of these screws in the coordinate system $\boldsymbol{S}'$ can be calculated by implementing the projective transformation. After constructing a system of linear equations for the plane of screws, the numerical matrix for the corresponding β-plane can be calculated and it has

$$\boldsymbol{B} = \begin{bmatrix} -0.344 & -0.860 & 0.376 \\ 0.215 & -0.462 & -0.860 \\ -0.914 & 0.215 & -0.344 \end{bmatrix} \tag{4.46}$$

Thus, it can be verified that matrix $\boldsymbol{B}$ presenting the β-plane corresponding to the plane of screws with the same pitch satisfies the following two conditions

$$\begin{aligned}
\boldsymbol{B}^{\mathrm{T}}\boldsymbol{B} &= \boldsymbol{I} \\
\det(\boldsymbol{B}) &= -1
\end{aligned} \tag{4.47}$$

It can be seen that matrix $\boldsymbol{B}$ belongs to $O(3)$ with the condition $\det(\boldsymbol{B}) = -1$. Thus, it has been validated that the corresponding projective points of the plane of screws with the same pitch constitutes an β-plane in $\mathbb{P}^5$. Then the plane of screws forms a three-system. The proposition proposed in corollary 2 on the linear dependence of a plane of screws whose axes lie in a common plane in $\mathbb{R}^3$ is thus verified.

Substituting the numerical form of matrix $\boldsymbol{B}$ into Equation (4.9), the skew-symmetric matrix of the position vector locating the plane π can be calculated as

$$[\boldsymbol{r}_0 \times] = \begin{bmatrix} 0 & -0.500 & 0.600 \\ -0.500 & 0 & -0.500 \\ 0.600 & -0.500 & 0 \end{bmatrix} \tag{4.48}$$

This result is coincident with Equation (4.43), hence the corollary 2 has been sufficiently verified.

4.6.3 Constructing Partitioned Matrix for the Intersection of the α-Plane and the β-Plane

In the third section of the example, a planar pencil of screws is given to verify corollary 4 in this chapter. The planar pencil of screws in $\mathbb{R}^3$ can be regarded as the intersection of the bundle of screws with the plane of screws. Hence, the direction vectors that lie in a series of parallel plane can be chosen as the direction vectors of the planar pencil of screws and the position vector in Equation (4.35) can be chosen as the position

vectors of the planar pencil of screws. Calculating the 6-dimensional homogenous coordinates, then applying the projective transformation, the coordinates of the planar pencil of screws in the coordinate system $\boldsymbol{S}'$ can be obtained as follows

$$\begin{aligned}
\boldsymbol{S}_1' &= \begin{pmatrix} -0.850 & 0.440 & 0.150 & 0.250 & 0.560 & -0.750 \end{pmatrix}^{\mathrm{T}} \\
\boldsymbol{S}_2' &= \begin{pmatrix} -0.630 & -0.636 & 0.930 & -0.770 & 1.036 & -0.010 \end{pmatrix}^{\mathrm{T}} \\
\boldsymbol{S}_3' &= \begin{pmatrix} 1.090 & -0.332 & -0.390 & -0.090 & -0.868 & 0.830 \end{pmatrix}^{\mathrm{T}} \\
\boldsymbol{S}_4' &= \begin{pmatrix} 1.100 & 0.260 & -0.900 & 0.500 & -1.260 & 0.500 \end{pmatrix}^{\mathrm{T}}
\end{aligned} \tag{4.49}$$

In $\mathbb{P}^5$, two projective points identify a projective line. Otherwise, it is known two projective points of the corresponding screws provide 8 effective constraints for the projective plane. Consequently, the projective line of the planar pencil of screws can be presented in the form of a system of linear equations with 8 unknowns as

$$\begin{bmatrix} 1 & 0 & 0 & 0 & e_1 & f_1 \\ 0 & 1 & 0 & 0 & e_2 & f_2 \\ 0 & 0 & 1 & 0 & e_3 & f_3 \\ 0 & 0 & 0 & 1 & e_4 & f_4 \end{bmatrix} \begin{pmatrix} x_1 \\ x_2 \\ x_3 \\ \hdashline y_1 \\ y_2 \\ y_3 \end{pmatrix} = \mathbf{0} \tag{4.50}$$

Taking any two screws in Equation (4.49) and constructing a system of linear equations as follows

$$\begin{bmatrix} s'_{15} & \mathbf{0} & \mathbf{0} & \mathbf{0} & s'_{25} & \mathbf{0} & \mathbf{0} & \mathbf{0} \\ s'_{16} & s'_{15} & \mathbf{0} & \mathbf{0} & s'_{26} & s'_{25} & \mathbf{0} & \mathbf{0} \\ \mathbf{0} & s'_{16} & s'_{15} & \mathbf{0} & \mathbf{0} & s'_{26} & s'_{25} & \mathbf{0} \\ \mathbf{0} & \mathbf{0} & s'_{16} & s'_{15} & \mathbf{0} & \mathbf{0} & s'_{26} & s'_{25} \\ \mathbf{0} & \mathbf{0} & \mathbf{0} & s'_{16} & \mathbf{0} & \mathbf{0} & \mathbf{0} & s'_{26} \end{bmatrix}^{\mathrm{T}} \begin{pmatrix} \boldsymbol{g}_1 \\ \boldsymbol{g}_2 \\ \boldsymbol{g}_3 \\ \boldsymbol{g}_3 \end{pmatrix} = \begin{pmatrix} \boldsymbol{s}'_{11} \\ s'_{14} \\ \boldsymbol{s}'_{21} \\ s'_{24} \end{pmatrix} \tag{4.51}$$

where the italic symbol s'_{ij} represents the jth component of screw $\boldsymbol{s}'_i$ in Equation (4.49), the italic and bold symbol $\boldsymbol{s}'_{ij}$ represents the primary part or secondary part of screw $\boldsymbol{s}'_i$ when j equals 1 or 2, and $\boldsymbol{g}_i$, $\mathbf{0}$ are 2-dimensional vectors and represent $(e_i, f_i)^{\mathrm{T}}$ and $(0, 0)^{\mathrm{T}}$ respectively. Solving this 8 × 8 linear equations, a unique solution is obtained and thus the coefficient matrix can be written as

$$\boldsymbol{B} = \begin{bmatrix} 1 & 0 & 0 & 0 & 0.602 & -0.684 \\ 0 & 1 & 0 & 0 & 0.624 & 1.053 \\ 0 & 0 & 1 & 0 & -0.902 & -0.474 \\ 0 & 0 & 0 & 1 & 0.752 & 0.895 \end{bmatrix} \tag{4.52}$$

This is the matrix representation of the corresponding projective line of the planar pencil of screws with the same pitch. Substituting $\boldsymbol{s}'_3$, $\boldsymbol{s}'_4$, and the linear combinations $\boldsymbol{s}'_3$, $\boldsymbol{s}'_4$ into Equation (4.50) with the above matrix $\boldsymbol{B}$ as the coefficient matrix, the equation always keeps balance. This indicates that all the projective points corresponding to a planar pencil of screws with the same pitch lie on a projective line. These screws constitute a two-system and three or more screws with the same pitch, crossing a common point and lying on a common plane are linearly dependent; otherwise, less than three screws of this geometrical property are linearly independent. Consequently, corollary 4 is verified. In a similar way, corollary 5 regarding a cluster of screws with the same pitch whose axes are parallel and coplanar can be verified.

4.7 Conclusions

In this chapter, conventional three-systems were rediscovered by corresponding the generators of hyperquadrics in 5-dimensional projective space to screws in 3-space. Intersection of α-planes and β-planes of screws with non-zero constant pitch were derived for the first time and thus two-systems were rediscovered. Researchers relate planes in the Klein quadric in the 5-dimensional projective space to screw systems in 3-space, while this chapter for the first time extended it to a general case that any hyperquadrics in 5-dimensional space corresponding to the screws with the same pitch can be related back to 3-space.

The equations and results in this chapter and chapter 3 have the potential to be used in mobility calculation and screw-system variations by researchers in mechanisms-theory community, and lay foundation for chapter 5 of constraint system construction based on screw theory, for chapter 7 of equivalence of screw systems generating the same computational submanifolds, and for Chapter 9 of Jacobian matrix derivation of a hybrid mechanism using screw theory.

Chapter 5 Screw-Based Jacobian of a Parallel Mechanism with a Reconfigurable Base

5.1 Introduction

Conventionally, parallel mechanisms contain a fixed base and a moving platform with several identical limbs. To enhance the mobility and dexterity, more actuations are introduced to the limbs. Apart of this method, the rigid moving platform can be changed into a reconfigurable structure to improve its performance. This chapter introduces a parallel mechanism with a reconfigurable base which is inspired by object in-hand manipulation with a metamorphic robotic hand [84-89]. This flexible base utilizes a spherical mechanism structure contributing to a larger workspace of the parallel mechanism compared with conventional rigid-base parallel manipulators [85]. The proposed parallel mechanism is presented with the theory of metamorphosis and its geometric constraint is explored based on the approach of screw algebra. The Jacobian

matrix of the mechanism [90-95] is developed based on screw theory with the velocity analysis of the mechanism derived.

5.2 A Novel Parallel Mechanism Design with a Spherical Base

5.2.1 Parallel Mechanism with a Reconfigurable Base Generated through Manipulation of a Metamorphic Hand

Figure 5.1 shows a metamorphic robotic hand grasps and manipulates an object. The metamorphic hand has a reconfigurable palm with three identical two-phalanx fingers attached. The reconfigurable palm is composed of a spherical linkage with link AE as a fixed link. The other four links are symmetrically distributed to link AE, in particular, links AB and ED, links BC and DC are of the same length, respectively. The three fingers are assembled individually on link AE at point A_1, link DC at point A_2 and link BC at point A_3. The points A_1, A_2 and A_3 are evenly arranged about the centre of the spherical linkage, denoted as O, in the configuration with all the links in the same plane, the reconfigurable palm with two active DoFs varies configuration of the robotic hand in such a way to increase the workspace, dexterity and manipulability [85][90][96-101]. The method to map the multi-fingered hand grasping an object to a parallel mechanism was introduced by Borras-Sol and Dollar [102,103]. The robotic hand grasps and manipulates an object shown in Figure 5.1, where contact points between the object and the fingertips can be treated as spherical joints, leading to an equivalent reconfigurable base integrated parallel mechanism generated in Figure 5.2.

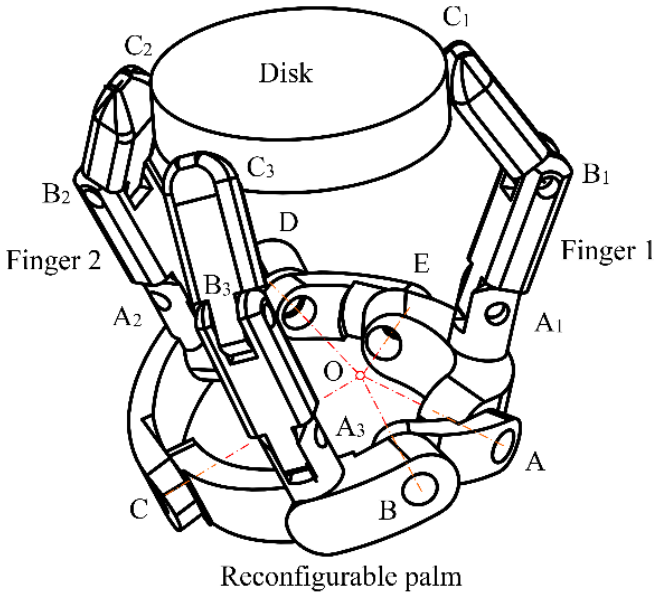

Figure 5.1 A three-fingered Metamorphic hand manipulates by on object

5.2.2 Structure of the Spherical-Base Integrated Parallel Mechanism

As illustrated in Figure 5.2, the spherical-base integrated parallel mechanism consists of a spherical non-rigid base, a moving platform and three RRS chains. The reconfigurable base is composed of five linkages connecting to each other to form a spherical five-bar linkage mechanism. In this presented design, link AE is fixed as the grounded link and joints A and E are the active joints to drive the palm to various configurations, while joints B, C and D are passive joints. The axes of these five joints intersect at the mechanism centre O. The angles of links AB, BC, CD, DE and EA are denoted by φ_1 to φ_5 respectively, and their sum satisfies $\varphi_1 + \varphi_2 + \varphi_3 + \varphi_4 + \varphi_5 = 2\pi$. Three identical limbs are mounted at point A_i (i = 1, 2 and 3), and the angles between OA_1 and OA, OB and OA_2, OA_3 and OD are denoted by δ_1, δ_2 and δ_3 respectively. The

angle between any two limbs is 120° when all the five links of the reconfigurable base are coplanar. However, the initial configuration of the mechanism is a singular state which is suitable for a theoretical representation rather than a practical starting configuration. Each limb is composed of two linkages linked by a revolute joint B_i (i = 1, 2 and 3). The three identical limbs are connected to the reconfigurable base by revolute joints A_i (i = 1, 2 and 3) on one end and the moving platform by spherical joints C_i (i = 1, 2 and 3) on the other end. The length of link A_iB_i is described by l_{i1}, while that of link B_iC_i as l_{i2} (i = 1, 2 and 3).

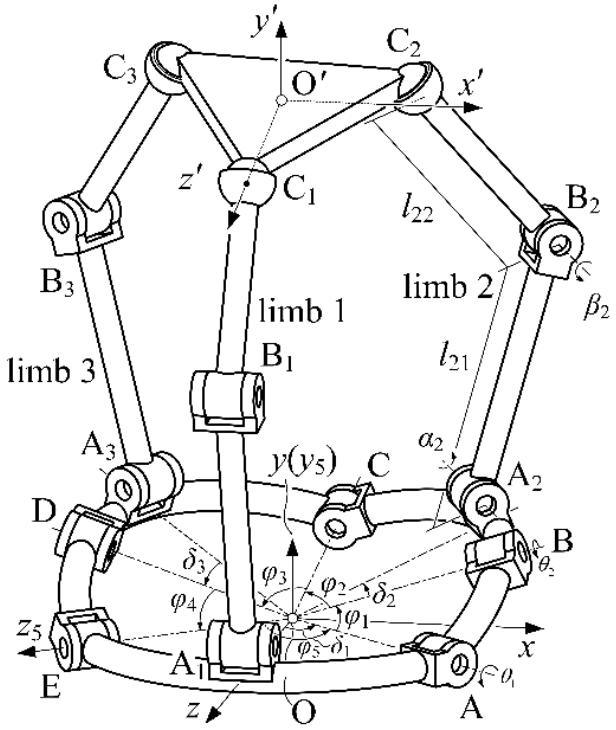

Figure 5.2 Structure of the reconfigurable-base integrated parallel mechanism

5.3 Jacobian Analysis based on Screw Theory

As stated in the former sections, since the parallel mechanism has three limbs fixed on a reconfigurable base, the kinematics decomposition method of the mechanism can be adopted to analysing the Jacobian matrix of the whole mechanism with the Jacobian analysis of the reconfigurable first presented, then followed by that of the full parallel mechanism.

5.3.1 Jacobian Derivation of the Reconfigurable Base

The velocity of point C is derived as a linear combination of angular velocity about axis OA and OB on one side, or the other side with angular velocity of axis OE and OD,

$$\boldsymbol{v}_{\mathrm{C}} = \dot{\theta}_1(\boldsymbol{P}_{\mathrm{A}} \times \boldsymbol{P}_{\mathrm{C}}) + \dot{\theta}_2(\boldsymbol{P}_{\mathrm{B}} \times \boldsymbol{P}_{\mathrm{C}}) \tag{5.1}$$

$$\boldsymbol{v}_{\mathrm{C}} = \dot{\theta}_5(\boldsymbol{P}_{\mathrm{E}} \times \boldsymbol{P}_{\mathrm{C}}) + \dot{\theta}_4(\boldsymbol{P}_{\mathrm{D}} \times \boldsymbol{P}_{\mathrm{C}}) \tag{5.2}$$

Since $\boldsymbol{v}_{\mathrm{C}}$ is an intermediate variable in the above calculation, it can be estimated from Equations (5.1) and (5.2). To take right inner product on both sides of the above equations with $\boldsymbol{P}_{\mathrm{D}}$, they have

$$\boldsymbol{P}_{\mathrm{D}} \cdot \boldsymbol{v}_{\mathrm{C}} = \dot{\theta}_1 \boldsymbol{P}_{\mathrm{D}} \cdot (\boldsymbol{P}_{\mathrm{A}} \times \boldsymbol{P}_{\mathrm{C}}) + \dot{\theta}_2 \boldsymbol{P}_{\mathrm{D}} \cdot (\boldsymbol{P}_{\mathrm{B}} \times \boldsymbol{P}_{\mathrm{C}}) \tag{5.3}$$

$$\boldsymbol{P}_{\mathrm{D}} \cdot \boldsymbol{v}_{\mathrm{C}} = \dot{\theta}_5 \boldsymbol{P}_{\mathrm{D}} \cdot (\boldsymbol{P}_{\mathrm{E}} \times \boldsymbol{P}_{\mathrm{C}}) \tag{5.4}$$

Substituting Equation (5.4) into Equation (5.3) yields,

$$\dot{\theta}_2 = -\frac{\boldsymbol{P}_{\mathrm{D}} \cdot (\boldsymbol{P}_{\mathrm{A}} \times \boldsymbol{P}_{\mathrm{C}})}{\boldsymbol{P}_{\mathrm{D}} \cdot (\boldsymbol{P}_{\mathrm{B}} \times \boldsymbol{P}_{\mathrm{C}})} \dot{\theta}_1 + \frac{\boldsymbol{P}_{\mathrm{D}} \cdot (\boldsymbol{P}_{\mathrm{E}} \times \boldsymbol{P}_{\mathrm{C}})}{\boldsymbol{P}_{\mathrm{D}} \cdot (\boldsymbol{P}_{\mathrm{B}} \times \boldsymbol{P}_{\mathrm{C}})} \dot{\theta}_5 \tag{5.5}$$

Similarly, the angular velocity $\dot{\theta}_4$ is obtained and expressed as,

$$\dot{\theta}_4 = \frac{\boldsymbol{P}_{\mathrm{B}} \cdot (\boldsymbol{P}_{\mathrm{A}} \times \boldsymbol{P}_{\mathrm{C}})}{\boldsymbol{P}_{\mathrm{B}} \cdot (\boldsymbol{P}_{\mathrm{D}} \times \boldsymbol{P}_{\mathrm{C}})} \dot{\theta}_1 - \frac{\boldsymbol{P}_{\mathrm{B}} \cdot (\boldsymbol{P}_{\mathrm{E}} \times \boldsymbol{P}_{\mathrm{C}})}{\boldsymbol{P}_{\mathrm{B}} \cdot (\boldsymbol{P}_{\mathrm{D}} \times \boldsymbol{P}_{\mathrm{C}})} \dot{\theta}_5 \tag{5.6}$$

Thus, the above two equations are expressed in matrix form as,

$$\begin{bmatrix} \dot{\theta}_2 \\ \dot{\theta}_4 \end{bmatrix} = \boldsymbol{J}_{\varphi} \begin{bmatrix} \dot{\theta}_1 \\ \dot{\theta}_5 \end{bmatrix} = \begin{bmatrix} -\dfrac{\boldsymbol{P}_{\mathrm{D}} \cdot (\boldsymbol{P}_{\mathrm{A}} \times \boldsymbol{P}_{\mathrm{C}})}{\boldsymbol{P}_{\mathrm{D}} \cdot (\boldsymbol{P}_{\mathrm{B}} \times \boldsymbol{P}_{\mathrm{C}})} & \dfrac{\boldsymbol{P}_{\mathrm{D}} \cdot (\boldsymbol{P}_{\mathrm{E}} \times \boldsymbol{P}_{\mathrm{C}})}{\boldsymbol{P}_{\mathrm{D}} \cdot (\boldsymbol{P}_{\mathrm{B}} \times \boldsymbol{P}_{\mathrm{C}})} \\ \dfrac{\boldsymbol{P}_{\mathrm{B}} \cdot (\boldsymbol{P}_{\mathrm{A}} \times \boldsymbol{P}_{\mathrm{C}})}{\boldsymbol{P}_{\mathrm{B}} \cdot (\boldsymbol{P}_{\mathrm{D}} \times \boldsymbol{P}_{\mathrm{C}})} & -\dfrac{\boldsymbol{P}_{\mathrm{B}} \cdot (\boldsymbol{P}_{\mathrm{E}} \times \boldsymbol{P}_{\mathrm{C}})}{\boldsymbol{P}_{\mathrm{B}} \cdot (\boldsymbol{P}_{\mathrm{D}} \times \boldsymbol{P}_{\mathrm{C}})} \end{bmatrix} \begin{bmatrix} \dot{\theta}_1 \\ \dot{\theta}_5 \end{bmatrix} \tag{5.7}$$

The angular velocity of passive joints B and D is derived through rotation rate of active joints A and E in light of the geometric constraints of the reconfigurable mechanism.

5.3.2 Jacobian Analysis for the Spherical-Base Integrated Parallel Mechanism Based on Screw theory

In this section, the screw theory is introduced to analyse the velocity of the spherical-base integrated parallel mechanism. A screw $\boldsymbol{S}$ is a six-dimensional vector to represent instantaneous velocity of a rigid body, which is expressed as,

$$\boldsymbol{S} = \begin{bmatrix} \boldsymbol{s} \\ \boldsymbol{s}_0 \end{bmatrix} = \begin{bmatrix} \boldsymbol{s} \\ \boldsymbol{r} \times \boldsymbol{s} + h\boldsymbol{s} \end{bmatrix} = \begin{bmatrix} s_x, s_y, s_z, s_{x0}, s_{y0}, s_{z0} \end{bmatrix}^{\mathrm{T}} \tag{5.8}$$

The first three components make up a unit vector $\boldsymbol{s}$ directing along the screw axis, describing a rotation of a joint axis. The last elements constitute $\boldsymbol{s}_0$ introducing the moment of the vector $\boldsymbol{s}$ about the origin of the reference frame. h expresses the screw pitch, which is equal to 0 for revolute joints and ∞ for prismatic joints. $\boldsymbol{r}$ is the position vector from the origin of the reference coordinate system directing to an arbitrary point on the screw axis $\boldsymbol{s}$.

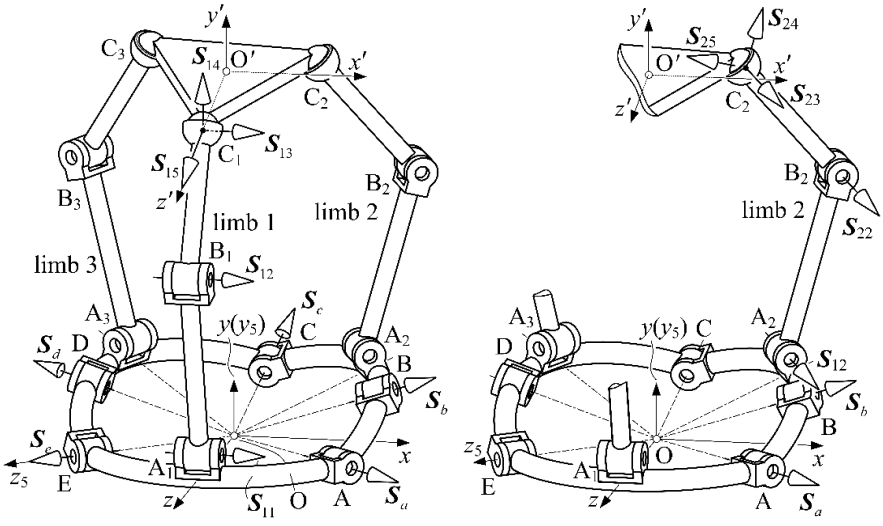

(a) (b)

Figure 5.3 Motion screw of the reconfigurable-base integrated parallel mechanism

The full Jacobian of the mechanism can be calculated from the twist of the mechanism based on screw algebra. Figure 5.3(a) shows motion screws of the spherical-base integrated parallel mechanism. We can treat each limb as an open-loop chain connecting the end-effector to the base shown in Figure 5.3(b). The instantaneous motion of the moving platform, denoted as $\boldsymbol{S_p}$ can be derived from the linear combination of the twist of each joint within this loop. Referring to Figure 5.3(a), twist $\boldsymbol{S_p}$ is obtained in terms of limb 1, 2 and 3 separately as

$$\boldsymbol{S}_p = \sum_{i=1}^{5} \dot{\theta}_{1i} \boldsymbol{S}_{1i} \tag{5.9}$$

$$\boldsymbol{S}_p = \dot{\theta}_1 \boldsymbol{S}_a + \dot{\theta}_2 \boldsymbol{S}_b + \sum_{i=1}^{5} \dot{\theta}_{2i} \boldsymbol{S}_{2i} \tag{5.10}$$

$$\boldsymbol{S}_p = \dot{\theta}_4 \boldsymbol{S}_d + \dot{\theta}_5 \boldsymbol{S}_e + \sum_{i=1}^{5} \dot{\theta}_{3i} \boldsymbol{S}_{3i} \tag{5.11}$$

Substituting Equations (5.5) and (5.6) into Equations. (5.10) and (5.11) respectively leads to,

$$\boldsymbol{S}_p = \dot{\theta}_1 \left(\boldsymbol{S}_a - m_1 \boldsymbol{S}_b \right) + m_2 \dot{\theta}_5 \boldsymbol{S}_b + \sum_{i=1}^{5} \dot{\theta}_{2i} \boldsymbol{S}_{2i} \tag{5.12}$$

$$\boldsymbol{S}_p = m_3 \dot{\theta}_1 \boldsymbol{S}_d + \dot{\theta}_5 \left(\boldsymbol{S}_e - m_4 \boldsymbol{S}_d \right) + \sum_{i=1}^{5} \dot{\theta}_{2i} \boldsymbol{S}_{2i} \tag{5.13}$$

where $m_1 = \dfrac{\boldsymbol{P}_{\mathrm{D}} \cdot (\boldsymbol{P}_{\mathrm{A}} \times \boldsymbol{P}_{\mathrm{C}})}{\boldsymbol{P}_{\mathrm{D}} \cdot (\boldsymbol{P}_{\mathrm{B}} \times \boldsymbol{P}_{\mathrm{C}})}$, $m_2 = \dfrac{\boldsymbol{P}_{\mathrm{D}} \cdot (\boldsymbol{P}_{\mathrm{E}} \times \boldsymbol{P}_{\mathrm{C}})}{\boldsymbol{P}_{\mathrm{D}} \cdot (\boldsymbol{P}_{\mathrm{B}} \times \boldsymbol{P}_{\mathrm{C}})}$, $m_3 = \dfrac{\boldsymbol{P}_{\mathrm{B}} \cdot (\boldsymbol{P}_{\mathrm{A}} \times \boldsymbol{P}_{\mathrm{C}})}{\boldsymbol{P}_{\mathrm{B}} \cdot (\boldsymbol{P}_{\mathrm{D}} \times \boldsymbol{P}_{\mathrm{C}})}$ and $m_4 = \dfrac{\boldsymbol{P}_{\mathrm{B}} \cdot (\boldsymbol{P}_{\mathrm{E}} \times \boldsymbol{P}_{\mathrm{C}})}{\boldsymbol{P}_{\mathrm{B}} \cdot (\boldsymbol{P}_{\mathrm{D}} \times \boldsymbol{P}_{\mathrm{C}})}$.

According to [85], we understand that the revolute-spherical screws dyad locate in a four-dimensional vector space. So, its reciprocal screws form a two-system with zero pitch, denoted as $\boldsymbol{S}_{i1}^{r}$ and $\boldsymbol{S}_{i2}^{r}$ (i = 1, 2 and 3) of the ith limb. Taking the reciprocal product of both sides of Equations (5.9), (5.11) and (5.12) with reciprocal screw $\boldsymbol{S}_{i1}^{r}$ and $\boldsymbol{S}_{i2}^{r}$ leads to six linear equations, which is expressed in the matrix form as,

$$\mathbf{J}_q^{\mathrm{T}} \Delta \boldsymbol{S}_p = \mathbf{J}_\theta \dot{\boldsymbol{\theta}}_a \tag{5.14}$$

where $\dot{\boldsymbol{\theta}}_a = \left[\dot{\theta}_1 , \dot{\theta}_5 , \dot{\theta}_{11} , \dot{\theta}_{21} , \dot{\theta}_{31}\right]^{\mathrm{T}}$ $\mathbf{J}_q^{\mathrm{T}} = \begin{bmatrix} \boldsymbol{S}_{11}^{r\,\mathrm{T}} \\ \boldsymbol{S}_{12}^{r\,\mathrm{T}} \\ \vdots \\ \boldsymbol{S}_{32}^{r\,\mathrm{T}} \end{bmatrix}$, $\mathbf{J}_\theta = \begin{bmatrix} \mathbf{J}_{\theta 1} \\ \mathbf{J}_{\theta 2} \\ \mathbf{J}_{\theta 3} \end{bmatrix}$ and Δ denotes the reciprocal operator expressed as $\Delta = \begin{bmatrix} \mathbf{0} & \mathbf{I} \\ \mathbf{I} & \mathbf{0} \end{bmatrix}$.

The term $\mathbf{J}_{\theta i}$ is detailed presented in Appendix B, and $\mathbf{J}_q^{\mathrm{T}}$, is a 6×6 nonsingular matrix in most cases. Multiplying both sides of Equation (5.14) by the inverse of $\mathbf{J}_q^{\mathrm{T}}$ results in the twist of the moving platform as,

$$\Delta \boldsymbol{S}_p = \left[\mathbf{J}_q^{\mathrm{T}}\right]^{-1} \mathbf{J}_\theta \dot{\boldsymbol{\theta}}_a \tag{5.15}$$

where $\Delta \boldsymbol{S}_p$ is the twist of the moving platform by interchanging the primary part and secondary part of $\boldsymbol{S}_p$. The left-hand side and right-hand side of Equation (5.14) represented the power of the platform and the active joints respectively, which give clues to the dynamic analysis of the proposed parallel mechanism with concept of kinetic energy.

5.3.3 Velocity Analysis of the reconfigurable-base Integrated Parallel Mechanism

To analysis the properties of the proposed reconfigurable-base integrated parallel mechanism, its construction can be treated as three single-loop mechanisms between any two of three limbs and a spare geometric constraint of the five-bar reconfigurable base. The instantaneous twist represents the motion of each link, and all the links' motion in a closed-loop form a linear combination of all the instantaneous twists within this loop. Using twist $\boldsymbol{S}_{ij}$ denotes the instantaneous motion along the *j*th joint in the *i*th limb and twist $\boldsymbol{S}_a, \boldsymbol{S}_b, \boldsymbol{S}_c, \boldsymbol{S}_d$ and $\boldsymbol{S}_e$ denote that along the joints of the reconfigurable base. Denote the rotation rate $\dot{\theta}_{ij}$ and $\dot{\theta}_k$ as the velocity of the *j*th joint in the *i*th limb and the velocity of the *k*th joint in the reconfigurable base. Twists of three closed-loop-mechanisms are expressed separately based on the introduced notations above, as follows,

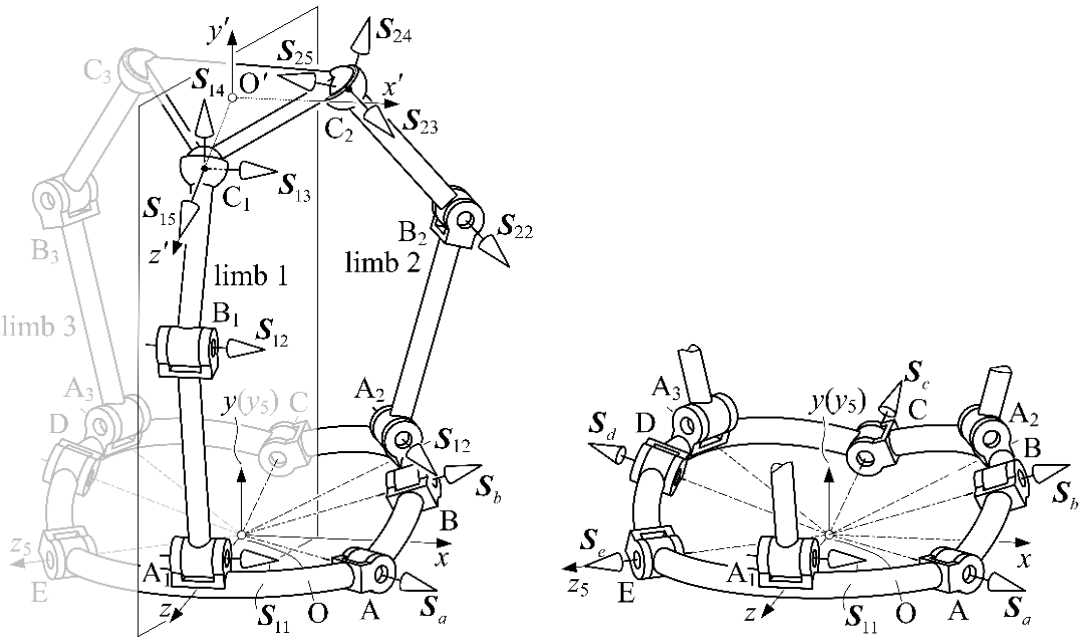

(a) (b)

Figure 5.4 Motion screw of closed-loop mechanism of the parallel mechanism

For the closed-loop composed of limb 1 and 2, shown in Fig. 5.4(a), the closed-loop-twist equation is expressed as,

$$\dot{\theta}_1 \boldsymbol{S}_a + \dot{\theta}_2 \boldsymbol{S}_b + \sum_{i=1}^{5} \dot{\theta}_{1i} \boldsymbol{S}_{1i} - \sum_{i=1}^{5} \dot{\theta}_{2i} \boldsymbol{S}_{2i} = \boldsymbol{0} \tag{5.16}$$

For limbs 2 and 3, the closed-loop-twist is,

$$\dot{\theta}_3 \boldsymbol{S}_c + \sum_{i=1}^{5} \dot{\theta}_{2i} \boldsymbol{S}_{2i} - \sum_{i=1}^{5} \dot{\theta}_{3i} \boldsymbol{S}_{3i} = \boldsymbol{0} \tag{5.17}$$

And for limbs 3 and 1, the closed-loop-twist is,

$$\dot{\theta}_4 \boldsymbol{S}_d + \dot{\theta}_5 \boldsymbol{S}_e + \sum_{i=1}^{5} \dot{\theta}_{3i} \boldsymbol{S}_{3i} - \sum_{i=1}^{5} \dot{\theta}_{1i} \boldsymbol{S}_{1i} = \boldsymbol{0} \tag{5.18}$$

Further, the closed-loop-twist of the reconfigurable base through its geometric constraint, shown in Fig. 5.4(b) is

$$\dot{\theta}_1 \boldsymbol{S}_a + \dot{\theta}_2 \boldsymbol{S}_b + \dot{\theta}_3 \boldsymbol{S}_c + \dot{\theta}_4 \boldsymbol{S}_d + \dot{\theta}_5 \boldsymbol{S}_e = \mathbf{0} \tag{5.19}$$

In each closed-loop-mechanism, the active joints can be separated from the rest passive joints in the twist equations given in Eqs. (7.67) throughout (7.70) as,

$$\dot{\theta}_1 \boldsymbol{S}_a + \dot{\theta}_{11} \boldsymbol{S}_{11} - \dot{\theta}_{21} \boldsymbol{S}_{21} = -\dot{\theta}_2 \boldsymbol{S}_b - \sum_{i=2}^{5} \dot{\theta}_{1i} \boldsymbol{S}_{1i} + \sum_{i=2}^{5} \dot{\theta}_{2i} \boldsymbol{S}_{2i} \tag{5.20}$$

$$\dot{\theta}_{21} \boldsymbol{S}_{21} - \dot{\theta}_{31} \boldsymbol{S}_{31} = -\dot{\theta}_3 \boldsymbol{S}_c - \sum_{i=2}^{5} \dot{\theta}_{2i} \boldsymbol{S}_{2i} + \sum_{i=2}^{5} \dot{\theta}_{3i} \boldsymbol{S}_{3i} \tag{5.21}$$

$$\dot{\theta}_5 \boldsymbol{S}_e + \dot{\theta}_{31} \boldsymbol{S}_{31} - \dot{\theta}_{11} \boldsymbol{S}_{11} = -\dot{\theta}_4 \boldsymbol{S}_d - \sum_{i=2}^{5} \dot{\theta}_{3i} \boldsymbol{S}_{3i} + \sum_{i=2}^{5} \dot{\theta}_{1i} \boldsymbol{S}_{1i} \tag{5.22}$$

$$\dot{\theta}_1 \boldsymbol{S}_a + \dot{\theta}_5 \boldsymbol{S}_e = -\dot{\theta}_2 \boldsymbol{S}_b - \dot{\theta}_3 \boldsymbol{S}_c - \dot{\theta}_4 \boldsymbol{S}_d \tag{5.23}$$

The Eqs. (5.16) to (5.19) can be rearranged in a matrix form that gives the relationship between velocity of the active joints and that passive joints as,

$$\mathbf{J}_a \dot{\boldsymbol{\theta}}_a = \mathbf{J}_p \dot{\boldsymbol{\theta}}_p \tag{5.24}$$

where $\dot{\boldsymbol{\theta}}_a$ and $\dot{\boldsymbol{\theta}}_p$ depict the velocity vectors of active joints and passive joints as,

$\dot{\boldsymbol{\theta}}_P = \left[\dot{\theta}_2 , \dot{\theta}_3 , \dot{\theta}_4 , \dot{\theta}_{12} , \dot{\theta}_{13} , \dot{\theta}_{14} , \dot{\theta}_{15} , \ \ldots \ , \dot{\theta}_{35} \right]^{\mathrm{T}}$, $\mathbf{J}_a$ and $\mathbf{J}_p$ dipict the active-Jacobian matrix and passive-Jacobian matrix respectively as

$$\mathbf{J}_a = \left[\begin{array}{ccc:ccc} \boldsymbol{S}_1 & \boldsymbol{0} & \boldsymbol{S}_{11} & -\boldsymbol{S}_{21} & \boldsymbol{0} \\ \boldsymbol{0} & \boldsymbol{0} & \boldsymbol{0} & \boldsymbol{S}_{21} & -\boldsymbol{S}_{31} \\ \boldsymbol{0} & \boldsymbol{S}_5 & -\boldsymbol{S}_{11} & \boldsymbol{0} & \boldsymbol{S}_{31} \\ \boldsymbol{S}_1 & \boldsymbol{S}_5 & \boldsymbol{0} & \boldsymbol{0} & \boldsymbol{0} \end{array}\right] \text{ and } \mathbf{J}_p = \left[\begin{array}{ccc:ccc} -\boldsymbol{S}_2 & \boldsymbol{0} & \boldsymbol{0} & -\mathbf{J}_{p1} & \mathbf{J}_{p2} & \boldsymbol{0} \\ \boldsymbol{0} & -\boldsymbol{S}_3 & \boldsymbol{0} & \boldsymbol{0} & -\mathbf{J}_{p2} & \mathbf{J}_{p3} \\ \boldsymbol{0} & \boldsymbol{0} & -\boldsymbol{S}_4 & \mathbf{J}_{p1} & \boldsymbol{0} & -\mathbf{J}_{p3} \\ -\boldsymbol{S}_2 & -\boldsymbol{S}_3 & -\boldsymbol{S}_4 & \boldsymbol{0} & \boldsymbol{0} & \boldsymbol{0} \end{array}\right]$$

where $\mathbf{J}_{pi} = \left[\boldsymbol{S}_{i2} \quad \boldsymbol{S}_{i3} \quad \boldsymbol{S}_{i4} \quad \boldsymbol{S}_{i5} \right], i = 1, 2 \text{ and } 3.$

The above derived Jacobian matrices are crucial for the singularity and dexterity analysis of the proposed integrated parallel mechanism.

5.4 Conclusions

In this chapter, a reconfigurable base integrated parallel mechanism was presented based on the manipulation of rigid objects with a Metamorphic hand for the first time through mechanism equivalent method. The structure of the proposed mechanism was introduced. By means of decomposing the mechanism into a typical 3RRS parallel mechanism and a reconfigurable linkage, the Jacobian based on screw theory was utilized to identify the relationship between active joints and passive joints through the screw system elimination with their reciprocal product. The Jacobian analysis

demonstrated the effectiveness of screw algebra approach in modelling the novel reconfigurable-base integrated parallel manipulator.

Chapter 6 Constraint Analysis of a Derivative Queer-Square Mechanism Using Lie Bracket

6.1 Introduction

This chapter investigates the kinematic constraints of a derivative queer-square mechanism. The derivative queer-square mechanism can be traced back to (Qin, Dai, and Gogu, 2014) [1] and the screw-system approach to identify the multi-furcation back to (Dai, Huang, and Lipkin, 2006) [23]. This chapter focuses on establishing kinematic constraints for the derivative queer-square mechanism using an approach with Lie bracket computation in terms of instantaneous screws. The research in this chapter for the first time applies the recursive algorithm based on Lie bracket to velocity and acceleration analysis of multi-loop mechanisms. By introducing the bilinear form representation, second-order constraints of the mechanism are simplified, and this operation lays a foundation for identifying motion branches in the next chapter.

6.2 Geometrical Structure of the Derivative Queer-Square Mechanism

The derivative queer-square mechanism consists of ten links connected by twelve revolute joints and in such a mechanism three loops are constructed by these joints. As illustrated in Figure 6.1, ten links are labelled by numbers 1, 2, …, 10, while twelve revolute joints can be described by letters A, B, C_1, D_1, E_1, F_1, C_2, D_2, E_2, F_2, G, H respectively in which revolute joints $C_1D_1E_1F_1$ form an inner loop and $C_2D_2E_2F_2$ form the other inner loop in the mechanism. If in some configurations links 4 and 5 are parallel, the loop C_1, D_1, E_1, F_1 constitutes a parallelogram, if not, the loop constitutes an anti-parallelogram. Similarly, the loop C_2, D_2, E_2, F_2 forms a parallelogram or an anti-parallelogram as well depending on whether links 7 and 8 are parallel or not.

When the mechanism moves to a configuration that all links lie in a same plane, as shown in Figure 6.2, the mechanism is singular, and the configuration is called as singularity configuration or *stationary configuration* [29]. This chapter and chapter 6 are to determine how many motion branches exist at this configuration and what the corresponding geometrical constraints are for each single motion branch.

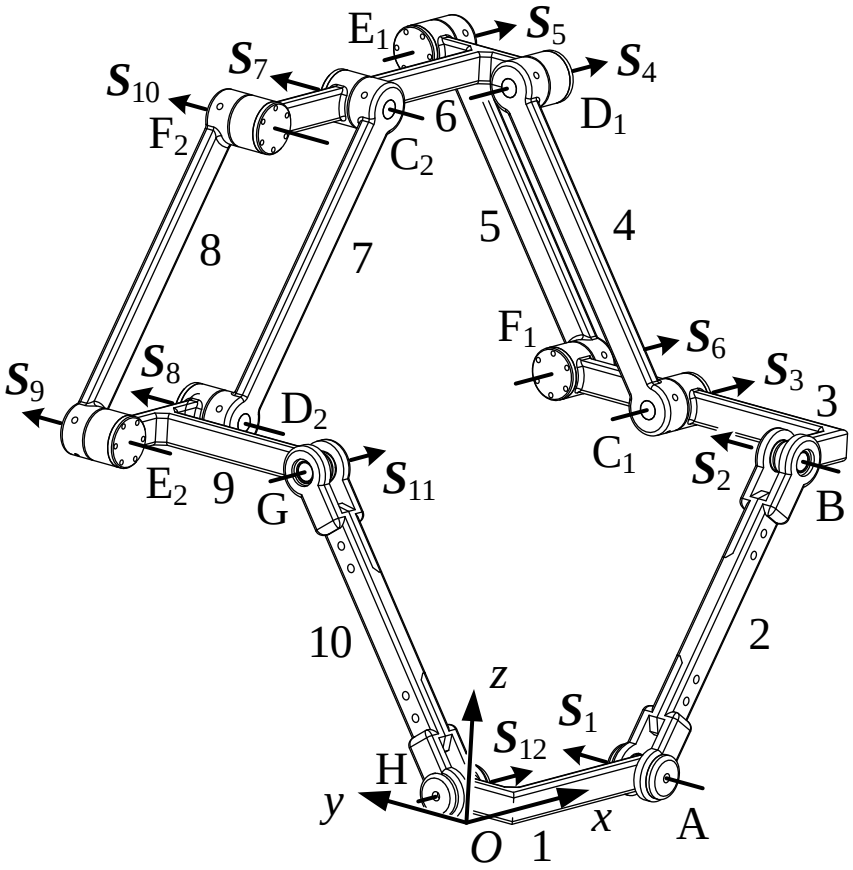

Figure 6.1 The 3D structure of the derivative mechanism

In the mechanism as shown in Figure 6.2, the length of the shorter link in loop $C_1D_1E_1F_1$ is denoted as *a* and the longer part of link 1 is denoted as *b*. The length of links 2, 4, 5, 7, 8, and 10 are equal to *a*+*b*. The length of the longer parts of links 6, 9 are equal to *a* while the length of the shorter parts of these two links are *b*. The two loops $C_1D_1E_1F_1$ and $C_2D_2E_2F_2$ are congruent in the singularity configuration. All the above lengths of links can be found in the following Figure 6.2. The coordinate frame *O*-*xyz* is established with the *x*-axis along with the longer part of link 1, the *y*-axis in the direction of the shorted part of link 1 and the origin at the intersection point of the *x*-axis with the axis of the joint E_2. It is straightforward to say all the joint axes are in the direction of either the *x*-axis or the *y*-axis at the singularity configuration and this is one of the reasons why the mechanism is named “square” mechanism.

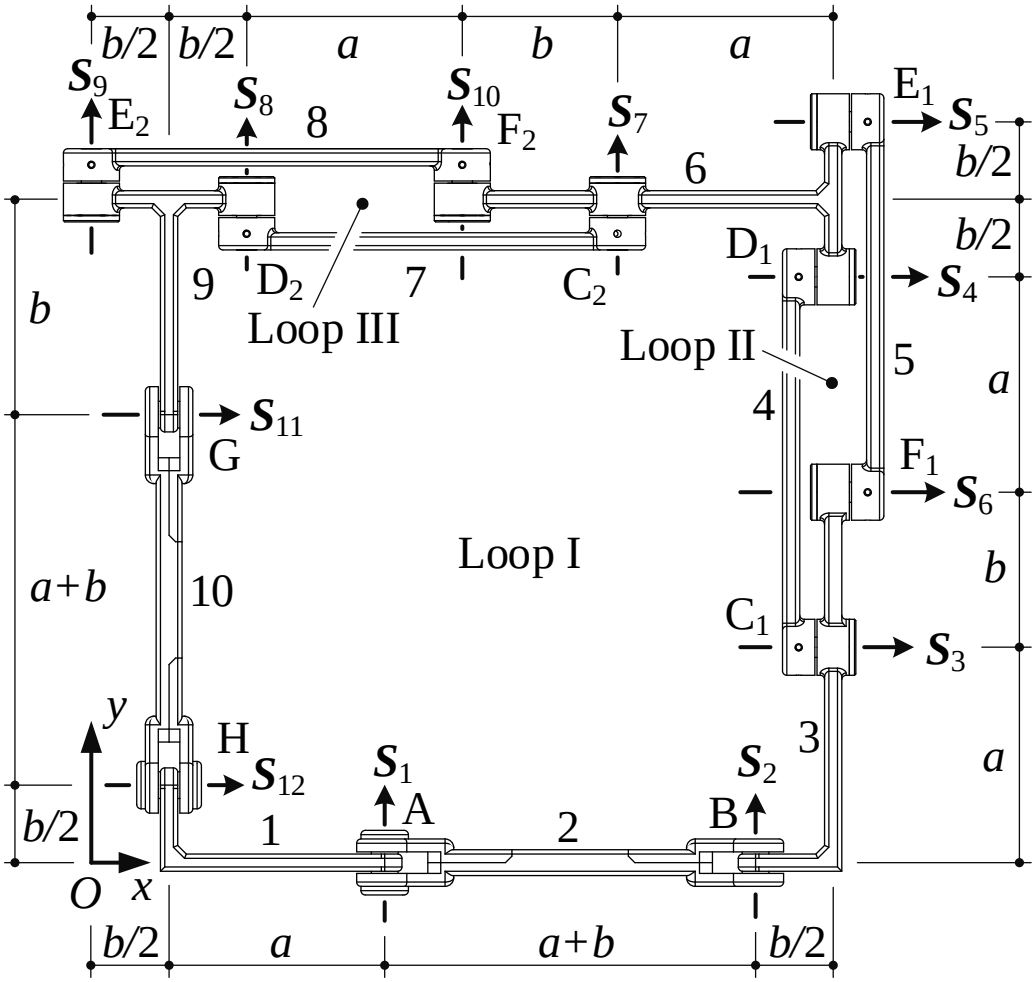

Figure 6.2 The singularity configuration of the mechanism

There are three independent loops I, II and III in the closed loop derivative queer-square mechanism and the topology of the queer-square mechanism can be indicated by the directed graph in Figure 6.3. All nodes in each single loop are connected by directed edges in a counter-clockwise direction, in which each node labels a link and each directed edge labels a revolute joint. The directed graph lays the foundation for the first-order constraint construction of the mechanism and this is discussed in detail in the following section.

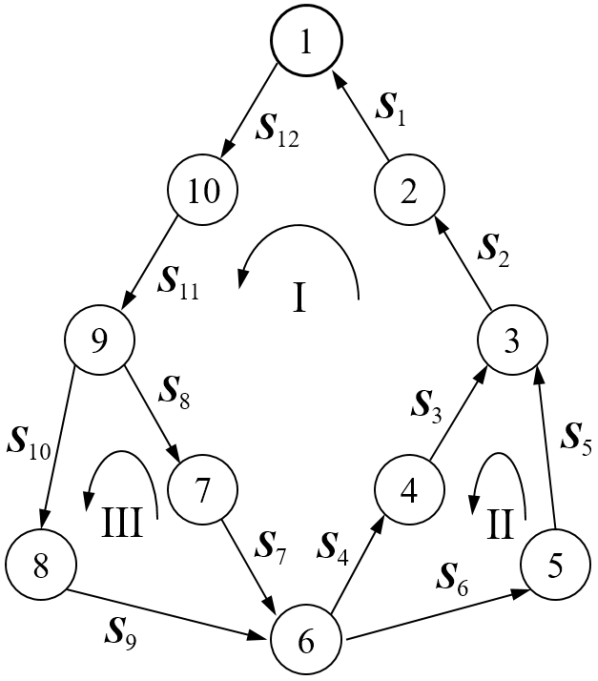

Figure 6.3 The directed graph of topology

6.3 Screws at the Singularity Configuration and First-Order Constraints

6.3.1 Screws and the Closed-Loop Velocity Formula

This section focuses on the instantaneous motion of the derivative queer-square mechanism at its singularity configuration and first-order constraints are revealed for the motion analysis. As stated in Chapter 3, a screw can represent the instantaneous velocity including linear velocity and angular velocity of a motion generated by a kinematic joint with respect to a coordinate system. In Figure 6.2, twelve screws are attached to the twelve revolute joints. According to the dimensions of the mechanism

described in Figure 6.2 and the form of a screw in Equation (3.1), the twelve screws can be calculated and written as

$$
\begin{aligned}
\boldsymbol{S}_1 &= \left[0 \quad 1 \quad 0 \quad 0 \quad 0 \quad a+\frac{1}{2}b\right]^{\mathrm{T}} \\
\boldsymbol{S}_2 &= \left[0 \quad 1 \quad 0 \quad 0 \quad 0 \quad 2a+\frac{3}{2}b\right]^{\mathrm{T}} \\
\boldsymbol{S}_3 &= \left[1 \quad 0 \quad 0 \quad 0 \quad 0 \quad -a\right]^{\mathrm{T}} \\
\boldsymbol{S}_4 &= \left[1 \quad 0 \quad 0 \quad 0 \quad 0 \quad -\left(2a+b\right)\right]^{\mathrm{T}} \\
\boldsymbol{S}_5 &= \left[1 \quad 0 \quad 0 \quad 0 \quad 0 \quad -2\left(a+b\right)\right]^{\mathrm{T}} \\
\boldsymbol{S}_6 &= \left[1 \quad 0 \quad 0 \quad 0 \quad 0 \quad -\left(a+b\right)\right]^{\mathrm{T}} \\
\boldsymbol{S}_7 &= \left[0 \quad 1 \quad 0 \quad 0 \quad 0 \quad a+2b\right]^{\mathrm{T}} \\
\boldsymbol{S}_8 &= \left[0 \quad 1 \quad 0 \quad 0 \quad 0 \quad b\right]^{\mathrm{T}} \\
\boldsymbol{S}_9 &= \left[0 \quad 1 \quad 0 \quad 0 \quad 0 \quad 0\right]^{\mathrm{T}} \\
\boldsymbol{S}_{10} &= \left[0 \quad 1 \quad 0 \quad 0 \quad 0 \quad a+b\right]^{\mathrm{T}} \\
\boldsymbol{S}_{11} &= \left[1 \quad 0 \quad 0 \quad 0 \quad 0 \quad -\left(a+\frac{3}{2}b\right)\right]^{\mathrm{T}} \\
\boldsymbol{S}_{12} &= \left[1 \quad 0 \quad 0 \quad 0 \quad 0 \quad -\frac{1}{2}b\right]^{\mathrm{T}}
\end{aligned}
\tag{6.1}
$$

It is known that any closed-loop mechanism with the end link connected with the base link fulfils the velocity formula of a closed-loop and the formula can be represented as follows

$$
\boldsymbol{J}\boldsymbol{\omega} = \mathbf{0} \tag{6.2}
$$

in which matrix $\boldsymbol{J}$ is called as Jacobian matrix of the closed-loop and can be obtained by assembling all screws corresponding to the kinematic joints; vector $\boldsymbol{\omega}$ represents the

scalar velocities of the kinematic joints in the mechanism. The dimension of $\boldsymbol{\omega}$ is determined by the number of kinematic joints.

Applying the above formula to loop I in Figure 6.3, the closed-loop velocity equation can be expressed as a linear combination of screws $\boldsymbol{S}_1$, $\boldsymbol{S}_2$, $\boldsymbol{S}_3$, $\boldsymbol{S}_4$, $\boldsymbol{S}_7$, $\boldsymbol{S}_8$, $\boldsymbol{S}_{11}$, $\boldsymbol{S}_{12}$ and written as follows

$$\sum_{i=1}^{4} \omega_i \boldsymbol{S}_i + \left(\omega_7 \boldsymbol{S}_7 + \omega_8 \boldsymbol{S}_8 + \omega_{11} \boldsymbol{S}_{11} + \omega_{12} \boldsymbol{S}_{12} \right) = 0 \tag{6.3}$$

Similarly, for loops II and III, the closed-loop velocity equation can be written as

$$-\omega_3 \boldsymbol{S}_3 - \omega_4 \boldsymbol{S}_4 + \omega_5 \boldsymbol{S}_5 + \omega_6 \boldsymbol{S}_6 = \boldsymbol{0} \tag{6.4}$$

$$-\omega_7 \boldsymbol{S}_7 - \omega_8 \boldsymbol{S}_8 + \omega_9 \boldsymbol{S}_9 + \omega_{10} \boldsymbol{S}_{10} = \boldsymbol{0} \tag{6.5}$$

The choice of symbols "+" or "–" in the above three equations depends on whether the direction of the loop coincides with the direction of the corresponding edge in the graph.

6.3.2 Jacobian Matrix and the First-Order Constraints

Assembling the above three equations into a linear equation system and expressing it in matrix form, it has

$$\begin{bmatrix} \boldsymbol{S}_1 & \boldsymbol{S}_2 & \boldsymbol{S}_3 & \boldsymbol{S}_4 & \mathbf{0} & \mathbf{0} & \boldsymbol{S}_7 & \boldsymbol{S}_8 & \mathbf{0} & \mathbf{0} & \boldsymbol{S}_{11} & \boldsymbol{S}_{12} \\ \mathbf{0} & \mathbf{0} & -\boldsymbol{S}_3 & -\boldsymbol{S}_4 & \boldsymbol{S}_5 & \boldsymbol{S}_6 & \mathbf{0} & \mathbf{0} & \mathbf{0} & \mathbf{0} & \mathbf{0} & \mathbf{0} \\ \mathbf{0} & \mathbf{0} & \mathbf{0} & \mathbf{0} & \mathbf{0} & \mathbf{0} & -\boldsymbol{S}_7 & -\boldsymbol{S}_8 & \boldsymbol{S}_9 & \boldsymbol{S}_{10} & \mathbf{0} & \mathbf{0} \end{bmatrix} \begin{bmatrix} \omega_1 \\ \omega_2 \\ \omega_3 \\ \omega_4 \\ \omega_5 \\ \omega_6 \\ \omega_7 \\ \omega_8 \\ \omega_9 \\ \omega_{10} \\ \omega_{11} \\ \omega_{12} \end{bmatrix} = \mathbf{0} \quad (6.6)$$

The above linear equation system gives the Jacobian matrix of the mechanism which implements instantaneous velocity analysis for the mechanism when the mechanism moves to the singularity configuration.

Substituting the twelve screws in Equation (6.1) to the above matrix in the left-hand side of the equation, the Jacobian matrix can be expressed as a function of the mechanism dimensions and thus the equation (6.2) gives the first-order constraints of the mechanism at the singularity configuration and the Jacobian matrix of the first-order constraints can be obtained as follows in Equation (6.7). The dimension of the matrix is 18×12 since the mechanism has three loops and twelve joints. It is straightforward to know that the rank of the first-order constraints is 7 and there are 12 angular velocity variables. Then the transitory mobility of the mechanism at this configuration can be identified as 5.

$$
\left[\begin{array}{cccc|cccc|cccc}
0 & 0 & 1 & 1 & 0 & 0 & 0 & 0 & 0 & 0 & 1 & 1 \\
1 & 1 & 0 & 0 & 0 & 0 & 1 & 1 & 0 & 0 & 0 & 0 \\
0 & 0 & 0 & 0 & 0 & 0 & 0 & 0 & 0 & 0 & 0 & 0 \\
\hdashline
0 & 0 & 0 & 0 & 0 & 0 & 0 & 0 & 0 & 0 & 0 & 0 \\
0 & 0 & 0 & 0 & 0 & 0 & 0 & 0 & 0 & 0 & 0 & 0 \\
a+\frac{1}{2}b & 2a+\frac{3}{2}b & -a & -(2a+b) & 0 & 0 & a+2b & b & 0 & 0 & -\left(a+\frac{3}{2}b\right) & -\frac{b}{2} \\
\hline
0 & 0 & -1 & -1 & 1 & 1 & 0 & 0 & 0 & 0 & 0 & 0 \\
0 & 0 & 0 & 0 & 0 & 0 & 0 & 0 & 0 & 0 & 0 & 0 \\
0 & 0 & 0 & 0 & 0 & 0 & 0 & 0 & 0 & 0 & 0 & 0 \\
\hdashline
0 & 0 & 0 & 0 & 0 & 0 & 0 & 0 & 0 & 0 & 0 & 0 \\
0 & 0 & 0 & 0 & 0 & 0 & 0 & 0 & 0 & 0 & 0 & 0 \\
0 & 0 & a & 2a+b & -2(a+b) & -(a+b) & 0 & 0 & 0 & 0 & 0 & 0 \\
\hline
0 & 0 & 0 & 0 & 0 & 0 & 0 & 0 & 0 & 0 & 0 & 0 \\
0 & 0 & 0 & 0 & 0 & 0 & -1 & -1 & 1 & 1 & 0 & 0 \\
0 & 0 & 0 & 0 & 0 & 0 & 0 & 0 & 0 & 0 & 0 & 0 \\
\hdashline
0 & 0 & 0 & 0 & 0 & 0 & 0 & 0 & 0 & 0 & 0 & 0 \\
0 & 0 & 0 & 0 & 0 & 0 & 0 & 0 & 0 & 0 & 0 & 0 \\
0 & 0 & 0 & 0 & 0 & 0 & -(a+2b) & -b & 0 & a+b & 0 & 0
\end{array}\right]
$$

(6.7)

This section derived the first-order constraints of the three-loop mechanism from Jacobian analysis and expressed it in matrix form as shown in Equation (6.7). The first-order constraints are only a part of the constraint system at the singularity configuration. The other second-order constraints it to be revealed from acceleration analysis in the following section.

6.4 Acceleration Analysis and Second-Order Constraints

To implementing acceleration analysis for the mechanism at the singularity, we take derivatives of both sides of Equation (6.2) and it has the following formula [20, 70]

$$\boldsymbol{J\alpha} = -\boldsymbol{S}_{\mathrm{L}} \tag{6.8}$$

in which matrix $\boldsymbol{J}$ is the same Jacobian matrix with that in Equation (6.6) ignoring units of elements; the 12-dimendional vector $\boldsymbol{\alpha}$ represents the angular accelerations of the corresponding revolute joints at the singularity configuration; the 6-dimensional vector on the left-hand side of the above equation $\boldsymbol{S}_{\mathrm{L}}$ can be computed by a recursive algorithm using Lie bracket of two screws and can be expressed as

$$\boldsymbol{S}_{\mathrm{L}} = \sum_{i<j} \omega_i \omega_j \left[\boldsymbol{S}_i, \boldsymbol{S}_j \right] \tag{6.9}$$

where i and j are 1, 2, 3, …, 12; screws $\boldsymbol{S}_i$, $\boldsymbol{S}_j$ are instantaneous screws attached to the revolute joints; the operator $[\boldsymbol{S}_1, \boldsymbol{S}_2]$ is Lie bracket which gives Lie product of any two screws.

The Lie bracket formula satisfies anti-commutativity which is $[\boldsymbol{S}_1, \boldsymbol{S}_2] = -[\boldsymbol{S}_2, \boldsymbol{S}_1]$. The rule of calculating Lie bracket of screws can be seen in Equation (3.8) in section 3.3. The above two formulae reveal the acceleration analysis of the mechanism by using a

recursive algorithm of Lie bracket calculation. The formulae can be applied to any configuration of a mechanism, even singularity configuration.

In fact, Equation (6.8) shares the same coefficient matrix with the linear equation system in Equation (6.6) ignoring the unit for each single entry and unknown, though the two equations are established for velocity analysis and acceleration analysis separately. The difference between the two equations in the algebraic point of view lies in Equation (6.8) is a non-homogeneous linear equation system, while the other is a homogeneous linear equation system. Both equations are derived from the same mechanism at the same singularity configuration, hence they will be solvable simultaneously under particular conditions, otherwise there are no solutions of the kinematics analysis including velocity and acceleration analysis which means there is no motion branch at the singularity configuration which can generate finite motions.

The algebraic condition for solving a non-homogenous linear equation system is that the corresponding homogenous linear equation system has non-zero solutions. This condition requires that the rank of the augmented matrix of the non-homogenous linear equation system are the same as the rank of the corresponding homogenous linear equation system. Therefore, consideration Equations (6.2), (6.8) and (6.9), the condition for solving Equation (6.8) can be expressed as below

$$\mathrm{Rank}\left(\boldsymbol{J}\right) = \mathrm{Rank}\left(\left[\boldsymbol{J} \quad -\boldsymbol{S}_{\mathrm{L}}\right]\right) \tag{6.10}$$

From Figure 6.1 and Equation (6.1), all axes of the twelve screws are parallel with either *x*-axis or *y*-axis, and due to the properties of Lie bracket calculation, the above Equation (6.10) holds if and only if the angular variables ω_i satisfy the condition below

$$\boldsymbol{S}_{\mathrm{L}} = \sum_{i<j} \omega_i \omega_j \left[\boldsymbol{S}_i, \boldsymbol{S}_j \right] = \mathbf{0} \tag{6.11}$$

This equation is a linear combination of second-order items of ω_i, ω_j and gives second-order constraints for the mechanism at the singularity configuration based on acceleration analysis and Lie bracket calculation.

6.5 Matrix Form of the Second Order Constraints

6.5.1 Bilinear Form of Second-Order Constraints

The section 5.4 gives the second-order constraints from acceleration analysis of the mechanism by using Lie algebra calculation. We substitute the twelve screws in Equation (6.1) into the second-order constraints in Equation (6.11), five algebraic conditions can be attained. These five second-order constraints are polynomials with regard to second-order items $\omega_i\omega_j$ and have very complicated expressions, for example, one of the polynomials obtained to represent the second-order constraint can be written as below

$$
\begin{aligned}
&(a+b)\omega_1\omega_2 - a\omega_1\omega_3 + (2a+b)\omega_1\omega_4 + \frac{3b}{2}\omega_1\omega_7 + \left(-a+\frac{b}{2}\right)\omega_1\omega_8 - \\
&\left(a+\frac{3b}{2}\right)\omega_1\omega_{11} - \frac{b}{2}\omega_1\omega_{12} - a\omega_2\omega_3 - (2a+b)\omega_2\omega_4 + \left(-a+\frac{b}{2}\right)\omega_2\omega_7 - \\
&\left(2a+\frac{b}{2}\right)\omega_2\omega_8 - \left(a+\frac{3b}{2}\right)\omega_2\omega_{11} - \frac{b}{2}\omega_2\omega_{12} + a\omega_3\omega_7 + a\omega_3\omega_8 + \\
&(2a+b)\omega_4\omega_7 + (2a+b)\omega_4\omega_8 - (a+b)\omega_7\omega_8 - \left(a+\frac{3b}{2}\right)\omega_7\omega_{11} - \\
&\frac{b}{2}\omega_7\omega_{12} - \left(a+\frac{3b}{2}\right)\omega_8\omega_{11} - \frac{b}{2}\omega_8\omega_{12} = 0
\end{aligned}
\tag{6.12}
$$

the meanings of scalars *a*, *b* in the above equation can be found in Figure 6.2. It is rather difficult to dig out any principles or geometrical meanings from the above complicated expression. Therefore, we introduce bilinear form to represent the second-order constraints. Considering Equation (6.11), since all elements of the combinational screw $\boldsymbol{S}_{\mathrm{L}}$ are polynomials of $\omega_i\omega_j$, such a screw can be rewritten by a bilinear form as below

$$
S_{\mathrm{L}k} = \boldsymbol{\omega}^{\mathrm{T}}\boldsymbol{A}_k\boldsymbol{\omega}, \quad k = 1, 2, \cdots, 5 \tag{6.13}
$$

where matrix $\boldsymbol{A}$ describes the coefficient matrix of the bilinear form. In this case, the second-order constraints can be obtained in the form of bilinear form

$$
\boldsymbol{\omega}^{\mathrm{T}}\boldsymbol{A}_k\boldsymbol{\omega} = 0 \tag{6.14}
$$

Therefore, each single constraint of second order can be represented by a specific matrix. Considering the above matrix operation, the dimension of the coefficient matrix of the bilinear form is 12×12. For instance, the polynomial in Equation (6.12) can be

expressed in the form of a 12×12 matrix which represents a bilinear form of the 12-dimensional vector $\boldsymbol{\omega}$ as below

$$\left[\begin{array}{cccc|cc|cc|cc|cc}
0 & a+b & -a & -(2a+b) & 0 & 0 & \frac{3b}{2} & -a+\frac{b}{2} & 0 & 0 & -\left(a+\frac{3b}{2}\right) & -\frac{b}{2} \\
0 & 0 & -a & -(2a+b) & 0 & 0 & -a+\frac{b}{2} & -\left(2a+\frac{b}{2}\right) & 0 & 0 & -\left(a+\frac{3b}{2}\right) & -\frac{b}{2} \\
0 & 0 & 0 & 0 & 0 & 0 & a & a & 0 & 0 & 0 & 0 \\
0 & 0 & 0 & 0 & 0 & 0 & 2a+b & 2a+b & 0 & 0 & 0 & 0 \\
\hline
0 & 0 & 0 & 0 & 0 & 0 & 0 & 0 & 0 & 0 & 0 & 0 \\
0 & 0 & 0 & 0 & 0 & 0 & 0 & 0 & 0 & 0 & 0 & 0 \\
0 & 0 & 0 & 0 & 0 & 0 & 0 & -(a+b) & 0 & 0 & -\left(a+\frac{3b}{2}\right) & -\frac{b}{2} \\
0 & 0 & 0 & 0 & 0 & 0 & 0 & 0 & 0 & 0 & -\left(a+\frac{3b}{2}\right) & -\frac{b}{2} \\
\hline
0 & 0 & 0 & 0 & 0 & 0 & 0 & 0 & 0 & 0 & 0 & 0 \\
0 & 0 & 0 & 0 & 0 & 0 & 0 & 0 & 0 & 0 & 0 & 0 \\
0 & 0 & 0 & 0 & 0 & 0 & 0 & 0 & 0 & 0 & 0 & 0 \\
0 & 0 & 0 & 0 & 0 & 0 & 0 & 0 & 0 & 0 & 0 & 0
\end{array}\right] \tag{6.15}$$

This is an upper triangular matrix which represents a second-order constraint of the mechanism in the form of a matrix. Considering the matrix form, it is possible to reduce some trivial items in the constraint and dig out its geometrical and physical meanings. This is discussed in detail in the next step.

6.5.2 Simplification of the Second-Order Constraints

By introducing bilinear forms, the second-constraints can be presented by 12×12 matrices. One of the constraints has been expressed in Equation (6.15). From the calculation in Section 5.4, five second-order constraints in total can be attained can then be rewritten in the form of matrices. The other four matrices are placed into Appendix A as four equations from (A.1) to (A.4).

If combining the first-order constraints shown in Equation (6.7) with the second-order constraints in section 5.5.1 and appendix A together, we can simplify the second-order constraints by elementary transformations of matrices and eliminating unknowns. For example, from the first four rows of the coefficient matrix of the first-order constraints, the following conditions of the unknowns ω_i can be obtained

$$\omega_3 + \omega_4 + \omega_{11} + \omega_{12} = 0 \tag{6.16}$$

$$\omega_1 + \omega_2 + \omega_9 + \omega_{10} = 0 \tag{6.17}$$

$$\begin{aligned}&\left(a+\frac{1}{2}b\right)\omega_1 + \left(2a+\frac{3}{2}b\right)\omega_2 - a\omega_3 - (2a+b)\omega_4 + (a+2b)\omega_9 + \\ &b\omega_{10} - \left(a+\frac{3}{2}b\right)\omega_{11} - \frac{b}{2}\omega_{12} = 0\end{aligned} \tag{6.18}$$

If only considering the first row in Equation (6.15) and extracting common factors, the following polynomial of $\omega_i\omega_j$ can be found and written as

$$\left(\left(a+b\right)\omega_2 - a\omega_3 - \left(2a+b\right)\omega_4 + \frac{3}{2}b\omega_9 + \left(-a+\frac{b}{2}\right)\omega_{10} - \left(a+\frac{3}{2}b\right)\omega_{11} - \frac{b}{2}\omega_{12}\right)\omega_1 \tag{6.19}$$

From Equation (6.18), it has

$$-a\omega_3 - \left(2a+b\right)\omega_4 + -\left(a+\frac{3}{2}b\right)\omega_{11} - \frac{b}{2}\omega_{12} = -\left(a+\frac{1}{2}b\right)\omega_1 - \left(2a+\frac{3}{2}b\right)\omega_2 - \left(a+2b\right)\omega_9 - b\omega_{10} \tag{6.20}$$

Substituting the above equation to the polynomial in Equation (6.19) and rearranging the items, the polynomial can be simplified as below

$$-\left(a+\frac{b}{2}\right)\left(\omega_1+\omega_2+\omega_9+\omega_{10}\right) \tag{6.21}$$

From the condition in Equation (6.17), the above simplified polynomial equals zero. In such a case all the items corresponding to the entries in the first row of the matrix in Equation (6.15) have been eliminated and the second-order constraint presented by the matrix has been simplified to a certain extent.

Using the same manner, the other rows of the matrix in Equation (6.15) can be simplified by combining the conditions obtained from the coefficient matrix of the first-order constraints. Then assembling all the simplified rows together, the fully simplified constraint of second order can be attained and expressed as below

$$\begin{aligned}&(a+b)\omega_1\omega_2+(a+b)\omega_9\omega_{10}+\\&\left(\left(a+\frac{b}{2}\right)(\omega_1+\omega_2)+(a+b)(\omega_2+\omega_{10})+b(\omega_9+\omega_{10})\right)(\omega_9+\omega_{10})=0\end{aligned}\tag{6.22}$$

It is straightforward that such a method of combining the first-order and second-order constraints can be applied to simplifying other second-order constraints given by the coefficient matrices of bilinear forms in Appendix A. The simplified second-order constraint related with the coefficient matrix (A.1) can be obtained as

$$(a+b)(\omega_3\omega_4+\omega_7\omega_8)+\left((a+b)\omega_4+\left(-a+\frac{b}{2}\right)\omega_7+\frac{3}{2}b\omega_8\right)(\omega_3+\omega_4)=0 \tag{6.23}$$

The simplified second-order constraint related to the coefficient matrix (A.2) can be written as below

$$(\omega_3+\omega_4-\omega_{11}-\omega_{12})(\omega_7+\omega_8)=0 \tag{6.24}$$

The polynomials corresponding to the coefficient matrix (A.3) and (A.4) are already simplified and can be obtained directly as

$$(a+b)\omega_3(\omega_4-\omega_6)-b\omega_3(\omega_5+\omega_6)+a\omega_5(\omega_4+\omega_6)-b\omega_6(\omega_4-\omega_5)=0 \tag{6.25}$$

$$a\omega_9(\omega_{10}-\omega_{12})+b\omega_9(\omega_{10}+\omega_{11})+(a+b)\omega_{11}(\omega_{10}+\omega_{12})+b\omega_{10}(\omega_{11}+\omega_{12})=0 \tag{6.26}$$

Finally, all second-order constraints have been attained and simplified by introducing bilinear form representation of the polynomials of constraints. The results were described by Equations from (6.22) to (6.26).

6.6 Conclusions

This chapter established the kinematic model including velocity and acceleration analysis of the derivative queer-square mechanism and first-order and second-order constraints have been attained by using Lie bracket calculation of screws. The recursive algorithm of screws based on Lie bracket was used to modelling the kinematic constraints of multi-loop mechanisms for the first time. To reduce the complexity introduced by three loops and twelve kinematic joints, this chapter employed bilinear form to represent the second-order constraint and simplified their expressions. This approach made it possible to simplify complicated constraints of second order so that the recursive algorithm can be applied to multi-loop mechanisms which are quite complicated in modelling. Finally, all first-order and second-order constraints were attained in the simplified form. This chapter demonstrated the effectiveness of screw theory discussed in Chapter 3 and 4 and paved a way of exploring motion branches of the derivative queer-square mechanism for Chapter 6.

Chapter 7 Multi-Furcation Recognition of a Derivative Queer-Square Mechanism Based on Constraint Analysis

7.1 Introduction

This chapter is an extension of chapter 5 focusing on working out motion branches of the derivative queer-square mechanisms. Following the modelling of first-order and second-order constraints in Chapter 5, this chapter is to construct the constraint system of the multi-loop mechanism in Section 6.2. Before solving the equation system of constraints, Section 6.3 recognises the geometrical conditions under which the order of the constraint system changes. Solutions to the constraint system of integrating first-order and second-order constraints are solved and given in Section 6.4 and all motion branches are listed in Section 6.5 with the corresponding geometrical conditions and prototype validations. Finally, this chapter implements motion simulation in commercial software SolidWorks to validate the derivations and equations numerically.

7.2 Construction of Constraint System

In chapter 5, first-order and second-order constraints were derived according to the velocity and acceleration analysis respectively using a recursive algorithm of Lie bracket of screws. The scalars of relative angular velocities of kinematic joints in the mechanism form the vector of unknowns. All the constraints are obtained at the singularity configuration so that the mechanism can move into a motion branch if and only if all the constraints of the mechanism at that moment are satisfied, that is to say, the constraint system compromised of the first-order and second-order constraints have nontrivial solutions and the number of solutions determines the number of the motion branches.

Assembling the first-order constraints in Equation (6.2) and the second-order constraints in Equation (6.14), the following constraint system with first-order and second-order integrated is obtained and can be expressed by an equation system in matrix form

$$\begin{cases} \boldsymbol{J}\boldsymbol{\omega} = \mathbf{0} \\ \boldsymbol{\omega}^{\mathrm{T}} \boldsymbol{A}_k \boldsymbol{\omega} = 0, \quad k = 1, 2, \cdots, 5 \end{cases} \tag{7.1}$$

In the above constraint system, there are seven independent first-order constraints which is represented by the matrix in Equation (6.7) and five second-order constraints described in Equations from (6.22) to (6.26). The dependence property is discussed in the next section. From the above constraint system and rearranging the five second-

order constraints, all possible constraints exerted to the mechanism at the singularity configuration can be listed as below

$$
\begin{cases}
\omega_3+\omega_4+\omega_{11}+\omega_{12}=0\\
\omega_1+\omega_2+\omega_7+\omega_8=0\\
\left(a+\frac{1}{2}b\right)\omega_1+\left(2a+\frac{3}{2}b\right)\omega_2-a\omega_3-(2a+b)\omega_4+(a+2b)\omega_9+b\omega_{10}-\\
\quad\left(a+\frac{3}{2}b\right)\omega_{11}-\frac{b}{2}\omega_{12}=0\\
\omega_3+\omega_4-\omega_5-\omega_6=0\\
a\omega_3+(2a+b)\omega_4-(a+b)\omega_5-2(a+b)\omega_6=0\\
-\omega_7-\omega_8+\omega_9+\omega_{10}=0\\
-(a+2b)\omega_7-b\omega_8+(a+b)\omega_9=0\\
(\omega_3+\omega_4-\omega_{11}-\omega_{12})(\omega_7+\omega_8)=0\\
(a+b)(\omega_1\omega_2-\omega_7\omega_8)+\left(a\omega_3+(2a+b)\omega_4-\left(a+\frac{3b}{2}\right)\omega_{11}-\frac{b}{2}\omega_{12}\right)(\omega_7+\omega_8)=0\\
(a+b)(\omega_3\omega_4-\omega_{11}\omega_{12})+\left(\frac{3b}{2}\omega_3+\left(-a+\frac{b}{2}\right)\omega_4+(a+2b)\omega_7+b\omega_8\right)(\omega_{11}+\omega_{12})-\\
\quad((a+2b)\omega_7+b\omega_8+(a+b)\omega_{12})(\omega_3+\omega_4)=0\\
(a+b)(\omega_3\omega_4-\omega_5\omega_6)-b\omega_3(\omega_5+\omega_6)+a(\omega_4\omega_6-\omega_3\omega_5)-b\omega_5(\omega_3+\omega_4)=0\\
(a+b)(\omega_9\omega_{10}-\omega_7\omega_8)+a(\omega_7\omega_9-\omega_8\omega_{10})+b\omega_7(\omega_9+\omega_{10})+b\omega_9(\omega_7+\omega_8)=0
\end{cases}
\tag{7.2}
$$

All constraints have been attained completely and shown in the above equation system. The kinematic constraints determine the motion branches of mechanisms and this is discussed in detail in the following context of this chapter.

7.3 Recognition of Geometrical Conditions for Motion Branches

In Equation (7.2), all the first-order constraints are independent and they are represented in a matrix. From Section 5.5.2, all the second-order constraints have been simplified considering the conditions provided by the first-order constraints, so any one of the second-order constraints is independent of the first-order constraints. However, the dependence amongst the second-order constraints has not been explored in the previous chapter and this issue is discussed in this section.

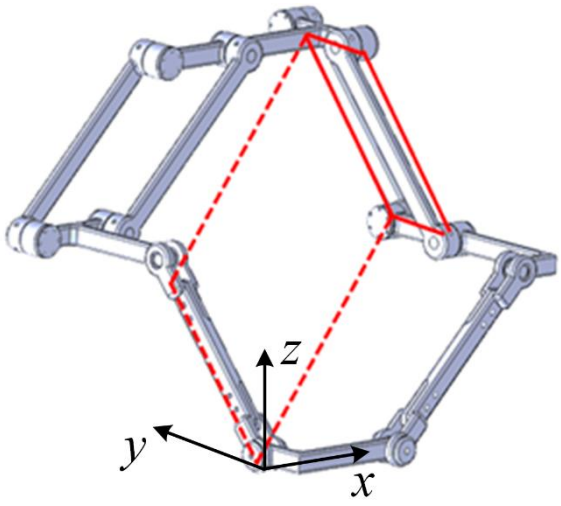

Figure 7.1 Loop II of the mechanism in a configuration of a parallelogram and the adjunct parallelogram

Considering the five second-order constraints listed in Equation (7.2) and at the same time check the three loops in the derivative queer-square mechanism, it can be found that the items in the second-order constraint are closely connected to the topology of

the multi-loop mechanism. For instance, if loop II is in a configuration of a parallel four-bar mechanism and there exists an adjunct parallelogram which is marked in red colour in Figure 7.1, the following algebraic items extracted from the second-order constraints always hold

$$\begin{aligned} &\omega_3 + \omega_4 = \omega_{11} + \omega_{12} = 0 \\ &\omega_3\omega_4 - \omega_{11}\omega_{12} = 0 \\ &\omega_3\omega_4 - \omega_5\omega_6 = 0 \end{aligned} \tag{7.3}$$

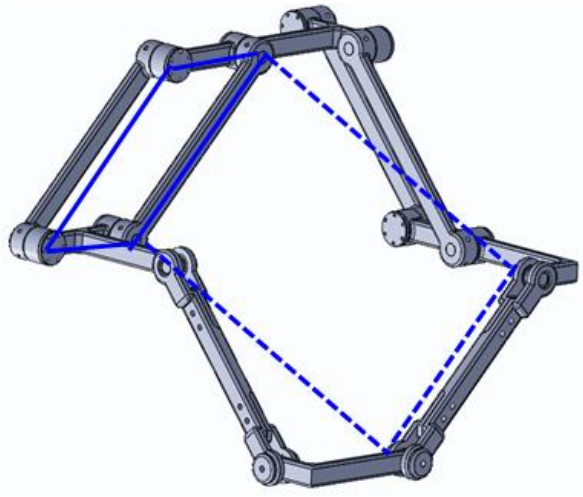

Figure 7.2 Loop III of the mechanism in a configuration of a parallelogram and the connotative parallelogram

Similarly, if loop III forms a parallelogram and there exists a connotative parallelogram which is marked in blue colour in Figure 7.2, the algebraic conditions below always hold in the mechanism

$$\begin{aligned}
&\omega_7+\omega_8=\omega_1+\omega_2=0\\
&\omega_1\omega_2-\omega_7\omega_8=0\\
&\omega_9\omega_{10}-\omega_7\omega_8=0
\end{aligned}\tag{7.4}$$

The above conditions in Equations (7.3) and (7.4) are determined by the topology of loops II and III in the mechanism and affects the degrees of freedom of the constraint system. For example, if only loop II is a parallelogram and there exists a connotative parallelogram as shown in Figure 7.1, one constraint $\omega_3+\omega_4=0$ is introduced to the constraint system, meanwhile, combining this constraint with the first-order constraints, it can be seen that the following two second-order constraints are trivial

$$\begin{aligned}
&\left(\omega_3+\omega_4-\omega_{11}-\omega_{12}\right)\left(\omega_7+\omega_8\right)=0\\
&\left(a+b\right)\left(\omega_3\omega_4-\omega_{11}\omega_{12}\right)+\left(\frac{3b}{2}\omega_3+\left(-a+\frac{b}{2}\right)\omega_4+\left(a+2b\right)\omega_7+b\omega_8\right)\left(\omega_{11}+\omega_{12}\right)-\\
&\left(\left(a+2b\right)\omega_7+b\omega_8+\left(a+b\right)\omega_{12}\right)\left(\omega_3+\omega_4\right)=0
\end{aligned}\tag{7.5}$$

Hence, the degrees of the freedom of the constraint system currently can be calculated as (5+7) + 1−2=11. Similarly, if both loop II and III are parallelograms and there exist two connotative parallelograms as shown in Figure 7.1 and Figure 7.2, there are two geometrical constraints which are $\omega_3+\omega_4=0$ and $\omega_7+\omega_8=0$ being introduced to the constraint system, however four constraint listed below in the constraint system including one first-order constraint become trivial

$$
\begin{aligned}
&\left(\omega_3+\omega_4-\omega_{11}-\omega_{12}\right)\left(\omega_7+\omega_8\right)=0\\
&\left(a+b\right)\left(\omega_1\omega_2-\omega_7\omega_8\right)+\left(a\omega_3+\left(2a+b\right)\omega_4-\left(a+\frac{3b}{2}\right)\omega_{11}-\frac{b}{2}\omega_{12}\right)\left(\omega_7+\omega_8\right)=0\\
&\left(a+b\right)\left(\omega_3\omega_4-\omega_{11}\omega_{12}\right)+\left(\frac{3b}{2}\omega_3+\left(-a+\frac{b}{2}\right)\omega_4+\left(a+2b\right)\omega_7+b\omega_8\right)\\
&\quad\left(\omega_{11}+\omega_{12}\right)-\left(\left(a+2b\right)\omega_7+b\omega_8+\left(a+b\right)\omega_{12}\right)\left(\omega_3+\omega_4\right)=0\\
&-\omega_7-\omega_8+\omega_9+\omega_{10}=0
\end{aligned}
\tag{7.6}
$$

Therefore, the degrees of freedom of the constraint system for the mechanism can be calculated as (5+7)+2−4=10. This method of calculating the degrees of freedom of the constraint system can be applied to other cases of the topology of the mechanism. It can be concluded that whether loop II and III are parallelograms and whether there exist connotative parallelograms are the determinants of the degrees of freedom of the constraint system. In such a case, geometrical conditions which are referred to the topology of the mechanism can be recognised, and such types of conditions determine the degree of freedom of the constraint system so that they determine the motion branches of the mechanism which is explored in the following section.

7.4 Solving the Constraint System of the Derivative Queer-Square Mechanism

The constraint system of the derivative mechanism presented in Equation (7.2) is relatively complicated with 12 first-order and second-order constraints mixed. We can use the commercial software Matlab to help solve the equation system. Firstly, the recursive algorithm of Lie bracket of screws can be calculated in Matlab. Secondly, the

first-order and second-order constraints can be obtained by symbol operation in the software based on the Lie product calculation. Finally, we employ the Matlab function *solve* to implement the symbolic solution of algebraic equations. All codes to implement the above operation and calculation are placed into Appendix B.

After running the programs presented in Appendix B, six solutions to the equation system of the constraints are given. If representing these solutions in the form of 12-dimensional column vectors $(\omega_1\ \omega_2\ \ldots\ \omega_{12})^{\mathrm{T}}$, the solution vectors can be expressed as follows

$$\begin{pmatrix}\omega_1 & -\omega_1 & -\omega_{12} & \omega_{12} & \omega_{12} & -\omega_{12} & \omega_1 & -\omega_1 & -\omega_1 & \omega_1 & -\omega_{12} & \omega_{12}\end{pmatrix}^{\mathrm{T}} \tag{7.7}$$

$$\begin{pmatrix}\omega_1 & -\omega_1 & \omega_1 & -\omega_1 & -\omega_1 & \omega_1 & -\omega_1 & \omega_1 & \omega_1 & -\omega_1 & -\omega_1 & \omega_1\end{pmatrix}^{\mathrm{T}} \tag{7.8}$$

$$\begin{pmatrix}\omega_1 & \frac{a}{a+2b}\omega_1 & -\frac{2a-b}{2a+4b}\omega_1 & \frac{2a-b}{2a+4b}\omega_1 & \frac{2a-b}{2a+4b}\omega_1 & -\frac{2a-b}{2a+4b}\omega_1 \\ -\frac{a}{a+2b}\omega_1 & -\omega_1 & -\frac{a}{a+2b}\omega_1 & -\omega_1 & \frac{2a-b}{2a+4b}\omega_1 & -\frac{2a-b}{2a+4b}\omega_1\end{pmatrix}^{\mathrm{T}} \tag{7.9}$$

$$\begin{pmatrix}\omega_1 & -\frac{a+b}{3a+b}\omega_1 & \frac{4a^2-b^2}{4(a+b)(3a+b)}\omega_1 & -\frac{4a^2-b^2}{4(a+b)(3a+b)}\omega_1 \\ -\frac{4a^2-b^2}{4(a+b)(3a+b)}\omega_1 & \frac{4a^2-b^2}{4(a+b)(3a+b)}\omega_1 & -\frac{a}{3a+b}\omega_1 & -\frac{a+2b}{3a+b}\omega_1 \\ -\frac{a}{3a+b}\omega_1 & -\frac{a+2b}{3a+b}\omega_1 & \frac{4a^2-b^2}{4(a+b)(3a+b)}\omega_1 & -\frac{4a^2-b^2}{4(a+b)(3a+b)}\omega_1\end{pmatrix} \tag{7.10}$$

$$\begin{pmatrix}\omega_1 & -\omega_1 & \frac{4a^2+4ab}{4a^2-b^2}\omega_1 & \frac{4a^2+12ab+8b^2}{4a^2-b^2}\omega_1 & \frac{4a^2+4ab}{4a^2-b^2}\omega_1 & \frac{4a^2+12ab+8b^2}{4a^2-b^2}\omega_1 \\ \omega_1 & -\omega_1 & -\omega_1 & \omega_1 & -\frac{12a^2+16ab+4b^2}{4a^2-b^2}\omega_1 & \frac{4a^2-4b^2}{4a^2-b^2}\omega_1\end{pmatrix}^{\mathrm{T}} \tag{7.11}$$

$$\begin{pmatrix} \omega_1 & -\omega_1 & -\frac{2a}{2a+b}\omega_1 & -\frac{2a+4b}{2a+b}\omega_1 & -\frac{2a}{2a+b}\omega_1 & -\frac{2a+4b}{2a+b}\omega_1 \\ -\omega_1 & \omega_1 & \omega_1 & -\omega_1 & \frac{2a}{2a+b}\omega_1 & \frac{2a+4b}{2a+b}\omega_1 \end{pmatrix}^{\mathrm{T}} \tag{7.12}$$

in which variables ω_i of angular velocities are given as the functions of ω_1 and ω_{12}. The above Equations from (7.7) to (7.11) gives the six solutions of the constraint system. The first solution in Equation (7.7) has two degrees of freedom and hence ω_1 and ω_{12} are chosen to represent other variables. The other five solutions have only one degree of freedom and ω_1 is chosen to represent other variables.

Till now it can be concluded that the constraint system of the derivative queer-square mechanism at the singularity configuration shown in Figure 6.2 has been established based on the recursive algorithm of Lie bracket of screws and the method of simplifying the second-order constraints using bilinear form. There are six solutions to the constraint system of the mechanism at the singularity configuration.

7.5 Six Motion Branches of the Derivative Queer-Square Mechanism

The number of the solutions to the constraint system of a mechanism at a singularity mechanism determines the quantity of the motion branches of the mechanism at the singularity configuration. From Section 6.4, six solutions are obtained as presented in Equations from (7.7) to (7.11) and that means the mechanism has six motions branches at this singularity configuration.

All feasible geometrical conditions for the constraint system were recognised in Section 6.3 based on the simplification of second-order constraints and the combination of the first-order and second-order constraints. These geometrical conditions were presented in Equations (7.3) and (7.4). Then we check the six solutions one by one to see which geometrical conditions they satisfy. In such a way we can correspond the six solutions to the geometrical conditions of the topology of the mechanism so that we can establish the relationship between the six solutions and the motion branches of the mechanism and in this way all the motion branches of the mechanism at the singularity configuration can be revealed completely.

For the first solution presented in Equation (7.7), we check all the feasible geometrical conditions and found the following conditions are fulfilled

$$\begin{cases} \omega_3 + \omega_4 = 0 \\ \omega_7 + \omega_8 = 0 \\ \omega_1\omega_2 - \omega_7\omega_8 = 0 \\ \omega_3\omega_4 - \omega_{11}\omega_{12} = 0 \end{cases} \tag{7.13}$$

which means loops II and III are parallelograms and there exist two connotative parallelograms in the mechanism. Therefore, the connection from solutions to the constraint system to the motion branches of the mechanism can be established so that the corresponding motion branch can be recognised. Since loops II and III are parallelograms and there exist two connotative parallelograms in the mechanism, the motion branch corresponding to the solution in Equation (7.7) and the conditions in

Equation (7.13) can be determined and shown as follows

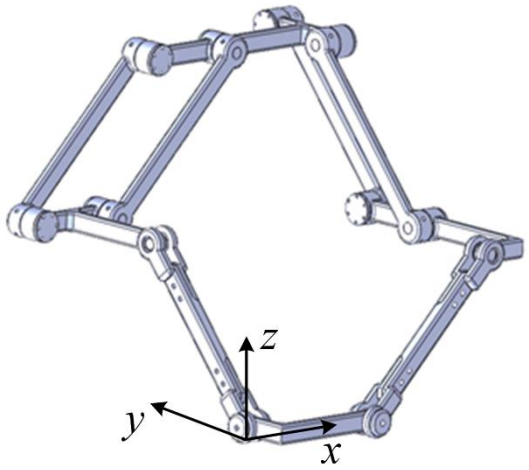

Figure 7.3 The motion branch I with two parallelograms and two connotative parallelograms

Considering the solution in Equation (7.7), there are two variables in the solution and that means in this motion branch I the mechanism has mobility two.

A 3D printed prototype of the derivative queer-mechanism was made to demonstrate the existence of the motion branch. It was proved that the prototype can move to this motion branch from the singularity configuration presented in Figure 6.2 and the photo of the prototype in this motion branch is shown in Figure 7.4

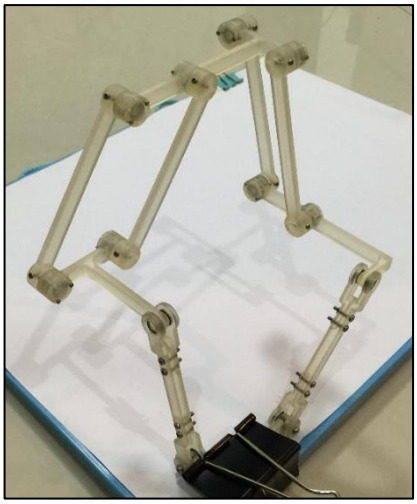

Figure 7.4 The prototype of the mechanism in motion branch I

In a similar way, the geometrical conditions which the second solution in Equation (7.8) satisfies can be obtained as below

$$\begin{cases} \omega_3 + \omega_4 = 0 \\ \omega_7 + \omega_8 = 0 \\ \omega_1 - \omega_{12} = 0 \end{cases} \tag{7.14}$$

which means loop I and II are parallelograms but there are no connotative parallelograms in the mechanism. The topology of the motion branch II can hence be presented in the following Figure 7.5

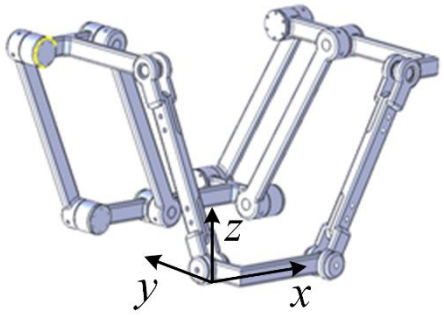

Figure 7.5 The motion branch II with two parallelograms and no connotative parallelograms

Then we check the 3D printed prototype, the motion branch is achievable and can be presented in the photo below. This motion branch has mobility one.

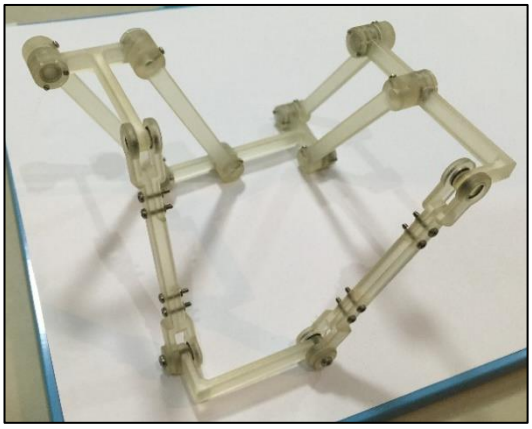

Figure 7.6 The prototype of the mechanism in motion branch II

Considering the solution in Equation (7.9), the following conditions hold

$$\begin{cases} \omega_3 + \omega_4 = 0 \\ \omega_1\omega_2 - \omega_7\omega_8 = 0 \\ \omega_7 + \omega_8 \neq 0 \end{cases} \tag{7.15}$$

which means loop I forms a parallelogram while loop II forms an anti-parallelogram, meanwhile, there is only one connotative parallelogram determined by joints *A*, *B*, C_2, and D_2 in Figure 6.2. This motion branch III can be presented in Figure 7.7.

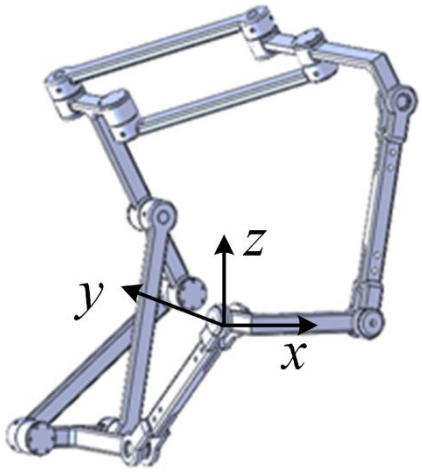

Figure 7.7 The motion branch III with one parallelogram and one connotative parallelogram

Using the 3D printed prototype, it is demonstrated that the mechanism can move to this motion III from the singularity configuration and the motion branch can be presented in Figure 7.8.

Figure 7.8 The prototype of the mechanism in motion branch II

Now check the solution in Equation (7.10) for geometrical conditions. It can be found the following conditions are satisfied of the solution

$$\begin{cases} \omega_3 + \omega_4 = 0 \\ \omega_7 + \omega_8 \neq 0 \\ \omega_1\omega_2 - \omega_7\omega_8 \neq 0 \end{cases} \tag{7.16}$$

which indicates loop I is a parallelogram and loop II is an anti-parallelogram and there is no connotative parallelogram in this motion branch IV. The configuration of the mechanism in this motion branch can be illustrated by the following Figure 7.9.

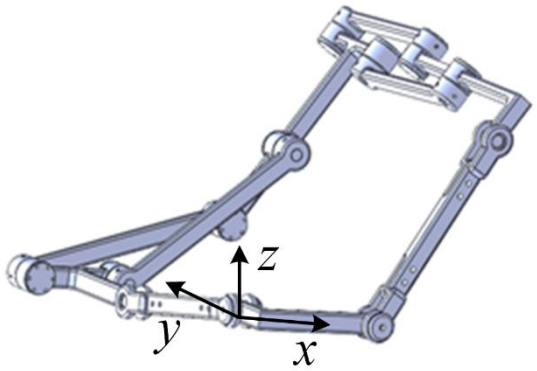

Figure 7.9 The motion branch IV with one parallelogram and no connotative parallelogram

In the 3D printed prototype, the mechanism can achieve the movement from the singularity configuration to the motion branch IV. The motion branch can be presented in the photo of the prototype in Figure 7.10.

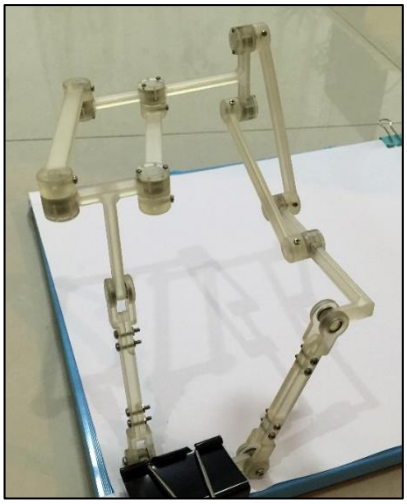

Figure 7.10 The motion branch IV with one parallelogram and no connotative parallelogram

Considering the solution in Equation (7.12), the following geometrical conditions can be satisfied

$$\begin{cases} \omega_7 + \omega_8 = 0 \\ \omega_3 + \omega_4 \neq 0 \\ \omega_5\omega_6 - \omega_{11}\omega_{12} \neq 0 \end{cases} \tag{7.17}$$

in which loop I is an anti-parallelogram and loop II is a parallelogram and there is no connotative parallelogram. The configuration of the motion branch can be presented in Figure 7.11.

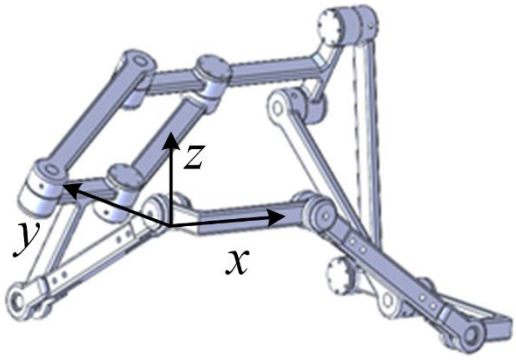

Figure 7.11 The motion branch V with one parallelogram and no connotative parallelogram

It can be demonstrated that the mechanism can move to the motion branch V from the singularity configuration. The 3D printed prototype in this motion branch is presented in Fig. 6.12

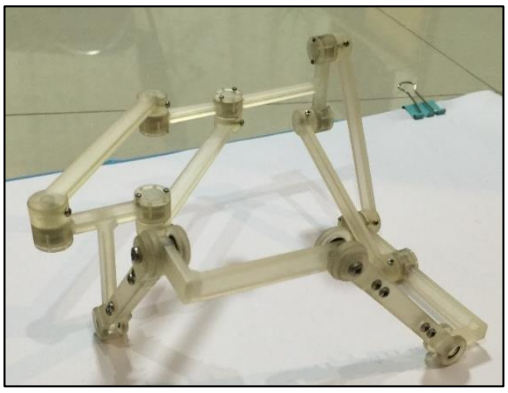

Figure 7.12 The prototype of the mechanism in motion branch V

Finally, check the solution in Equation (7.11) for the geometrical constraints. The following constraints satisfying the solution can be obtained as

$$\begin{cases} \omega_7 + \omega_8 = 0 \\ \omega_3 + \omega_4 \neq 0 \\ \omega_5\omega_6 - \omega_{11}\omega_{12} = 0 \end{cases} \tag{7.18}$$

which means loop II is a parallelogram and loop I is an anti-parallelogram and there exists one connotative parallelogram in this motion branch VI. The configuration of the motion branch can be presented by Figure 7.13.

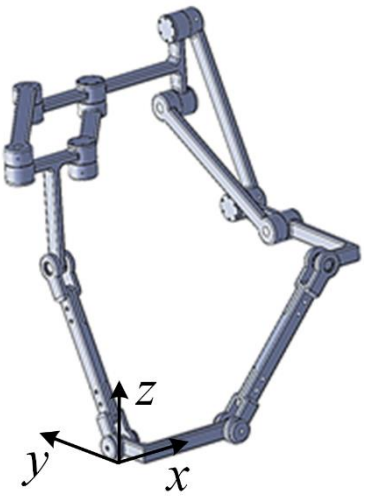

Figure 7.13 The motion branch VI with one parallelogram and one connotative parallelogram

The 3D printed prototype in the configuration of motion branch VI can be presented by the photo in Figure 7.14.

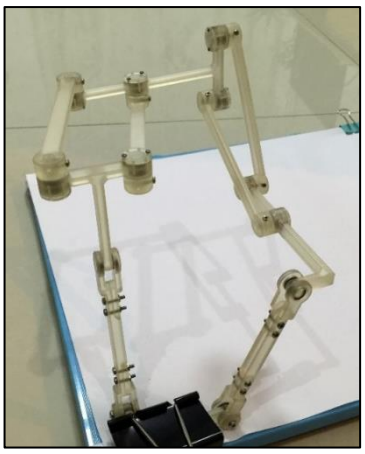

Figure 7.14 The prototype of the mechanism in motion branch VI

Now this section gives all the six motion branches of the derivative queer-square mechanism at the singularity configuration together with the corresponding geometrical constraints and the demonstration with a 3D printed prototype.

7.6 Validation of the Solutions to the Constraint System

7.6.1. Angular Velocities of the Six Motion Branches

Considering the solutions in Equations from (7.7) to (7.11), angular velocity ω_3 can be represented as functions of ω_1 and ω_{12} in six motion branches respectively. Therefore, ω_{3i} can be presented as below

$$\omega_{3i} = \begin{cases} -\omega_{12}, & i = 1 \\ \omega_1, & i = 2 \\ -\dfrac{2a-b}{2a+4b}\omega_1, & \vdots \\ \dfrac{4a^2-b^2}{4(a+b)(3a+b)}\omega_1, & \vdots \\ -\dfrac{2a}{2a+b}\omega_1, & \vdots \\ \dfrac{4a^2+4ab}{4a^2-b^2}\omega_1 & i = 6 \end{cases} \tag{7.19}$$

where the subscript i from 1 to 6 in ω_{3i} indicates the number of the motion branches. Here the angular velocity ω_3 is arbitrarily chosen and we can also choose other angular velocities as the argument. Plotting the curves defined by the functions in Equation (7.19) in a coordinate system, the following figure with curves of angular velocities can be attained.

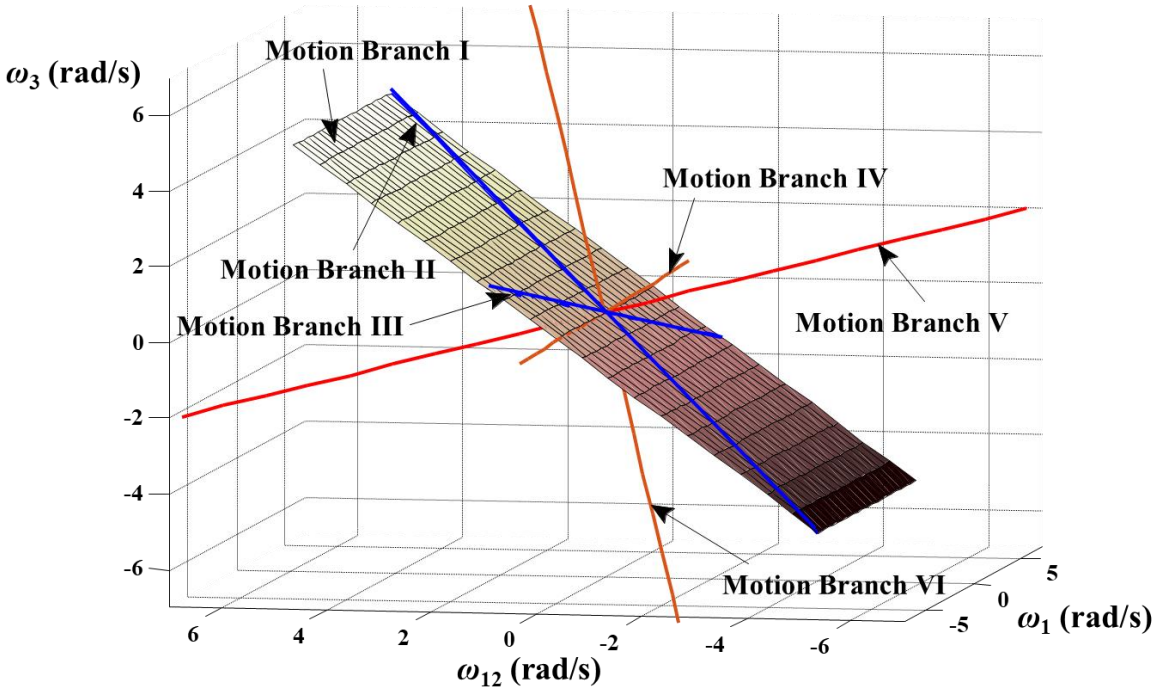

Figure 7.15 Multifurcation represented by angular velocities

In this figure, lines in red and blue colour indicate the corresponding motion branches have mobility one and the plane for motion branch I means it has mobility two. All lines and the plane intersect at a point and this indicates the configuration spaces of all motion branches intersect at the singularity configuration.

When the mechanism moves to the singularity configuration, the mechanism will divide into six motion branches and this is coined *multi-furcation* of mechanism. The

mechanism can switch its motion branch when going through the intersection point and this point can thus be coined *constraint singularity*. Figure 7.16 gives the correspondence between the curves of angular velocities and the configuration of the motion branches.

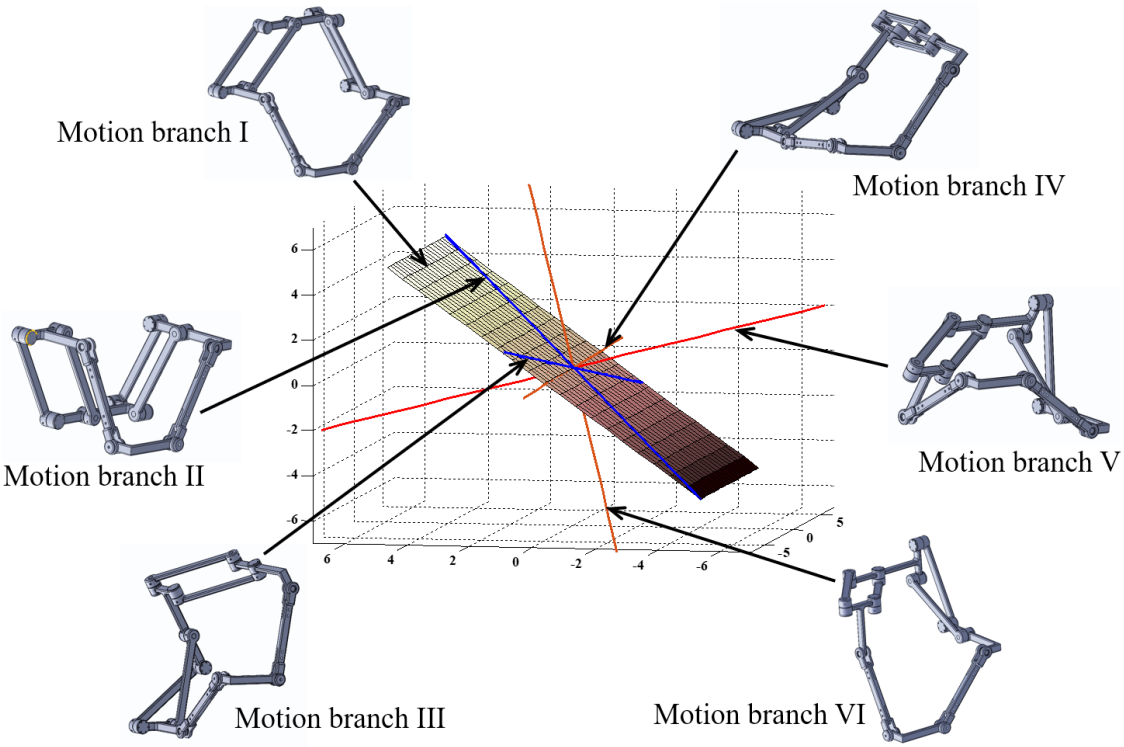

Figure 7.16 Correspondence between the curves of angular velocities and the configuration of the motion branches

7.6.2. Numerical Validation of the Solutions to the Constraint System

An arbitrary trajectory given to ω_1, we can get the results of other angular velocities when the mechanism is at the singularity configuration from the Equations from (7.7) to (7.11) and these calculations have been presented in Figure 7.15. On the other hand, we can implement the kinematics simulation for every motion branch one by one to collect the information of the angular velocities.

Since the relationship between angular velocities in motion branches I and II are rather simple, this section only does the simulation for motion branches from III to VI. This section uses the commercial software module Solidworks Motion to implement the kinematics simulation for the motion branches. The results can be given by the following Figure 7.17.

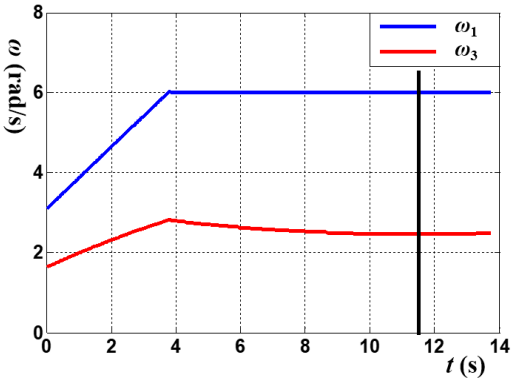

Motion branch III

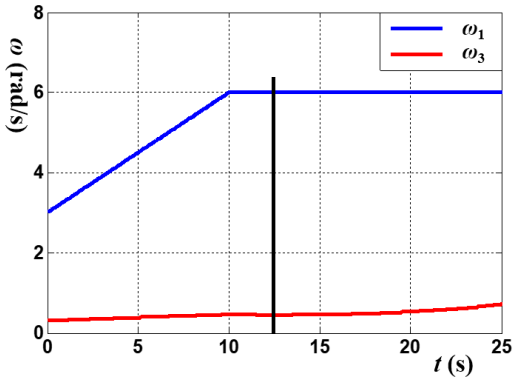

Motion branch IV

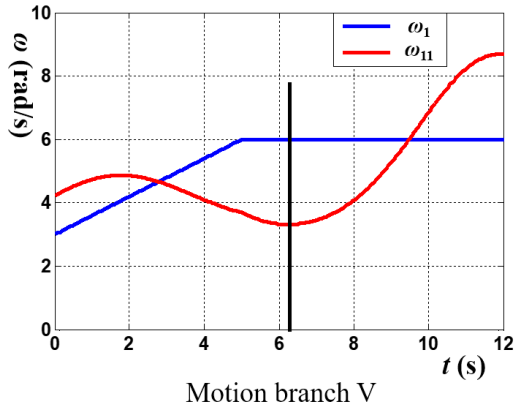

Motion branch V

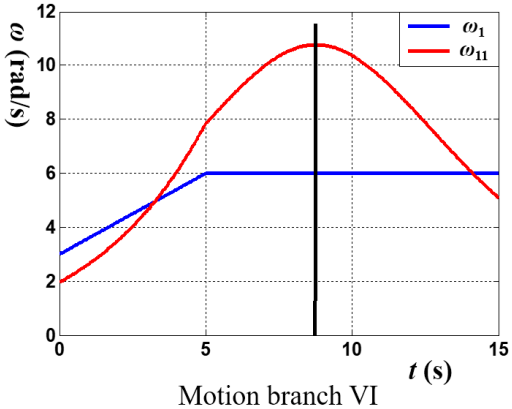

Motion branch VI

Figure 7.17 Numerical validation of motion branches from III to VI

The above curves reveal the numerical results of ω_3 in motion branches III and IV and ω_{11} in motion branches IV and V and these results are presented by curves in red colour in the above figures. The vertical line in the figures gives the moment when the mechanism moves through the singularity configuration and hence the angular velocities at that moment can be attained. Through comparison between the results of the angular velocity at singularity configuration calculated by the solutions in Section 6.4 and by simulation in Solidworks Motion, it can be validated that the two results coincide with each other precisely and this proves the validation of the solutions to the constraint system.

7.7 Conclusions

This chapter for the first time revealed the six motion branches of the derivative queer-square mechanism. Though reference [1] gave 14 motion states of the same mechanisms, this dissertation found 12 of the 14 motion states can be regarded as six motion branches because there are 6 six solutions for sure to the constraint system of the mechanism. In fact, different motion ranges of the same motion branch were seen as different motion states in reference [1]. However, this chapter found the other 2 of the 14 motion states cannot go through the same singularity configuration we were focusing on, so it should be eliminated from the motion branch classification.

After attaining six motion branches by solving the constraint system of the derivative queer-square mechanism, this chapter presented the prototype of each single motion branch and implemented numerical simulation in the commercial software module Solidworks Motion and it was verified that the results of angular velocities obtaining from the solutions to the constraint system coincided precisely with the simulation results. This chapter has shown the effectiveness of the screw-algebra approach together with the bilinear form representations of constraints in recognising the multi-furcation in complicated multi-loop mechanisms.

Chapter 8 Compositional Submanifold Analysis of Mechanisms

8.1 Introduction

The kinematic chains that generate the planar motion group in which the prismatic-joint direction is always perpendicular to the revolute-joint axis have shown their effectiveness in type synthesis and mechanism analysis in parallel mechanisms. This chapter extends the standard PRP (Prismatic-Revolute-Prismatic) kinematic chain generating the planar motion group to a relatively generic case by means of the equivalence of screw spaces as the tangent spaces of compositional submanifolds, in which one of the prismatic joint-directions is not necessarily perpendicular to the revolute-joint axis, leading to the discovery of a pseudo-helical motion with a variable pitch in a kinematic chain. The displacements of such a PRP chain generate a submanifold of the Schoenflies motion subgroup. This chapter investigates for the first time this type of motion that is the variable-pitched pseudo-planar motion described by

the above submanifold. The motion representation of a PRP-schoenflies parallel mechanism is presented in this chapter.

8.2 Compositional Submanifolds and Lie Subgroups

This section is to retrieve several fundamental concepts on Lie groups and composition of submanifolds, paving a way for using a composition of submanifolds in the context of Lie group to perform bifurcation analysis of a 3-PUP parallel mechanism.

A subset of the rigid motion group SE(3) is denoted by $C \subseteq SE(3)$. A submanifold M of SE(3) can be regarded as a subset of SE(3) endowed with the smooth group operations and denoted as $M \subseteq$ SE(3). If the closure under composition is satisfied by M, a subgroup S of SE(3) can be obtained and written as $S \leq$ SE(3). Table 1 enlists the subgroups of SE(3) and presents the notation to be used in this dissertation.

The composition of subsets is the binary operation $\circ : P(\mathrm{SE}(3)) \times P(\mathrm{SE}(3)) \rightarrow P(\mathrm{SE}(3))$, where P(SE(3)) is the power set of SE(3). Such that, for any $A, B \in P(\mathrm{SE}(3))$:

$$A \circ B = \{ab \mid a \in A, b \in B\} \in P(\mathrm{SE}(3)) \tag{8.1}$$

where A and B are not necessarily subgroups of SE(3), even if A and B are subgroups, $A \circ B$ is in general not a subgroup of SE(3). Therefore $A \circ B$ can be referred to as *compositional submanifold* to indicate the general case in which the result is not a

subgroup. The composition of subsets is associative but not commutative. In fact, $A \circ B$ is a subgroup of SE(3) if and only if $A \circ B = B \circ A$.

Table 8.1 List of subgroups of SE(3). When applied, L($\hat{\boldsymbol{x}}$, Q) denotes a line that is parallel to $\hat{\boldsymbol{x}}$ and contains Q.

Dimension	Name	Description
0	{e}	The trivial set containing only the identity of SE(3)
1	$T(\hat{\boldsymbol{x}})$	The set of translations along a straight line parallel to $\hat{\boldsymbol{x}}$
1	$R(Q,\hat{\boldsymbol{x}})$	The set of rotations about a fixed axis L($\hat{\boldsymbol{x}}$, Q)
1	$H(Q,\hat{\boldsymbol{x}},h)$	The set of helical displacements with fixed pitch h and fixed axis L($\hat{\boldsymbol{x}}$, Q)
2	$T(\hat{\boldsymbol{x}}_1, \hat{\boldsymbol{x}}_2)$	The set of translations in a plane that contains $\hat{\boldsymbol{x}}_1$ and $\hat{\boldsymbol{x}}_2$
2	$C(Q,\hat{\boldsymbol{x}})$	The set of cylindrical displacements: rotations about the fixed axis L($\hat{\boldsymbol{x}}$, Q) and translations along a straight line parallel to $\hat{\boldsymbol{x}}$.
3	T	The set of spatial translations.
3	$G(\hat{\boldsymbol{x}})$	The set of general planar displacements: translations in a plane perpendicular to $\hat{\boldsymbol{x}}$ and rotations about an axis parallel to $\hat{\boldsymbol{x}}$.
3	$S(Q)$	The set of spherical displacements: rotations about any axis containing Q.
3	$Y(\hat{\boldsymbol{x}}, h)$	The set of translations in plane perpendicular to $\hat{\boldsymbol{x}}$ and helical motions with pitch h and axis parallel to $\hat{\boldsymbol{x}}$.
4	$X(\hat{\boldsymbol{x}})$	The set of Schoenflies displacements: transitions in space and rotations about an axis that is parallel to $\hat{\boldsymbol{x}}$.

6	SE(3)	The improper subset containing the whole Euclidean group.

In an n-link kinematic chain the *kinematic bond* or *mechanical liaison* between links i and j, $i<j\in\{1,\ldots,n\}$, $L(i,j) \in P(\mathrm{SE}(3))$ is the set of all possible Euclidean displacements between links i and j. In such a case, if the kinematic chain is constructed purely by revolute, prismatic and helical joints, the kinematic bond between links i and j can be obtained by:

$$L(i,j) = A_{i,i+1} \circ A_{i+1,i+2} \circ \ldots \circ A_{j-1,j} \in P(\mathrm{SE}(3)) \tag{8.2}$$

where $A_{k,k+1} \leq \mathrm{SE}(3)$, $k = i \ldots j\text{-}1$, is the subgroup of all possible displacements between adjacent links k and $k+1$ which are joined by a 1-DOF kinematic pair and thus $A_{k,k+1}$ is a subgroup of SE(3).

In mechanism analysis and kinematics, the displacement of the end-effector of an open kinematic chain can be completely described by the concepts related to the composition of submanifolds in the above. An illustrative example is given by employing a PRP kinematic chain in Figure 8.1. In this PRP chain, the two prismatic joints are lying in the plane π perpendicular to the axis of the revolute joint. Each single joint in this kinematic chain generates a subgroup of SE(3). The corresponding tangent space of the manifold of a kinematic joint at the identity can be presented by the axis and type of the joint. In that case, the displacement of the end effector of the PRP chain can be represented by a compositional submanifold M constituted by the subgroups M_1, M_2, and M_3 of the kinematic joints which represents the kinematic bond between the fixed link and the end effector.

Further, it is possible to use various bases to represent the tangent space at the identity of the composition submanifold M by applying a linear transformation to the current basis generating such tangent space. Since the kinematic bond between the end effector and the fixed link of the kinematic chain in Figure 8.1 is the subgroup of general planar displacements $G(\widehat{\boldsymbol{k}})$, it is possible to apply linear transformations to the current basis of the tangent space at identity to obtain equivalent kinematic chains. The kinematic equivalence is ensured not only instantaneously but also under finite displacements since the kinematic bond is a subgroup, and thus its tangent space at the identity is a subalgebra of se(3). The equivalent kinematic chains of the PRP chain can be obtained as PRP, PPR(Prismatic-Prismatic-Revolute), RPR(Revolute-Prismatic-Revolute), PRR(Prismatic-Revolute-Revolute), and RRR(Revolute-Revolute-Revolute) kinematic chains in which the direction of the prismatic joint axis is always perpendicular to the axis of the revolute joint in each chain.

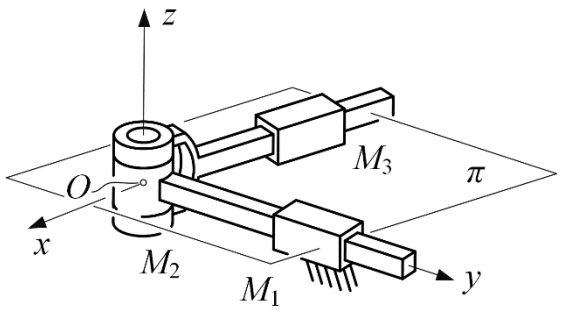

Figure 8.1 PRP chain and the related submanifolds.

8.3 Tangent Spaces of Compositional Submanifolds Generated by Screws

A *complex* of the rigid motion group SE(3) can be defined as a subset of elements of SE(3) and coined $C \subseteq \mathrm{SE}(3)$. With the concept of the complex of SE(3), a submanifold M of SE(3) can be regarded as a complex of SE(3) attached with the smooth group operations and we coin it $M \leq \mathrm{SE}(3)$. If the closure property is satisfied for M, a subgroup S of SE(3) can be obtained and written as $S \leq \mathrm{SE}(3)$. Alternatively, a subgroup of SE(3) can be directly obtained from a complex of SE(3) in the case the group axioms are fulfilled for the complex.

The product $C_1 \cdot C_2$ of two complexes C_1, C_2 of $SE(3)$ is defined as the subset $C=\{c_1 \cdot c_2: c_1 \in C_1, c_2 \in C_2\}$ in which the product is the group multiplication of SE(3). Similar with the definition of the submanifold of SE(3) in the above, if integrating smooth group operations with the subset C attaining from the product of two complexes, the submanifold M of SE(3) can be obtained from the subset C and it is coined *compositional submanifold* or *product submanifold* in this dissertation. It is not difficult to prove that M is the product of two submanifolds M_1, M_2 growing from the complexes C_1, C_2. It is noteworthy that the product operation in the product submanifold is distinctive with the product in the concept of product submanifold in the theory of differential manifolds. The former product is nothing more than the group multiplication of SE(3), while the latter product refers to the direct product or the Cartesian product of two submanifolds.

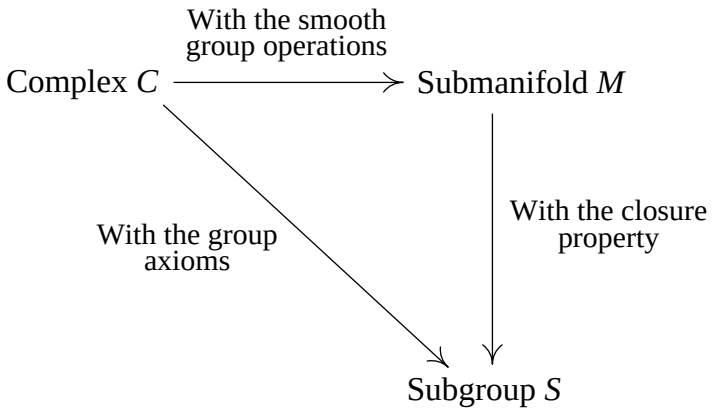

Figure 8.2 The relationship among the complex, submanifold, and subgroup of se(3)

If more strictly, let the two complexes C_1, C_2 fulfil the group axioms, then two subgroups S_1, S_2 are given. The product of subgroups S_1, S_2 of SE(3) does not necessarily gives another subgroup unless the closure property is satisfied for the resultant subset of the product, but usually gives an product submanifold according to the above definitions. In the same manner we can derive the product of three or more submanifolds or subgroups to generate a product submanifold of SE(3).

In kinematics, the product submanifold is in fact a mathematical representation for the well-known kinematic bond put forward by Hervé.

In certain instances, the tangent space of a product submanifold plays an essential role in mechanism analysis. From the differential geometry, the tangent space of a product submanifold is equivalent to the product of the tangent spaces of the submanifolds. Let M_1, M_2, … , M_n be a sequence of differential manifolds of dimension d_1, d_2, … , d_n respectively, a product submanifold M of dimension $(d_1 + d_2 + ... + d_n)$ can be obtained by taking the product of these manifolds and can be denoted as $M = M_1 \times M_2 \times \ldots \times M$

$_n$. Hence, manifolds M_1, M_2, … , M_n come as submanifolds of M. As to the tangent spaces of product submanifold and its submanifolds, we have an isomorphism as follows

$$\phi : \mathrm{T}_p M \to \mathrm{T}_{p1} M_1 \times \mathrm{T}_{p2} M_2 \times \cdots \times \mathrm{T}_{pn} M_n \tag{8.3}$$

in which p_1, p_2, … , p_n are the projections of p on M_1, M_2, … , M_n respectively. That is to say, the tangent space of a product submanifold is equivalent to the product of the tangent spaces of the corresponding submanifolds. Considering the exponential map between a manifold with its tangent space, the relationship amongst the product submanifold of the submanifolds and the related tangent spaces can be described by a commutative diagram in Figure 8.3.

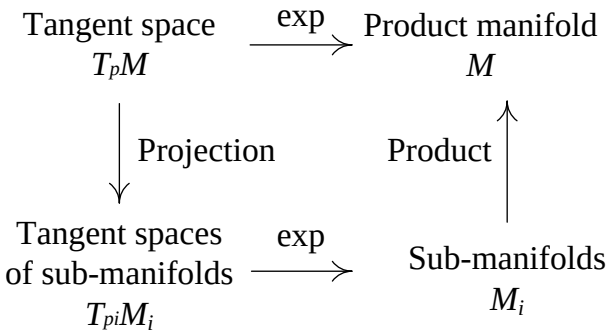

Figure 8.3 A commutative diagram for the product submanifold, the submanifolds, and the related tangent spaces

From Figure 8.3, a submanifold of $SE(3)$ can be obtained through two approaches, in which one is to take the product of its submanifolds to gain a product submanifold, and the other is to obtain its tangent space followed by taking the exponential map of the tangent space.

8.4 Motion Representation of a Tilting-Angled PRP Chain as a Subset of the Schoenflies Motion Subgroup

The planar motion group SE(2) can be achieved by five types of kinematic chains. This section is to prove the particular PRP kinematic chain with a tilting angle in Figure 8.4(a) that is instantaneously equivalent to the chain PRH(Prismatic-Revolute-Helical) kinematic chain shown in Figure 8.4 (b), in which a helical joint is involved to compensate for the tilting angle. In other words, the chain PRP with a tilting angle receives a pseudo-helical motion due to the tilting angle compared with a standard PRP chain.

Let $M(\hat{\boldsymbol{s}}, \alpha) \triangleq L(1,4)$ be the kinematic bond between the end-effector and the fixed link in the PRP kinematic chain in Figure 8.4(a). Then,

$$\exp(m_1E_4)\exp(\theta(E_3+m_1E_5))\exp(m_2(\cos\alpha\cos\theta E_4+\cos\alpha\sin\theta E_5+\sin\alpha E_6)) \in M(\hat{\boldsymbol{s}}, \alpha) \tag{8.4}$$

where $\hat{\boldsymbol{s}}$ coincides with z-axis, representing a normal vector of plane π of the kinematic chain, and scalars θ, m_1 and m_2 indicate the amplitudes of the revolute joint and the two prismatic joints respectively. In this dissertation, E_i, i=1,…,6, form a standard basis for

the Lie algebra se(3) of SE(3), E_1, E_2, and E_3 representing the rotations about x-, y-, and z-axis respectively, and E_4, E_5, and E_6 representing the translations along the three axes respectively.

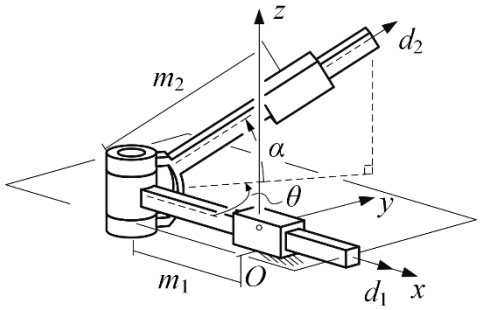

(a) PRP chain with a tilting angle α

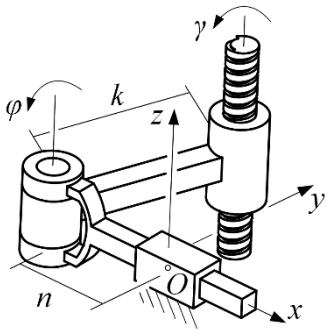

(b) PRH kinematic chain

Figure 8.4 Geometrical structures of the PRP chain with a tilting angle and the PRH chain.

Considering the open kinematic chain of Figure 8.4(a), the basis $\{S_1, S_2, S_3\}$ for the tangent space of the manifold $M(\hat{\boldsymbol{s}}, \alpha)$ at identity can be written as follows:

$$\begin{aligned} &S_1 = E_4, \quad S_2 = E_3 + m_1 E_5, \\ &S_3 = \cos\alpha\cos\theta E_4 + \cos\alpha\sin\theta E_5 + \sin\alpha E_6 \end{aligned} \tag{8.5}$$

Now consider $M^*(\hat{\boldsymbol{s}}, h) \triangleq L(1,4)$ be the kinematic bond between the end-effector and the fixed link in the PRP kinematic chain in Figure 8.4 (b). Then,

$$\exp(nE_4)\exp(\varphi(E_3+nE_5))\exp(\gamma(E_3+k\sin\varphi E_4+(n-k\cos\varphi)E_5+hE_6)) \in M^*(\hat{\boldsymbol{s}}, h) \quad (8.6)$$

where scalars φ, n and γ indicate the amplitudes of the prismatic joint, revolute joint and helical joint respectively, h is the pitch of the helical joint, and k is the distance between the revolute joint and the helical joint. Hence, the tangent space at the identity, $T_eM^*(\hat{\boldsymbol{s}}, h)$, of the displacement manifold produced by the PRH kinematic chain can be generated by the following basis

$$\begin{aligned} &V_1 = E_4, \quad V_2 = E_3 + nE_5, \\ &V_3 = E_3 + k\sin\varphi E_4 + (n - k\cos\varphi)E_5 + hE_6 \end{aligned} \quad (8.7)$$

Comparing Equation (7.5) with Equation (7.7) and simply using elementary operations for matrices, the basis $\{V_1, V_2, V_3\}$ can be transformed into the basis $\{S_1, S_2, S_3\}$ by the following linear transformation

$$\begin{bmatrix} V_1 \\ V_2 \\ V_3 \end{bmatrix} = \begin{bmatrix} 1 & 0 & 0 \\ 0 & 1 & 0 \\ \dfrac{k\cos(\varphi-\theta)}{\sin\theta} & 1 & \dfrac{-k\cos\varphi}{\cos\alpha\sin\theta} \end{bmatrix} \begin{bmatrix} S_1 \\ S_2 \\ S_3 \end{bmatrix} \quad (8.8)$$

where we take $m_1=n$ and the variable pitch of the pseudo-helical motion is derived as

$$h = -k \tan\alpha \frac{\cos\varphi}{\sin\theta} \tag{8.9}$$

It should be noted that the pitch of the pseudo-helical motion included in $M^*(\hat{\boldsymbol{s}}, h)$ is a variable, rather than a constant scalar which can be expressed by a mechanical helical joint. Instantaneously, the motion of kinematic chain in Figure 8.4(a) is equivalent to that of the kinematic chain in Figure 8.4(b). Since $M(\hat{\boldsymbol{s}},\alpha)$ is not a subgroup of SE(3), this equivalence does not hold for finite displacements and $M(\hat{\boldsymbol{s}},\alpha) \neq M^*(\hat{\boldsymbol{s}}, h)$. Other instantaneously-equivalent generators can be found by means of the change of basis, for example HRH(Helical-Revolute-Helical) kinematic chain.

A point in the end effector of the skewed PRP kinematic chain generating $M(\hat{\boldsymbol{s}},\alpha)$ describes a family of one-sheet hyperboloids whose centers can translate along a straight line. Each hyperboloid is generated by the composition of the second and third kinematic pairs, an RP chain, and each center of the hyperboloid lies in a line parallel to the first prismatic pair. This gives a total of ∞^3 points, in concordance with the dimension of $M(\hat{\boldsymbol{s}},\alpha)$. The end effector undergoes a rotation about the axis of the hyperboloid, such rotation is dependent of its position in the hyperboloid.

A simpler way of describing $M(\hat{\boldsymbol{s}},\alpha)$ is thinking of it as $G(\hat{\boldsymbol{s}})$ adding a translation through $\hat{\boldsymbol{s}}$, which is dependent of $G(\hat{\boldsymbol{s}})$. However, unlike in $Y(\hat{\boldsymbol{s}},h)$, this dependence is not related to the rotational component of $G(\hat{\boldsymbol{s}})$. If $G(\hat{\boldsymbol{s}})$ is generated by a PRP chain, then the translation through $\hat{\boldsymbol{s}}$ is given is by $(\tan\alpha)s$, where s is a displacement of the final P joint, this relationship is linear, in a similar way that the translation through $\hat{\boldsymbol{s}}$ in $Y(\hat{\boldsymbol{s}},h)$ is linearly dependent on the rotation about $\hat{\boldsymbol{s}}$. It can be seen that due to this translation

the smallest subgroup containing $M(\hat{\boldsymbol{s}},\alpha)$ is the 5-dimensional subgroup of Schoenflies displacements, $X(\hat{\boldsymbol{s}})$.

8.5 Motion Representation of a PRP-Schoenflies Parallel Mechanism

Since a PRP chain with tilting angle is a generator of the $M(\hat{\boldsymbol{s}},\alpha)$ submanifold of the Schoenflies motions subgroup, $X(\hat{\boldsymbol{s}})$, it is possible to build a parallel manipulator whose end effector motions generates $M(\hat{\boldsymbol{s}},\alpha)$. Such manipulator can be obtained by taking the skewed PRP chain with tilting angle as a limb and other two limbs that generate manifolds of the Shoenflies motion.

An example of such a mechanism is shown in Figure 8.5. The two generators of the Schoenflies motions subgroup are the limbs 2 and 3, which are RPC and RCH(Revolute-Cylindrical-Helical) chains respectively. In limb 2 the axes of the C and R joints are parallel to $\hat{\boldsymbol{u}}$ and the direction of P joint axis is perpendicular to $\hat{\boldsymbol{u}}$. In limb 3 the axes of the three joints are parallel to $\hat{\boldsymbol{u}}$. Permutation of the joints in these two limbs is allowed. These two limbs can be replaced by any other mechanical generator of the Schoenflies subgroup of motions.

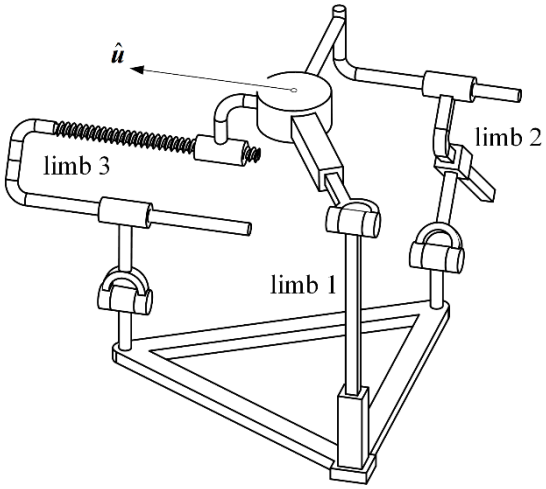

Figure 8.5 The 3-DOF PRP-Schoenflies parallel mechanism

The manifold generated by the possible displacements of the moving platform with respect to the fixed platform is the intersection of three manifolds generated bylimbs. Since $M(\hat{\boldsymbol{u}},\alpha)$ is a submanifold of $X(\hat{\boldsymbol{u}})$, then the manifold of displacements of the moving platform with respect to the fixed one is

$$\mathrm{M}_1 \cap \mathrm{M}_2 \cap \mathrm{M}_3 = M(\hat{\boldsymbol{u}},\alpha) \cap X(\hat{\boldsymbol{u}}) \cap X(\hat{\boldsymbol{u}}) = M(\hat{\boldsymbol{u}},\alpha). \tag{8.10}$$

Therefore, this parallel mechanism is able to generate exactly the same submanifold of the skewed PRP kinematic chain with a tilting angle. The parallel mechanism has 3 degrees of freedom since no passive degree of freedom is present in the limbs. The three limbs allow to control each degree of freedom using each limb.

8.6 Conclusions

Serial chains with kinematic equivalence that generate the same Lie subgroups of SE(3) play an essential role in mechanism synthesis and analysis. By introducing the concept of computational submanifolds of SE(3) with its tangent spaces and the relevant products, this chapter extended the standard PRP kinematic chain producing the planar motion subgroup SE(2) to a relatively generic kinematic chain in which the prismatic-joint direction is not necessary to be perpendicular to the revolute-joint axis. To the knowledge of the candidate, although such a PRP kinematic chain has been investigated in [39][66] through screw systems, the type of motion described by this skewed PRP kinematic chain is not included in previous dissertations or books dealing with submanifolds of SE(3) that are not subgroups. Finally, this chapter ended up with investigating the motion representation of a PRP-schoenflies parallel mechanism.

Chapter 9 Bifurcation Analysis of a 3-PUP Parallel Mechanism

9.1 Introduction

Following the extraction of a pseudo-helical motion from the skewed PRP kinematic chain in Chapter 7, this chapter investigates the bifurcated motion in a 3-PUP parallel mechanism by changing the active geometrical constraint in its configuration space. The representation of motion of the 3-PUP parallel mechanism and its motion branches will be derived using computational submanifolds of $SE(3)$. An experimental test is set up based on a 3D printed prototype of the 3-PUP parallel mechanism to detect the inconspicuous translation of the pseudo-helical motion.

9.2 Geometrical Structure of the 3-PUP Parallel Mechanism

The elementary concept of Lie group and product submanifold in chapter 8 is to be applied in the displacement and mobility analysis of a parallel mechanism with bifurcated motion by exploring the characteristics of the displacement of a 3-PUP parallel mechanism.

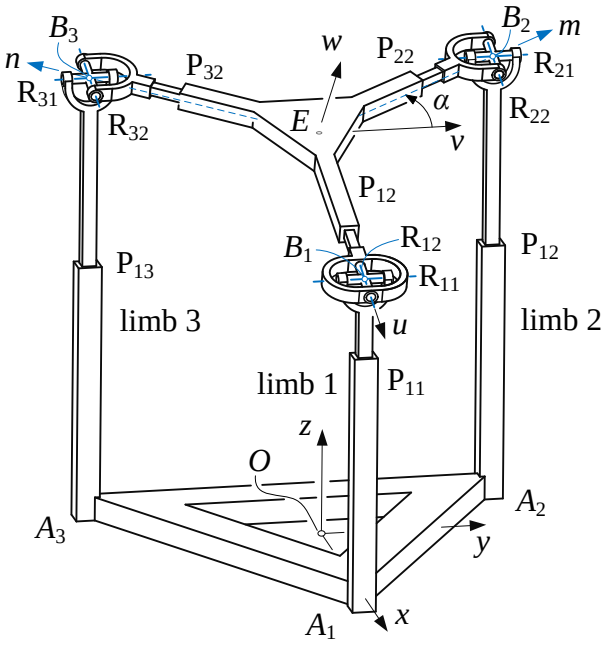

Figure 9.1 The 3-PUP Parallel Mechanism

As illustrated in Figure 9.1, the 3-PUP parallel mechanism contains three PUP limbs denoted as limb i (i=1, 2, 3) where U represents the Hook joint. In each limb, the prismatic joint of the limb labelled as P_{i1} is perpendicular to the base and is called base-prismatic joint. The three base-prismatic joints are symmetrically distributed, and thus constitute an equilateral triangle $A_1A_2A_3$ attached with the base. The rotation axes in

three Hook joints U_i allocated respectively at each joint between a limb and the platform form two sets of rotation axes R_{i1} and R_{i2}, where the first subscript indicates the limb number and the second subscript indicates the set number. In this arrangement, the same set rotation axes in three limbs respectively are parallel to each other. Three rotation axes R_{i1} are parallel with A_2A_3. For three platform-prismatic joints P_{i2} on the platform, P_{12} corresponding to limb 1 is collinear with the rotation axis of R_{12} while P_{22} and P_{32} have an angle α with R_{22} and R_{32} respectively.

As in Figure 9.1, a global reference frame $\{O\text{-}xyz\}$ is located at the central point O of triangle $A_1A_2A_3$ with its x-axis passing through point A_1 and y-axis parallel with A_2A_3, while a local reference frame $\{E\text{-}uvw\}$ is attached to the platform with its origin at the central point E of the platform, u-axis going through the point B_1, and v-axis parallel with B_2B_3.

In the global reference frame, the three base-prismatic joints P_{i1} are in the direction of the z-axis and the first set of revolute joint R_{i1} in the three hook joints directs towards the y-axis. In the local reference frame, the second set of revolute joints in the three hook joints is lying in the direction of the u-axis and the revolute joint R_{12} is in the direction of the u-axis, while the revolute joints R_{22} and R_{23} form an angle α with v-axis. Hence, the joints in limb 1 from the base to the platform can be written as $P(\boldsymbol{z})$, $U(B_1, \boldsymbol{y}, \boldsymbol{u})$, and $P(\boldsymbol{u})$, in which the prismatic joint is represented by a direction vector and the hook joint by two direction vectors perpendicular to each other together with the point where the axes of the two revolute joints intersect. In such a case, the joints in limb 2 can be denoted as $P(\boldsymbol{z})$, $U(B_2, \boldsymbol{y}, \boldsymbol{u})$, and $P(\boldsymbol{m})$; the joints in limb 3 can be denoted

as $P(\boldsymbol{z})$, $U(B_3, \boldsymbol{y}, \boldsymbol{u})$. Vector $\boldsymbol{m}$ and $\boldsymbol{n}$ are the position vectors from origin E to point B_2 and B_3 respectively.

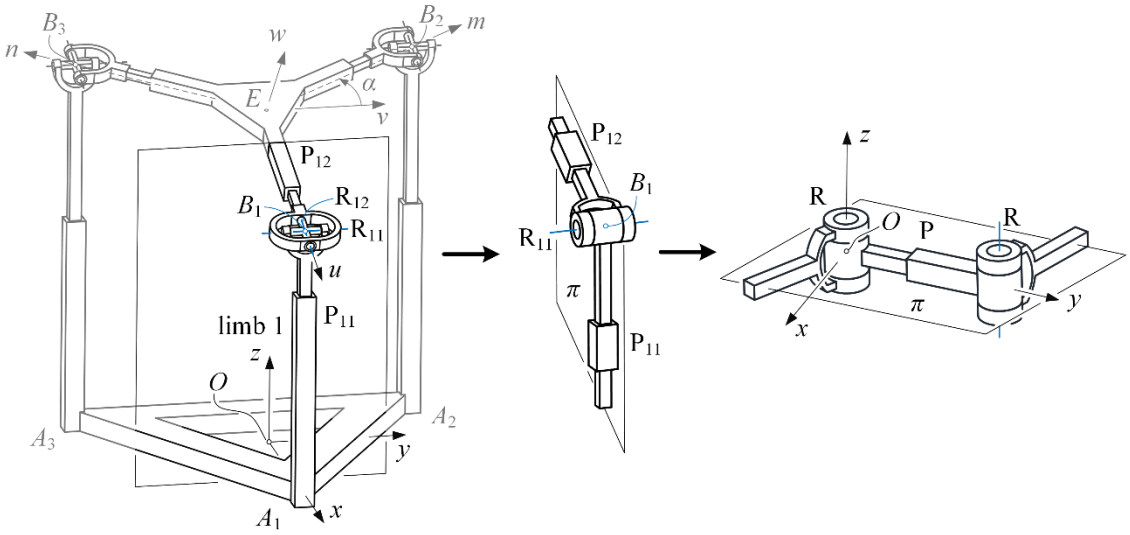

Figure 9.2 The PRP Chain Extracted from Limb 1 and Its Equivalent RPR Chain

As in Figure 9.2, a PRP chain in which two prismatic joints lie in a plane perpendicular to the revolute-joint axis can be extracted from limb 1 of the 3-PUP parallel mechanism. This is one of the kinematic chains that generate the planar motion group SE(2). According to the description this chapter, chain PRP in limb 1 and chain RPR are said to be equivalent with each other. If we switch these two chains, the displacement and mobility of the platform of the 3-PUP parallel mechanism do not change as both of the two kinematic chains generate the same product submanifold, strictly the planar motion group SE(2). Such a sort of kinematic equivalence brings benefits to this dissertation because the displacement submanifold of the platform of the 3-PUP parallel mechanism can be derived by means of finding out the kinematic equivalence chains of particular chains.

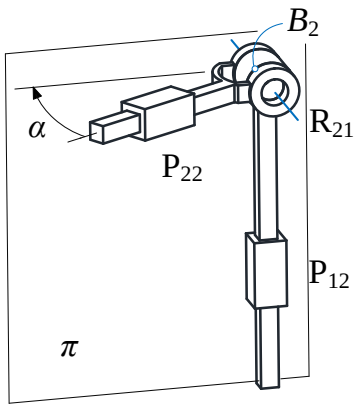

Figure 9.3 The PRP Chain with an Offset Angle Extracted From Limb 2

Likewise, a PRP chain with an offset angle α can be obtained from limb 2 as illustrated in Figure 9.3. This particular PRP chain can be regarded as a variation of PRP chain in Figure 8.1 and there is no difference between them other than the offset angle α. However, the two kinematic chains are distinctive in kinematics because the PRP chain with an offset angle generates a 2-dimensional submanifold of $SE(3)$ and thus cannot generate the planar motion group $SE(2)$ anymore due to the existence of the offset angle α. Finding out the equivalence manifold of this submanifold to obtain submanifold of the platform of the 3-PUP parallel mechanism is an essential issue of this dissertation and is to be further investigated in the following sections.

9.3 Manifold Representation of The PUP Motion and the Parallel Mechanism

In a 3-PUP parallel manipulator (Figure 9.1) the three base-prismatic joints P_{i1} are in the direction of $\boldsymbol{k}(z)$ and the first set of revolute joints R_{i1} in the universal joints directs towards the $\boldsymbol{k}(z)$ of the global fixed frame. In the local reference frame, the second set of revolute joints in the three universal joints is lying in the direction of the u thus the revolute joint R_{12} is in the direction of the u, while the revolute joints R_{22} and R_{32} form an angle α with v. Hence, the joints in limb 1 from the base to the platform can be written as $P(\hat{\boldsymbol{k}})$, $U(B_1, \hat{\boldsymbol{j}}, \hat{\boldsymbol{u}})$, and $P(\hat{\boldsymbol{u}})$, in which the prismatic joint is represented by a direction vector and the universal joint by two direction vectors perpendicular to each other together with the point where the axes of the two revolute joints intersect. In such a case, the joints in limb 2 can be denoted as $P(\hat{\boldsymbol{k}})$, $U(B_2, \hat{\boldsymbol{j}}, \hat{\boldsymbol{u}})$, and $P(\hat{\boldsymbol{m}})$; the joints in limb 3 can be denoted as $P(\hat{\boldsymbol{k}})$, $U(B_2, \hat{\boldsymbol{j}}, \hat{\boldsymbol{u}})$, and $P(\hat{\boldsymbol{n}})$. Vector $\hat{\boldsymbol{m}}$ and $\hat{\boldsymbol{n}}$ are the unit vectors in the direction of EB_2 and EB_3, respectively.

As shown in Figure 8.1, a standard PRP chain in which two prismatic joints lie in a plane perpendicular to the revolute-joint axis can be extracted from limb 1 of the 3-PUP parallel mechanism. This is one of the kinematic chains that generate the planar motion group SE(2).

As in Figure 9.4, the submanifolds generated by the kinematic joints in limb 1 and can be expressed as $T(\hat{\boldsymbol{k}})$, $R(B_1, \hat{\boldsymbol{j}})$, $R(B_1, \hat{\boldsymbol{u}})$ and $T(\hat{\boldsymbol{u}})$, respectively. Based on the related concepts of composition of submanifolds given in chapter 7, the kinematic bond

between the fixed and the moving platforms generated by limb 1 is represented by the compositional submanifold as follows,

$$M_1 = T(\hat{\boldsymbol{k}})R\,(B_1, \hat{\boldsymbol{j}})R\,(B_1, \hat{\boldsymbol{u}})T\,(\hat{\boldsymbol{u}}) \tag{9.1}$$

This presents a compositional submanifold generated by limb 1 that is a pivoting limb of a 3-PUP parallel mechanism.

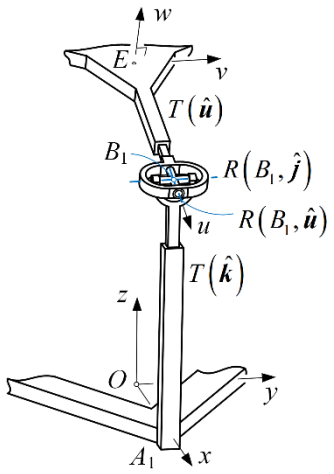

Figure 9.4 The Lie subgroups in limb 1.

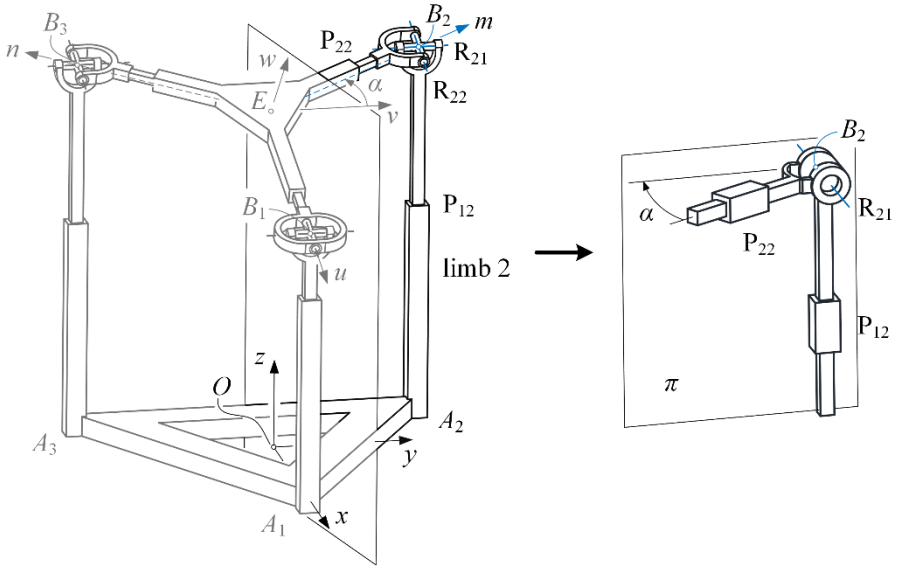

Figure 9.5 The skewed PRP chain with a tilting angle extracted from limb 2.

According to the geometrical structure of the 3-PUP parallel mechanism given in this chapter, the displacement manifolds generated by limb 2 and limb 3 are respectively written as

$$M_2 = T(\hat{\boldsymbol{k}})R\,(B_2, \hat{\boldsymbol{j}})R\,(B_2, \hat{\boldsymbol{u}})T\,(\hat{\boldsymbol{m}}) \tag{9.2}$$

$$M_3 = T(\hat{\boldsymbol{k}})R\,(B_3, \hat{\boldsymbol{j}})R\,(B_3, \hat{\boldsymbol{u}})T\,(\hat{\boldsymbol{n}}) \tag{9.3}$$

It can be seen that M_1, M_2 and M_3 are four-dimensional submanifolds of SE(3).

Since the displacements of the platform of a parallel mechanism are the intersection of displacements of its limbs, the displacement submanifold M of the platform of the 3-PUP parallel mechanism can be represented by the intersection of the submanifolds M_1, M_2 and M_3 in the form of

$$M = M_1 \cap M_2 \cap M_3 \tag{9.4}$$

The displacement subset M is not necessarily a differential manifold due to the fact that it may contain more than one displacement branch. This phenomenon will be further explored. Consequently, the displacements of the platform of the 3-PUP parallel mechanism can be presented using the intersection of three product submanifolds. However, the result of the intersection of the three product submanifolds in Equation (8.4) remains unsolved and it is changeable with respect to the change of the geometrical conditions in configuration space of the 3-PUP parallel mechanism.

9.4 Motion Branches of the 3-PUP Parallel Mechanism

9.4.1 Motion Branch with a Pure Rotation and a Translation

To solve the intersection of the three submanifolds in Equation (8.4), motion branch A of the configuration space of the 3-PUP parallel mechanism can be obtained when the geometrical condition that the rotation axis of revolute joint R_{21} coincides with the rotation axis of revolute joint R_{31} is effective. In this case, the constraint $d_2 = d_3$, where d_2 and d_3 represent the amplitudes of the prismatic joints P_{21} and P_{31} respectively, is a consequence of R_{21} and R_{31} being co-axial. The denotations R_{21}, R_{31}, P_{21} and P_{31} are given in Figure 9.1. Hence, the group equality $R(B_2, \hat{\boldsymbol{j}}) = R(B_1, \hat{\boldsymbol{j}})$ is satisfied, since B_1B_2 is parallel to $\hat{\boldsymbol{j}}$. In this motion branch, the displacement manifold M_{A1} produced by limb 1 can be obtained from Equation (8.4) and derived as follows:

$$M_{A1} = T(\hat{\boldsymbol{k}}) \circ R(B_1, \hat{\boldsymbol{j}}) \circ R(B_1, \hat{\boldsymbol{u}}) \circ T(\hat{\boldsymbol{u}}) = T(\hat{\boldsymbol{k}}) \circ R(B_1, \hat{\boldsymbol{j}}) \circ T(\hat{\boldsymbol{u}}) \circ R(B_1, \hat{\boldsymbol{u}}) = G(\hat{\boldsymbol{j}}) \circ R(B_1, \hat{\boldsymbol{u}}) \tag{9.5}$$

where $R(B_1, \hat{\boldsymbol{u}}) \circ T(\hat{\boldsymbol{u}})$ has commuted to $T(\hat{\boldsymbol{u}}) \circ R(B_1, \hat{\boldsymbol{u}})$, this is allowed since the axes of rotation and translation are parallel. The result, $G(\hat{\boldsymbol{j}}) \circ R(B_1, \hat{\boldsymbol{u}})$, is a 4-dimensional submanifold which was studied by Fanghella and Galletti [81] and Rico [82] et al (see

Table 8.1, row 10)[1]. From such research it is known that $G(\hat{\boldsymbol{j}}) \circ R(B_1, \hat{\boldsymbol{u}})$ contains 3 translations and 2 rotations that are not independent, so that the dimension of this submanifold is four. The smallest subgroup of SE(3) that contains $G(\hat{\boldsymbol{j}}) \circ R(B_1, \hat{\boldsymbol{u}})$ is the improper subgroup SE(3).

For the second and third limb we have:

$$M_{A2} = T(\hat{\boldsymbol{k}}) \circ R(B_2, \hat{\boldsymbol{j}}) \circ R(B_2, \hat{\boldsymbol{u}}) \circ T(\hat{\boldsymbol{m}}) \tag{9.6}$$

$$M_{A3} = T(\hat{\boldsymbol{k}}) \circ R(B_2, \hat{\boldsymbol{j}}) \circ R(B_2, \hat{\boldsymbol{u}}) \circ T(\hat{\boldsymbol{n}}) \tag{9.7}$$

Which are 4-dimensional submanifolds of SE(3). The smallest subgroup containing them is the whole group SE(3). However, both, M_{A2} and M_{A3} are subsets of the double Schoenflies submanifold, $X(\hat{\boldsymbol{j}}) \circ X(\hat{\boldsymbol{u}})$, which was studied by Lee and Hervé [54]. It can be seen that:

$$M_{A2} \cap M_{A3} = T(\hat{\boldsymbol{k}}) \circ R(B_2, \hat{\boldsymbol{j}}) \circ R(B_2, \hat{\boldsymbol{u}}) \tag{9.8}$$

Since intersection is an associative operation it follows that:

$$M_A = M_{A1} \cap M_{A2} \cap M_{A3} = M_{A1} \cap (M_{A2} \cap M_{A3}) = G(\hat{\boldsymbol{j}}) \circ R(B_1, \hat{\boldsymbol{u}}) \cap T(\hat{\boldsymbol{k}}) \circ R(B_2, \hat{\boldsymbol{j}}) \circ R(B_2, \hat{\boldsymbol{u}})$$

$$= T(\hat{\boldsymbol{k}}) \circ R(B_2, \hat{\boldsymbol{j}}) \tag{9.9}$$

[1] In both references $R(B_1, \hat{\boldsymbol{u}}) \circ G(\hat{\boldsymbol{j}})$ was analyzed. Even though the composition of sets is non-commutative, $G(\hat{\boldsymbol{j}}) \circ R(B_1, \hat{\boldsymbol{u}})$ can be analyzed by kinematic inversion, i.e. considering the end-effector as fixed link and the fixed link as end-effector.

In such a case, the feasible mobility of the platform of the 3-PUP parallel mechanism in branch A of the configuration space restricted by the condition $d_2 = d_3$ is a translation along z-axis together with a rotation about the axis R_{21} getting through the point B_2, parallel with y-axis. The displacement of the platform described by the submanifold M_A can be illustrated by the 3D printed prototype given in Figure 9.6.

(a) (b) (c)

Figure 9. 6 Feasible displacements in motion branch A: (a) home configuration (see Sec. 6.3); (b), (c) from the test set up in Section 8.5, the platform is performing pure rotation, without any translation along x- and y-axis.

9.4.2 Motion Branch with a Pseudo-helical motion and a Translation

When the geometrical condition that rotation axes R_{22} and R_{32} are perpendicular to the yz-plane of the global reference frame $\{O\text{-}xyz\}$ is effective (then $\hat{\boldsymbol{u}} = \hat{\boldsymbol{\imath}}$), Eq. (9.8) has a solution. Observe that if R_{22} is parallel to R_{32}, then revolute joints R_{21} and R_{31} must be idle. With such a constraint exerted by the geometrical

structure of the 3-PUP parallel mechanism, the configuration of the parallel mechanism goes into another branch denoted as motion branch B in this dissertation. For the first limb we have the same set of displacements:

$$M_{B1} = T(\hat{\boldsymbol{k}}) \circ R(B_1, \hat{\boldsymbol{j}}) \circ R(B_1, \hat{\boldsymbol{\imath}}) \circ T(\hat{\boldsymbol{\imath}}) = T(\hat{\boldsymbol{k}}) \circ R(B_1, \hat{\boldsymbol{j}}) \circ T(\hat{\boldsymbol{\imath}}) \circ [T(\hat{\boldsymbol{\imath}}) \circ R(B_1, \hat{\boldsymbol{\imath}})] = G(\hat{\boldsymbol{j}}) \circ C(B_1, \hat{\boldsymbol{\imath}}) \quad (9.10)$$

Both limbs are generators of the 3-dimensional submanifold described in chapter 7. To find $M_{B2} \cap M_{B3}$ observe that, if the end effectors of both limbs are rigidly connected the translational component along $\hat{\boldsymbol{\imath}}$, appearing due to the pseudo-helical motion described in Chapter 7, has to be the same for both kinematic chains. Therefore:

$$M_{B2} \cap M_{B3} = M_{-1}(\hat{\boldsymbol{\imath}}, \alpha) = M_{-1}(\hat{\boldsymbol{\imath}}, \pi\text{-}\alpha) \quad (9.11)$$

where $M_{-1}(\hat{\boldsymbol{\imath}}, \beta)$, $\beta = \alpha,\ \pi - \alpha$, indicates a submanifold of $M(\hat{\boldsymbol{\imath}}, \beta)$ whose dimension is 2 and includes the pseudo-helical motion component of $M(\hat{\boldsymbol{\imath}}, \beta)$. Therefore $M_{-1}(\hat{\boldsymbol{\imath}}, \beta)$ includes the pseudo-helical motion of $M(\hat{\boldsymbol{\imath}}, \beta)$ and $T(\hat{\boldsymbol{k}})$, so that:

$$M_{B2} \cap M_{B3} = M_{-1}(\hat{\boldsymbol{\imath}}, \alpha) = T(\hat{\boldsymbol{k}}) \circ M_{-2}(\hat{\boldsymbol{\imath}}, \alpha) = M_{-1}(\hat{\boldsymbol{\imath}}, \pi\text{-}\alpha) = T(\hat{\boldsymbol{k}}) \circ M_{-2}(\hat{\boldsymbol{\imath}}, \pi\text{-}\alpha) \quad (9.12)$$

where $M_{-2}(\hat{\boldsymbol{\imath}}, \beta)$, $(\beta = \alpha,\ \pi - \alpha)$, represents the 1-dimensional submanifold of pseudo-helical motions with variable pitch. Observe that $M_{-1}(\hat{\boldsymbol{\imath}}, \alpha) = M_{-1}(\hat{\boldsymbol{\imath}}, \pi\text{-}\alpha)$ since the translation of both end-effectors, which have been rigidly connected occurs in the x-direction due to the symmetry of the isosceles triangle conformed by the moving platform. If the displacements in this direction have to be the same for both limbs we

have $s_{22}\sin\alpha = s_{32}\sin(\pi-\alpha) \Leftrightarrow s_{22} = s_{32}$, where s_{22} and s_{32} are the displacements of pairs P_{22} and P_{32} respectively, and the translations in the y- direction are cancelled.

It is now straightforward to determine the set of displacements of the moving platform with respect to the fixed platform:

$$M_B = M_{B1} \cap M_{B2} \cap M_{B3} = M_{B1} \cap (M_{B2} \cap M_{B3}) = G(\hat{\boldsymbol{j}}) \circ C(B_1, \hat{\boldsymbol{i}}) \cap T(\hat{\boldsymbol{k}}) \circ M_{-2}(\hat{\boldsymbol{i}}, \pi-\alpha) = T(\hat{\boldsymbol{k}}) \circ M_{-2}(\hat{\boldsymbol{i}}, \pi-\alpha) \quad (9.13)$$

This is due to the fact that $T(\hat{\boldsymbol{k}}) \leq G(\hat{\boldsymbol{j}})$ and $M_{-2}(\hat{\boldsymbol{i}}, \pi-\alpha) \subseteq C(B_1, \hat{\boldsymbol{i}})$. Observe that due to symmetry the axis of rotation of $M_{-2}(\hat{\boldsymbol{i}}, \pi-\alpha)$ passes through E and B_1. It can be concluded that in this branch of motion the parallel platform undergoes a pseudo-helical motion and a pure translation. Revolute joint R_{11} is idle too since the rotational component of $G(\hat{\boldsymbol{j}})$ is lost in the intersection.

Imagine that P_{11} is locked, then the pure translation of the moving platform is lost. If s_{21} and s_{31} are the displacements of prismatic joints P_{21} and P_{31}, respectively, then $d_2 = d_3$. If P_{11} is released and the pure translation is now allowed, then $d_2 + d_1 = d_3 + d_1$, where s_{11} is the displacement of kinematic pair P_{11}. Thus, the geometric constraint for this motion branch is $d_2 + d_3 = 2d_1$

The displacement of the platform described by submanifold M_B can be illustrated by the prototype given in Figure 9.7.

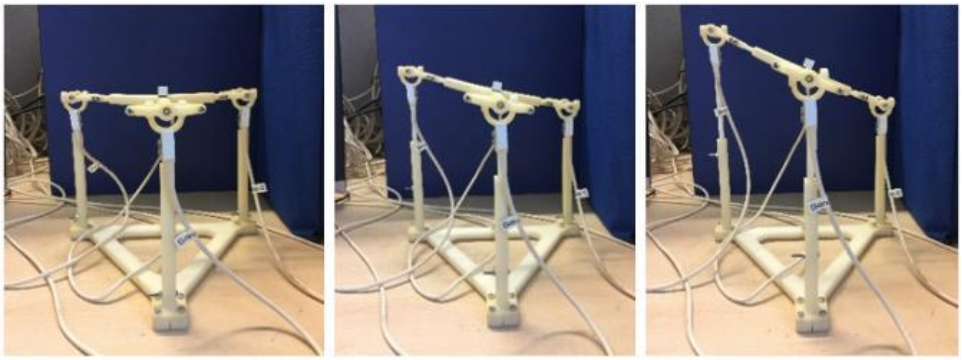

(a) (b) (c)

Figure 9.7 Feasible displacements in motion branch B. (a) home configuration; (b), (c) the photos only illustrate the rotation of the platform, and the translation of the pseudo-helical motion is to be detected in Sec. 7.

9.4.3 Home Configuration and the Bifurcated Motion

The home configuration of the 3-PUP parallel mechanism is a configuration where the two motion branches of the configuration space switch over. In the home configuration, the constraints in motion branches A and B are both effective, due to that the home configuration is also named *constraint singularity* in configuration space.

Note that $M_A \cap M_B = T(\widehat{\boldsymbol{k}})$, therefore there is a continuum of points in the configuration space that are singularities. If coordinate system $\{E\text{-}uvw\}$ coincides with $\{O\text{-}xyz\}$, applying pure translation in the z direction will lead to singular configurations in which it is possible to escape to any of both motion branches. Hence, all these configurations belong to both components of the configuration space and both geometric constraints ($d_2 + d_3 = 2d_1$ and $d_2 = d_3$) are satisfied, therefore, in such continuum of singular

configurations $d_1 = d_2 = d_3$. These properties are summarized in the diagram in Figure 9.8.

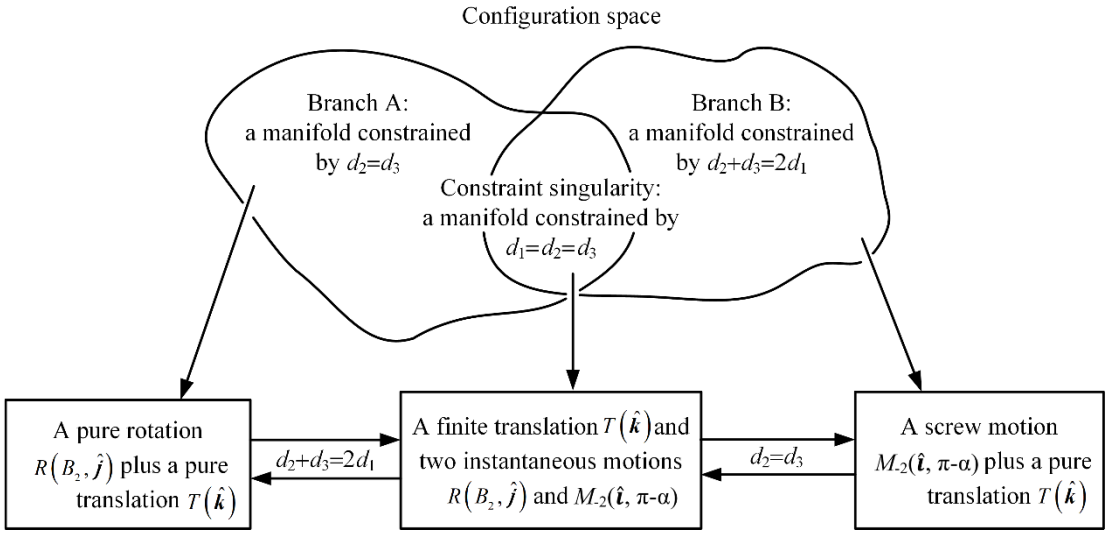

Figure 9.8 Bifurcated motion and constraint singularity in the 3-PUP parallel mechanism.

As in Figure 9.8, the translation of the platform $T(\boldsymbol{z})$, common to branches A and B, is still feasible at home configuration. However, the rotation of the platform $R(B_2, \boldsymbol{y})$, included in motion branch A but not in motion branch B, becomes instantaneous displacement because the constraint space of motion branch A is a proper subset of the constraint space of the home configuration. That is to say, in home configuration the instantaneous rotation $R(B_2, \boldsymbol{y})$ exists since home configuration is a specific case of motion branch A, but this instantaneous rotation $R(B_2, \boldsymbol{y})$ cannot generate any finite motion in home configuration since this rotation is not permitted by the constraints of motion branch B. In a similar way, we can obtain an instantaneous screw motion $M(E, \boldsymbol{u}, h)$ as well in home configuration. Hence, in home configuration determined by the conditions $d_2=d_3$ and $d_2+d_3=2d_1$, i.e. $d_1=d_2=d_3$, the platform of the 3-PUP parallel

mechanism has a finite rotation as $T(\boldsymbol{z})$, an instantaneous rotation as $R(B_2, \boldsymbol{y})$, and an instantaneous screw motion as $M(E, \boldsymbol{u}, h)$. This result can be verified by taking the intersection of three manifolds of limbs under the geometrical constraint $d_1=d_2=d_3$. In this home configuration the displacement manifold M_{C1} generated by limb 1 can be derived as follows

$$\begin{aligned} M_{C1} &= T(\boldsymbol{z})R(B_1, \boldsymbol{y})R(B_1, \boldsymbol{u})T(\boldsymbol{u}) \\ &= T(\boldsymbol{z})\left[T(\boldsymbol{z})R(B_1, \boldsymbol{y})T(\boldsymbol{u})\right]\left[R(B_1, \boldsymbol{u})T(\boldsymbol{u})\right] \\ &= T(\boldsymbol{z})\,PL(\boldsymbol{y})C(B_1, \boldsymbol{u}) \end{aligned} \tag{9.14}$$

where $PL(\boldsymbol{y})$ and $C(B_1, \boldsymbol{u})$ was given in previous sections. Due to the geometrical constraint $d_1= d_2= d_3$, $PL(\boldsymbol{y})$ and $C(B_1, \boldsymbol{u})$ in the above represents the potential displacements in home configuration and thus cannot produce a finite displacement. In like manner, we can obtain the displacement manifold M_{C2} and M_{C3} generated by limb 2 and 3

$$\begin{aligned} M_{C2} &= T(\boldsymbol{z})R(B_2, \boldsymbol{y})R(B_2, \boldsymbol{u})T(\boldsymbol{n}) \\ &= T(\boldsymbol{z})R(B_2, \boldsymbol{y})M(E, \boldsymbol{u}, h) \end{aligned} \tag{9.15}$$

$$\begin{aligned} M_{C3} &= T(\boldsymbol{z})R(B_3, \boldsymbol{y})R(B_3, \boldsymbol{u})T(\boldsymbol{n}) \\ &= T(\boldsymbol{z})R(B_3, \boldsymbol{y})M(E, \boldsymbol{u}, h) \\ &= T(\boldsymbol{z})R(B_2, \boldsymbol{y})M(E, \boldsymbol{u}, h) \end{aligned} \tag{9.16}$$

where we have $R(B_1, \boldsymbol{y})$ $R(B_2, \boldsymbol{y}) \subset PL(\boldsymbol{y})$, and $M(C, \boldsymbol{u}, h) \subset C(B_1, \boldsymbol{u})$. Similarly, the displacements represented by $R(B_1, \boldsymbol{y})$ $R(B_2, \boldsymbol{y})$, $PL(\boldsymbol{y})$, $M(C, \boldsymbol{u}, h)$, and $C(B_1, \boldsymbol{u})$ in the

above are all instantaneous that cannot generate finite displacement due to the geometrical constraint d_1=d_2= d_3. Taking the intersection of the three product submanifold M_{C1}, M_{C2} and M_{C3}, the displacement of the platform in the home configuration can be derived as follows

$$\begin{aligned} M_C &= M_{C1} \cap M_{C2} \cap M_{C3} \\ &= T(\boldsymbol{z})\left[PL(\boldsymbol{y}) \cap R(B_2, \boldsymbol{y}) \cap R(B_2, \boldsymbol{y})\right] \\ &\quad \left[C(B_1, \boldsymbol{u}) \cap M(E, \boldsymbol{u}, h) \cap M(E, \boldsymbol{u}, h)\right] \\ &= T(\boldsymbol{z}) R(B_2, \boldsymbol{y}) M(E, \boldsymbol{u}, h) \end{aligned} \tag{9.17}$$

In such a case, the platform of the 3-PUP parallel mechanism has a finite rotation T ($\boldsymbol{z}$), an instantaneous rotation $R(B_2, \boldsymbol{y})$, and an instantaneous screw motion $M(E, \boldsymbol{u}, h)$, and hence the result has been verified by the above derivation. The displacement of the platform given by product submanifold M_C can be illustrated by the forward kinematics simulation given in Figure 9.9.

In terms of the bifurcated motion of the 3-PUP parallel mechanism, this paragraph returns to Figure 9.8. Assuming the 3-PUP parallel mechanism is moving in motion branch A under the geometrical constraint d_2=d_3, the other geometrical constraint d_2+d_3=2d_1, will be automatically activated when the configuration of the 3-PUP parallel mechanism arrives in the home configuration. Then, if the constraint d_2=d_3 is released, the mechanism will move into motion branch B from the home configuration. Otherwise, if the constraint d_2+d_3=2d_1 is deactivated, the mechanism will return back to motion branch A from the home configuration. Due to the geometrical structure, the two constraints d_2=d_3 and d_2+d_3=2d_1 of the 3-PUP parallel mechanism can be effective

simultaneously in which case the mechanism receives the constraint singularity in the home configuration. But the case that these two constraints are deactivated simultaneously will never happen. That is to say, for the 3-PUP parallel mechanism at least one of the two constraints are effective such that the mechanism is either in motion branch A, or in motion branch B, and switches from each other at the home configuration.

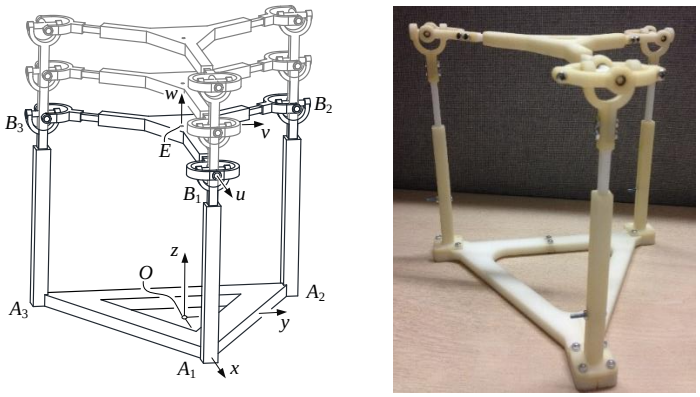

Figure 9.9 Feasible displacements in Home configuration

9.5 Experimental validation of the bifurcated motion

In Section 8.4, when the 3-PUP parallel mechanism moved within motion branch B, the derivations revealed a pseudo-helical motion of the platform. Though Figure 9.7 illustrated the feasible displacements in motion branch B, the variable-pitched translation of the pseudo-helical motion in that motion branch cannot be shown only by photos of the prototype. Thus, this section is to set up an experiment on the 3D printed prototype of the 3-PUP parallel mechanism, then detect the translation of the screw motion to validate the extraction of the pseudo-helical motion.

Figure 9.10 gives the experimental test environment which consists of a 3D printed prototype of the 3-PUP parallel mechanism, four 6-DOF tracking sensors (Ascension, Model 800), a transmitter (Ascension wide-range transmitter), and a sensor driver (3D Guidance trakSTAR, Class 1 Type B). Three tracking sensors, i.e. sensor 1, 2, 3 are attached to sliders in limbs 1, 2, 3 of the 3-PUP parallel mechanism respectively to measure the displacement of each single slider, while the remaining tracking sensor, i.e. sensor 4 is attached to the platform aligning with the symmetry axis of the platform to gather the motion-output information. The platform of the 3-PUP parallel mechanism moves upon the adjustment of the height of each single slider, where the three tracking sensors can ensure the three sliders moving along the same direction during test.

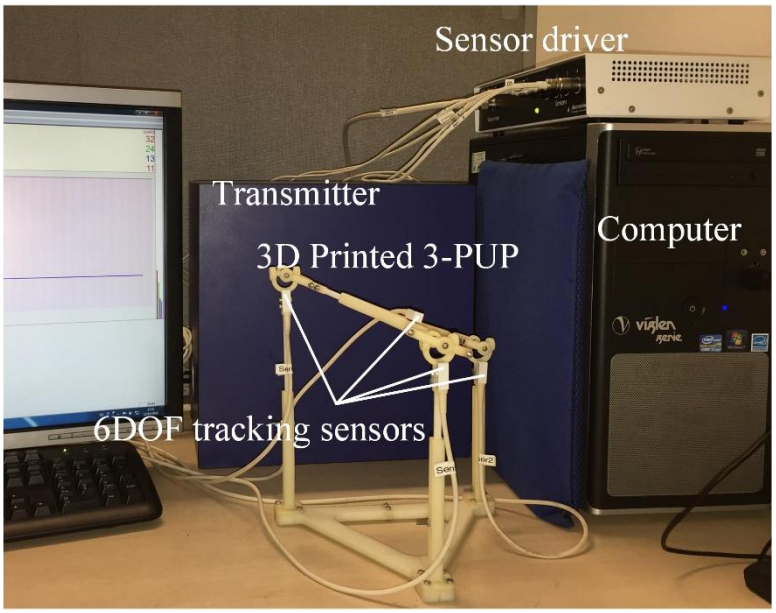

Figure 9.10 The experimental environment for detecting the translation of the pseudo-helical motion.

Figure 9.7(a) gives the home configuration of motion branch B, where the initial data of configuration of each single sensor is acquired as shown in Table 9.1. At the initial

configuration, the value of component z of sensors 1 and 3 are measured as 10.16mm and 10.49mm respectively. Then adjust sliders 1 and 3 upwards, and simultaneously ensure the geometrical condition $d_2+d_3=2d_1$ held during the adjustment by subscribing to the real-time sensor data. The prototype reaches the configuration shown in Figure 9.7(b) when slider 3 is moved upwards for 30mm, then move sliders 1 and 3 forwards for another increment 30mm for slider 3, to the third configuration described in Figure 9.7(c). During the movement we always keep slider 2 still, hence the condition $d_1=d_3/2$ holds. The data of sensors 1 and 3 are recorded when the prototype reaches the two configurations illustrated in Figure 9.7(b) and Figure 9.7(c), as shown in Table 9.2.

Table 9.1 Data acquisition of all sensors at initial configuration.

Sensors	x(mm)	y(mm)	z(mm)	azimuth(°)	elevation(°)	roll(°)
Sensor 1	-2.68	453.18	10.16	163.15	84.97	100.79
Sensor 2	312.87	55.48	3.35	97.82	82.49	127.70
Sensor 3	-61.84	327.72	10.49	158.98	78.04	121.20
Sensor 4	6.92	381.74	15.40	98.30	1.96	1.23

Table 9.2 Data acquisition for sensors 1 and 3 at configurations (b) and (c) in Figure 9.7.

Configurations	Sensors	x(mm)	y(mm)	z(mm)	azimuth(°)	elevation(°)	roll(°)
Configuration (b)	Sensor 1	-2.46	453.18	-4.80	174.42	84.49	78.50
	Sensor 3	-63.40	328.05	-19.53	168.70	79.36	89.11
Configuration (c)	Sensor 1	-3.01	453.52	-19.76	165.38	83.34	39.51
	Sensor 3	-69.43	327.38	-49.56	144.63	77.67	62.57

From Tables 9.1 and 9.2, looking at the component z of sensors 1 and 3, it can be calculated easily that the increments for the two sensors are measured as about 30mm and 60mm respectively. During the movement of sliders 1 and 3 from configurations 8.7(a) to 8.7(c), the translation of the pseudo-helical motion would be captured if sensor 4 attached to the platform detects any movements along x- and y-axis of the transmitter reference frame which can be seen from the data x and y in tables. For convenience we gather all the data measured by sensor 4 in Table 9.2 as below.

Table 9.3 Data acquisition for sensor 4 at configurations 8.7(a), 8.7(b) and 8.7(c).

Configurations	x(mm)	y(mm)	z(mm)	azimuth(°)	elevation (°)	roll(°)
Configuration (a)	6.92	381.74	15.40	98.30	1.96	1.23
Configuration (b)	4.58	382.86	29.58	97.56	0.01	-10.74
Configuration (c)	3.91	384.76	43.42	96.53	-1.41	-20.96

In Table 9.3, the data of components x and y are decreasing upon the adjustments of slider 1 and 3 under the geometrical condition $d_2 + d_3 = 2d_1$, i.e. $d_1 = d_3/2$ if keeping slider 2 still. That means that the minor translation of the platform are happening and detected during the movement of the platform from configurations 8.7(a) to 8.7(c). The corresponding rotation in motion branch B is also detected, seeing the data in the last two columns of Table 9.2. In such ways the experiment discloses the inconspicuous translation of the screw and hence validates the extraction of pseudo-helical motion based on the composition of submanifolds analysis.

9.6 Conclusions

Following the analysis of the skewed PRP chain which extracted a special pseudo-helical motion in chapter 7, this chapter investigated the displacement representation, bifurcated motion, and constraint singularity of a 3-PUP parallel mechanism parallel mechanism with a Lie group interpretation, presenting a Lie group method for the displacement analysis of a parallel mechanism with bifurcated motion. The method facilitated the analysis of the parallel platform since it did not need to deal with instantaneous constraints or motions as in the previous publications and simplified the analysis of such parallel mechanism without resorting to in-depth geometry analysis. At last this chapter implemented an experimental test using commercial 6-DOF tracking sensors to detect the translation of the pseudo-helical motion and validated the derivations.

Chapter 10 Conclusions and Future Work

10.1 General Conclusions

The dissertation addressed the problems in recognising reconfiguration of mechanisms using screw algebra-based kinematics analysis and its extensions in mechanisms theory.

The dependency of screws with non-zero constant pitch was identified by introducing a projective transformation in the 5-dimensional projective space and by revealing the generators α- and β-planes of the corresponding hyperquadrics. Based on screw algebra calculations, a method of integrating high-order kinematic analysis and bilinear form representations was for the first time proposed for recognising the six motion branches with the related geometrical conditions of the derivative queer-square mechanism. The dissertation then investigated the equivalence between two screw spaces and extended the results to the field of compositional submanifolds of SE(3), by which the bifurcation of the 3-PUP parallel mechanism parallel mechanism was analysed using compositional submanifold representations. Finally, the dissertation constructed the Jacobian matrix

for a hybrid mechanism with a reconfigurable base using screw algebra-based approach. The general conclusions of this dissertation can be presented below.

Chapter 1 introduced the research problems related with recognising motion branches of reconfigurable mechanisms and the aims and objectives, and structure of the dissertation were briefly presented.

Chapter 2 reviewed the background and historical development of reconfigurable mechanisms, line geometry, screw dependency, and Lie group, etc. The basic concepts and connection between these fields were presented mainly with the timeline of development of these relevant research topics.

Chapter 3 introduced a projective transformation for the first time proposed for the hyperquadrics of screws with non-zero pitch in the 5-dimensional projective space and any hyperquadrics corresponding to screw systems with a constant pitch can be represented in a matrix form. By using this method, it was attained that the hyperquadrics were generated by two bundles of planes as α-planes and β-planes. This chapter laid the foundation of recognising the dependency of screws for the next chapter and basic concepts and operations were used in the remaining part of the dissertation, especially Chapter 5 the Lie bracket computation and bilinear form representation of constraints and Chapter 7 the tangent spaces of compositional submanifolds of mechanisms.

Chapter 4 rediscovered the conventional three-systems by corresponding the generators of hyperquadrics in 5-dimensional projective space to screws in 3-space. Intersection

of α-planes and β-planes of screws with non-zero constant pitch were derived for the first time and thus two-systems were rediscovered. Researchers relate planes in the Klein quadric in the 5-dimensional projective space to screw systems in 3-space, while this chapter for the first time extended it to a general case that any hyperquadrics in 5-dimensional space corresponding to the screws with the same pitch can be related back to 3-space. The equations and results in this chapter and chapter 3 can be used in mobility calculation and screw-system variations and lay foundation for chapter 5 of constraint system construction based on screw theory, for chapter 7 of equivalence of screw systems generating the same computational submanifolds, and for Chapter 9 of Jacobian matrix derivation of a hybrid mechanism using screw theory.

Chapter 5 presented a reconfigurable base integrated parallel mechanism based on the manipulation of rigid objects with a Metamorphic hand for the first time through mechanism equivalent method. By means of decomposing the mechanism into a typical 3RRS parallel mechanism and a reconfigurable linkage, the Jacobian based on screw theory was utilized to identify the relationship between active joints and passive joints through the screw system elimination with their reciprocal product. The Jacobian analysis demonstrated the effectiveness of screw algebra approach in modelling the novel reconfigurable-base integrated parallel manipulator.

Chapter 6 established the kinematic model including velocity and acceleration analysis of the derivative queer-square mechanism and first-order and second-order constraints were attained by using Lie bracket calculation of screws. The recursive algorithm of screws based on Lie bracket was used to analyse the kinematic constraints of multi-loop mechanisms for the first time. This chapter employed bilinear form to represent

the second-order constraint and simplified their expressions. This approach made it possible to simplify complicated constraints of second order so that the recursive algorithm can be applied to multi-loop mechanisms which are quite complicated in modelling. Finally, all first-order and second-order constraints were attained in the simplified form. This chapter demonstrated the effectiveness of screw theory discussed in Chapter 3 and 4 and paved a way of exploring motion branches of the derivative queer-square mechanism for Chapter 6.

Chapter 7 for the first time revealed the six motion branches of the derivative queer-square mechanism. After attaining six motion branches by solving the constraint system of the derivative queer-square mechanism, this chapter presented the prototype of each single motion branch and implemented numerical simulation in the commercial software module Solidworks Motion and it was verified that the results of angular velocities obtaining from the solutions to the constraint system coincided precisely with the simulation results. This chapter shown the effectiveness of the screw-algebra approach together with the bilinear form representations of constraints in recognising the multi-furcation in complicated multi-loop mechanisms.

Chapter 8 introduced the concept of computational submanifolds of SE(3) with its tangent spaces and the relevant products, then this chapter extended the standard PRP kinematic chain producing the planar motion subgroup SE*(*2) to a relatively generic kinematic chain in which the prismatic-joint direction is not necessary to be perpendicular to the revolute-joint axis. To the knowledge of the candidate, the type of motion described by the skewed PRP chain is not included in previous dissertations or books dealing with submanifolds of SE(3) that are not subgroups. Finally, this chapter

ended up with investigating the motion representation of a PRP-Schoenflies parallel mechanism.

Chapter 9 followed the analysis of this PRP chain which extracted a special pseudo-helical motion in chapter 7 and investigated the displacement representation, bifurcated motion, and constraint singularity of a 3-PUP parallel mechanism with a Lie group interpretation, presenting a Lie group method for the displacement analysis of a parallel mechanism with bifurcated motion. The method facilitates the analysis of the parallel platform since it did not need to deal with instantaneous constraints or motions as in the previous publications and simplified the analysis of such parallel mechanism without resorting to in-depth geometry analysis.

Chapter 10 concluded the dissertation with general conclusions of all chapters, contributions and future work within the related fields.

10.2 Main Achievements of the Dissertation

Screw algebra-based kinematics analysis of mechanisms was investigated thoroughly in this dissertation, and this theory was extended to high-order kinematic analysis of multi-loop reconfigurable mechanisms and to the equivalence of screw spaces and then to the compositional representations of reconfigurable mechanisms. The main contributions of the dissertation can be concluded as below.

(I) The Klein quadric in the 5-dimensional projective space was extended to a relatively general hyperquadric corresponding to screws in 3-space with non-zero constant pitch by constructing a projective transformation. By this means, α- and β-planes of the hyperquadrics were derived and several conventional screw systems were rediscovered. This research laid the foundation of the whole picture of the dissertation in recognising motion branches and geometrical conditions of reconfigurable mechanisms.

(II) This dissertation for the first time obtained the six motion branches of the queer-square mechanism completely with their geometrical conditions by establishing an explicit way of recognition. The constraint system of the mechanism was constructed by integrating high-order kinematic analysis based on Lie bracket computation and the bilinear form representation of the second-order constraints.

(III) The dissertation for the first time extracted the pseudo-helical motion with a variable pitch from the skewed PUP kinematic chain with a tilting angle and the pseudo-helical motion was presented by a compositional submanifold of SE(3). This extended the research within the context of Lie subgroups of SE(3) to compositional submanifolds of SE(3) based on the equivalence of screw spaces as tangent spaces of compositional submanifolds. Therefore, the bifurcation in the 3-PUP parallel mechanism was analysed and represented in a compact way.

(IV) Kinematic characteristics of a hybrid mechanism with a reconfigurable base was investigated by mechanism decomposition and its Jacobian matrix was derived using screw algebra approach.

10.3 Future Work

This dissertation investigated the hyperquadrics in the 5-dimensional projective space corresponding to the screws with non-zero constant pitch and hence the research on Klein quadric was extended. However, this dissertation has not yet explored the hyperquadrics corresponding to the screw systems in which the pitch of screws is variable. In mechanisms, normally all helical joints are of the same pitch. In the future, if any results on the hyperquadrics corresponding to the screw systems with variable pitches are attained, it is expected novel mechanisms can be invited by arranging helical joints with different pitches.

The essence of why the movement of the derivative queer-square mechanism can be divided into six motion branches at the singularity configuration was revealed in this dissertation, that is, the multi-furcation in this mechanism is caused by the existence of the parallelogram and connotative parallelogram. In this manner, it has the potential that more reconfigurable mechanisms of this type can be discovered by rearranges the parallelogram and connotative parallelogram.

The bifurcation of the 3-PUP parallel mechanism was analysed, and the pseudo-helical motion produced by the skewed PRP kinematic chain was extracted. This mechanism can rotate along x- or y-axis in the horizontal plane and it can avoid the other motion branch when moves in one motion branch. This property provides a function of self-locking in mechanical system which brings safety in real application such as ankle rehabilitation devices and other medical robots. Exploiting real applications by using the 3-PUP parallel mechanism can be future direction for mechanisms research.

List of Publications

Journal Papers

- Zhang, X., Lopez-Custodio P., and Dai, J. S. (2017), Compositional submanifolds of pup and PRP kinematic chains and their derived parallel mechanisms, *ASME Transactions: Journal of Mechanisms and Robotics*, JMR-16-1303, Accepted.
- Sun, J., Zhang, X., Wei, G., and Dai, J. S. (2016). Geometry and kinematics for a spherical-base integrated parallel mechanism. *Meccanica*, **51**(7), pp. 1-15.
- Zhen W., Kang X., Zhang X., Dai J. (2016). Gait planning of a novel metamorphic quadruped robot. *Chinese Journal of Mechanical Engineering*, **52**(11), pp. 26-33.

Journal Papers to be Submitted

- Zhang, X., Lopez-Custodio P., and Dai, J. S. Constraint-based reconfiguration of the derivative queer-square mechanism using Lie bracket analysis. 2017.
- Zhang X. and Dai J. S. Dependency of screws based on alpha- and beta- planes of hyperquadrics in the 5-dimensional projective space. 2017.

Conference Papers

- Zhang, X., & Dai, J. S. (2016). Product Submanifold Based Analysis of Kinematic Chains and a 3-PUP Parallel Mechanism. In ASME IDETC/CIE, pp. V05BT07A061-V05BT07A061.

- Wei, G., Sun, J., Zhang, X., Pensky, D., Piater, J., & Dai, J. S. (2015). Metamorphic hand based grasp constraint and affordance. In ASME IDETC/CIE, pp. V05BT08A008-V05BT08A008.
- Sun J., Zhang X., Wei G., Dai J. Geometry and Kinematics of a Parallel Manipulator with a Reconfigurable Base. The third International Workshop on Fundamental Issues and Future Research Directions for Parallel Mechanisms and Manipulators, Tianjin, China, July 7-8, 2014.

References

[1] Qin, Y., Dai, J. S., & Gogu, G. (2014). Multi-furcation in a derivative queer-square mechanism. *Mechanism and Machine Theory*, **81**, 36-53.

[2] Dai, J. S., & Gogu, G. (2016). Special Issue on Reconfigurable Mechanisms. *Mechanism and Machine Theory*, **96**, 213-214.

[3] Wohlhart, K. (1996). Kinematotropic linkages. *Recent Advances in Robot Kinematics*, 359368.

[4] Dai, J. S., & Jones, J. R. (1999). Mobility in metamorphic mechanisms of foldable/erectable kinds. *Journal of mechanical design*, **121**(3), 375-382.

[5] Lee, C. C., & Hervé, J. M. (2002). Discontinuous mobility of one family of spatial 6R mechanisms through the group algebraic structure of displacement set. *In Proceedings of ASME IDETC/CIE*, pp. 645-653.

[6] Galletti, C., & Fanghella, P. (2001). Single-loop kinematotropic mechanisms. *Mechanism and Machine Theory*, **36**(6), 743-761.

[7] Galletti, C., & Giannotti, E. (2002). Multiloop kinematotropic mechanisms. *In Proceedings of ASME IDETC/CIE*, pp. 455-460.

[8] Kong, X., & Gosselin, C. M. (2007). *Type synthesis of parallel mechanisms*. Springer Publishing Company, Incorporated.

[9] Gan, D., Dai, J. S., & Caldwell, D. G. (2011). Constraint-based limb synthesis and mobility-change-aimed mechanism construction. *Journal of Mechanical Design*, **133**(5), 051001.

[10] Aimedee, F., Gogu, G., Dai, J. S., Bouzgarrou, C., & Bouton, N. (2016). Systematization of morphing in reconfigurable mechanisms. *Mechanism and Machine Theory*, **96**, 215-224.

[11] Dai, J. S., Zoppi, M., & Kong, X. (2009). *Advances in reconfigurable mechanisms and Robots I*, London: Springer.

[12] Dai, J. S., Zoppi, M., & Kong, X. (2012). *Advances in reconfigurable mechanisms and Robots II*, Springer.

[13] Ding, X., Kong, X., & Dai, J. S. (2015). *Advances in reconfigurable mechanisms and robots III* , Springer.

[14] Gan, D., Dai, J. S., & Liao, Q. (2009). Mobility change in two types of metamorphic parallel mechanisms. *Journal of Mechanisms and Robotics*, **1**(4), 041007.

[15] Zhang, K., Dai, J. S., & Fang, Y. (2010). Topology and constraint analysis of phase change in the metamorphic chain and its evolved mechanism. *Journal of Mechanical Design*, **132**(12), 121001.

[16] Zlatanov, D., Bonev, I. A., & Gosselin, C. M. (2002). Constraint singularities of parallel mechanisms. In Robotics and Automation, *Proceedings. ICRA'02. IEEE International Conference on*, Vol. 1, pp. 496-502.

[17] Lerbet, J. (1998). Analytic geometry and singularities of mechanisms. *ZAMM‐Journal of Applied Mathematics and Mechanics/Zeitschrift für Angewandte Mathematik und Mechanik*, **78**(10), 687-694.

[18] Diez-Martínez, C. R., Rico, J. M., Cervantes-Sanchez, J. J., & Gallardo, J. (2006). Mobility and connectivity in multiloop linkages. *In Advances in Robot Kinematics* (pp. 455-464). Springer Netherlands.

[19] Müller, A. (2014). Higher derivatives of the kinematic mapping and some applications. *Mechanism and Machine Theory*, **76**, 70-85.

[20] López-Custodio, P. C., Rico, J. M., Cervantes-Sánchez, J. J., Pérez-Soto, G. I., & Díez-Martínez, C. R. (2017). Verification of the higher order kinematic analyses equations. *European Journal of Mechanics-A/Solids*, **61**, 198-215.

[21] Kong, X. (2017). Reconfiguration Analysis of Multimode Single-Loop Spatial Mechanisms Using Dual Quaternions. *Journal of Mechanisms and Robotics*, **9**(5), 051002.

[22] Ball, R. S. (1900). *A Treatise on the Theory of Screws*. Cambridge university press.

[23] Dai, J. S., Huang, Z., & Lipkin, H. (2006). Mobility of overconstrained parallel mechanisms. *Journal of Mechanical Design*, **128**(1), 220-229.

[24] Gallardo-Alvarado, J., Rico-Martínez, J. M., & Alici, G. (2006). Kinematics and singularity analyses of a 4-dof parallel manipulator using screw theory. *Mechanism and Machine Theory*, **41**(9), 1048-1061.

[25] Huang, Z., & Li, Q. C. (2002). General methodology for type synthesis of symmetrical lower-mobility parallel manipulators and several novel manipulators. *The International Journal of Robotics Research*, **21**(2), 131-145.

[26] Dai, J. S., & Ding, X. (2006). Compliance analysis of a three-legged rigidly-connected platform device. *Journal of mechanical design*, **128**(4), 755-764.

[27] Veblen, O., & Young, J. W. (1918). *Projective geometry (Vol. 2)*. Ginn.

[28] Dandurand, A. (1984). The rigidity of compound spatial grids. *Structural Topology 1984 núm 10*.

[29] Hunt, K. H. (1978). *Kinematic geometry of mechanisms* . Oxford University Press, USA.

[30] Dimentberg, F. M. E. (1968). *The screw calculus and its applications in mechanics*. foreign technology div wright-pattersonafb oh.

[31] Woo, L., & Freudenstein, F. (1970). Application of line geometry to theoretical kinematics and the kinematic analysis of mechanical systems. *Journal of Mechanisms*, **5**(3), 417-460.

[32] Dai, J. S., & Jones, J. R. (2001). Interrelationship between screw systems and corresponding reciprocal systems and applications. *Mechanism and machine theory*, **36**(5), 633-651.

[33] Hao, K. (1998). Dual number method, rank of a screw system and generation of Lie sub-algebras. *Mechanism and Machine Theory*, **33**(7), 1063-1084.

[34] Herve, J. M. (1978). Analyse structurelle des mécanismes par groupe des déplacements. *Mechanism and Machine Theory*, **13**(4), 437-450.

[35] Gibson, C. G., & Hunt, K. H. (1990). Geometry of screw systems—1: screws: Genesis and geometry. *Mechanism and Machine Theory*, **25**(1), 1-10.

[36] Martínez, J. R., & Duffy, J. (1992). Orthogonal spaces and screw systems. *Mechanism and Machine Theory*, **27**(4), 451-458.

[37] Zlatanov, D., Agrawal, S., & Gosselin, C. M. (2005). Convex cones in screw spaces. *Mechanism and machine theory*, **40**(6), 710-727.

[38] Selig, J. M. (2004). *Geometric fundamentals of robotics*. Springer Science & Business Media.

[39] Gan, D., & Dai, J. S. (2013). Geometry constraint and branch motion evolution of 3-PUP parallel mechanisms with bifurcated motion. *Mechanism and Machine Theory*, **61**, 168-183.

[40] Su, H. J., & Tari, H. (2011). On line screw systems and their application to flexure synthesis. *Journal of Mechanisms and Robotics*, **3**(1), 011009.

[41] Zlatanov, D. (2012). The representation of the general three-system of screws by a sphere. *Mechanism and Machine Theory*, **49**, 315-331.

[42] Carricato, M., & Zlatanov, D. (2014). Persistent screw systems. *Mechanism and Machine Theory*, **73**, 296-313.

[43] Wei, G., Chen, Y., & Dai, J. S. (2014). Synthesis, mobility, and multifurcation of deployable polyhedral mechanisms with radially reciprocating motion. *Journal of Mechanical Design*, **136**(9), 091003.

[44] Kong, X. (2014). Reconfiguration analysis of a 3-DOF parallel mechanism using Euler parameter quaternions and algebraic geometry method. *Mechanism and Machine Theory*, **74**, 188-201.

[45] Walter, D. R., Husty, M. L., & Pfurner, M. (2009). A complete kinematic analysis of the SNU 3-UPU parallel robot. *Contemporary Mathematics*, **496**, 331.

[46] Nurahmi, L., Caro, S., Wenger, P., Schadlbauer, J., & Husty, M. (2016). Reconfiguration analysis of a 4-RUU parallel manipulator. *Mechanism and Machine Theory*, **96**, 269-289.

[47] Lopez-Custodio, P. C., Rico, J. M., Cervantes-Sánchez, J. J., & Pérez-Soto, G. I. (2016). Reconfigurable mechanisms from the intersection of surfaces. *Journal of Mechanisms and Robotics*, **8**(2), 021029.

[48] Gan, D., Dai, J. S., Dias, J., & Seneviratne, L. (2013). Unified kinematics and singularity analysis of a metamorphic parallel mechanism with bifurcated motion. *Journal of Mechanisms and Robotics*, **5**(3), 031004.

[49] Carbonari, L., Callegari, M., Palmieri, G., & Palpacelli, M. C. (2014). A new class of reconfigurable parallel kinematic machines. *Mechanism and Machine Theory*, **79**, 173-183.

[50] Rodriguez-Leal, E., Dai, J. S., & Pennock, G. R. (2009). Inverse kinematics and motion simulation of a 2-DOF parallel manipulator with 3-PUP legs. *Computational Kinematics, Proceedings*, 85-92.

[51] Tu, L. W. (2008). *Lie algebras. An Introduction to Manifolds*, 161-171.

[52] Karouia, M., & Hervé, J. M. (2002). A family of novel orientational 3-dof parallel robots. In Romansy 14 (pp. 359-368). Springer Vienna.

[53] Meng, J., Liu, G., & Li, Z. (2007). A geometric theory for analysis and synthesis of sub-6 DoF parallel manipulators. *IEEE Transactions on Robotics*, **23**(4), 625-649.

[54] Lee, C. C., & Hervé, J. M. (2006). Translational parallel manipulators with doubly planar limbs. *Mechanism and Machine Theory*, **41**(4), 433-455.

[55] Pérez-Soto, G., & Tadeo, A. (2006). *Síntesis de Número de Cadenas Cinemáticas, un Nuevo Enfoque y Nuevas Herramientas Matemáticas* (Doctoral dissertation, M. Sc. thesis, Universidad de Guanajuato, Salamanca, Gto. Mexico).

[56] Lee, C. C., & Hervé, J. M. (2007). Cartesian parallel manipulators with pseudoplanar limbs. *Journal of Mechanical Design*, **129**(12), 1256-1264.

[57] Lee, C. C., & Hervé, J. M. (2009). Type synthesis of primitive Schoenflies-motion generators. *Mechanism and Machine theory*, **44**(10), 1980-1997.

[58] Dai, J. S. (2012). Finite displacement screw operators with embedded Chasles' motion. *Journal of Mechanisms and Robotics*, **4**(4), 041002.

[59] Dai, J. S. (2015). Euler–Rodrigues formula variations, quaternion conjugation and intrinsic connections. *Mechanism and Machine Theory*, **92**, 144-152.

[60] Dai, J. S. (2006). An historical review of the theoretical development of rigid body displacements from Rodrigues parameters to the finite twist. *Mechanism and Machine Theory*, **41**(1), 41-52.

[61] Li, Q., Huang, Z., & Hervé, J. M. (2004). Type synthesis of 3R2T 5-DOF parallel mechanisms using the Lie group of displacements. *IEEE transactions on robotics and automation*, **20**(2), 173-180.

[62] Gogu, G. (2008). *Structural synthesis of parallel robots*. Dordrecht: Springer.

[63] Rico, J. M., Cervantes-Sánchez, J. J., Tadeo-Chávez, A., Pérez-Soto, G. I., & Rocha-Chavarría, J. (2008). New considerations on the theory of type synthesis of fully parallel platforms. *Journal of Mechanical Design*, **130**(11), 112302.

[64] Tadeo-Chávez, A., Rico, J. M., Cervantes-Sánchez, J. J., Pérez-Soto, G. I., & Muller, A. (2011, January). Screw systems generated by subalgebras: a further analysis. In ASME IDETC/CIT, pp. 1037-1049.

[65] Wu, Y., Löwe, H., Carricato, M., & Li, Z. (2016). Inversion symmetry of the euclidean group: theory and application to robot kinematics. *IEEE Transactions on Robotics*, **32**(2), 312-326.

[66] Zhang, K., Dai, J. S., & Fang, Y. (2012). Constraint analysis and bifurcated motion of the 3PUP parallel mechanism. *Mechanism and Machine Theory*, **49**, 256-269.

[67] Rico, J. M., Cervantes, J. J., Tadeo, A., Gallardo, J., Aguilera, L. D., & Diez, C. R. (2009). Infinitesimal kinematics methods in the mobility determination of kinematic chains. In AMSE IDETC/CIE, pp. 1195-1204.

[68] Rico, J. M., & Duffy, J. (1996). An efficient inverse acceleration analysis of in-parallel manipulators. In AMSE IDECT/CIT.

[69] Martínez, J. R., & Duffy, J. (1996). An application of screw algebra to the acceleration analysis of serial chains. Mechanism and Machine theory, **31**(4), 445-457.

[70] Rico, J. M., Gallardo, J., & Duffy, J. (1999). Screw theory and higher order kinematic analysis of open serial and closed chains. *Mechanism and Machine Theory*, **34**(4), 559-586.

[71] Alvarado, J. G. (1999). *Análisis cinemáticos de orden superior de cadenas espaciales mediante el algebra de tornillos y sus aplicaciones* (Doctoral dissertation, Tesis de doctorado, Instituto tecnológico de la Laguna).

[72] Dai, J. S. (2014) Screw algebra and Lie groups and Lie algebras, Higher Education Press, Beijing.

[73] Dai, J. S. (2014) Screw algebra and kinematic approaches for mechanisms and robotics, Springer, London.

[74] Rees, S. (1985). C 3 geometries arising from the Klein quadric. *Geometriae Dedicata*, **18(**1), 67-85.

[75] Edge, W. L. (1944). XI—The Identification of Klein's Quartic. *Proceedings of the Royal Society of Edinburgh Section A: Mathematics*, **62**(1), 83-91.

[76] Semple, J. G., & Roth, L. (1985). *Introduction to algebraic geometry*. Oxford University Press, USA.

[77] Gibson, C. G., & Hunt, K. H. (1990). Geometry of screw systems—2: classification of screw systems. *Mechanism and Machine Theory*, **25**(1), 11-27.

[78] Schreier, O., & Sperner, E. (1961). *Projective geometry of dimensions*. Chelsea Pub. Co..

[79] Bottema, O., & Roth, B. (1979). *Theoretical kinematics*. North-Holland publ. Co., n. Y., 1979, 558.

[80] Özkaldı, S., & Gündoğan, H. (2010). Cayley formula, Euler parameters and rotations in 3-dimensional Lorentzian space. *Advances in applied Clifford algebras*, **20**(2), 367-377.

[81] Fanghella, P., & Galletti, C. (1995). Metric relations and displacement groups in mechanism and robot kinematics. *Journal of Mechanical Design*, **117**(3), 470-478.

[82] Rico, J. M., & Ravani, B. (2002). On mobillity analysis of linkages using group theory. In ASME IDETC/CIE, pp. 429-446.

[83] Rico, J. M., Cervantes-Sánchez, J. J., Tadeo-Chávez, A., Pérez-Soto, G. I., & Rocha-Chavarría, J. (2008). New considerations on the theory of type synthesis of fully parallel platforms. *Journal of Mechanical Design*, **130**(11), 112302.

[84] Dai, J. S., Wang, D., & Cui, L. (2009). Orientation and workspace analysis of the multifingered metamorphic hand—Metahand. *IEEE Transactions on Robotics*, **25**(4), 942-947.

[85] Cui, L., & Dai, J. S. (2011). Posture, workspace, and manipulability of the metamorphic multifingered hand with an articulated palm. *Journal of mechanisms and robotics*, **3**(2), 021001.

[86] Wei, G., Dai, J. S., Wang, S., & Luo, H. (2011). Kinematic analysis and prototype of a metamorphic anthropomorphic hand with a reconfigurable palm. *International Journal of Humanoid Robotics*, **8**(03), 459-479.

[87] Dai, J. S., & Wang, D. (2007). Geometric analysis and synthesis of the metamorphic robotic hand. *Journal of mechanical design*, **129**(11), 1191-1197.

[88] Gao, Z., Wei, G., & Dai, J. S. (2015). Inverse kinematics and workspace analysis of the metamorphic hand. *Proceedings of the Institution of Mechanical*

Engineers, Part C: Journal of Mechanical Engineering Science, **229**(5), 965-975.

[89] Cui, L., & Dai, J. S. (2012). Reciprocity-based singular value decomposition for inverse kinematic analysis of the metamorphic multifingered hand. *Journal of Mechanisms and Robotics*, **4**(3), 034502.

[90] Yoshikawa, T. (1985). Manipulability of robotic mechanisms. *The international journal of Robotics Research*, **4**(2), 3-9.

[91] Waldron, K. J., Wang, S. L., & Bolin, S. J. (1985). A study of the Jacobian matrix of serial manipulators. *Journal of Mechanisms, Transmissions, and Automation in Design*, **107**(2), 230-237.

[92] Kim, S. G., & Ryu, J. (2003). New dimensionally homogeneous Jacobian matrix formulation by three end-effector points for optimal design of parallel manipulators. *IEEE Transactions on Robotics and Automation*, **19**(4), 731-736.

[93] Waldron, K. J., & Hunt, K. H. (1991). Series-parallel dualities in actively coordinated mechanisms. *The International Journal of Robotics Research*, **10**(5), 473-480.

[94] Wang, Y., Liu, H., Huang, T., & Chetwynd, D. G. (2009). Stiffness modeling of the Tricept robot using the overall Jacobian matrix. *Journal of Mechanisms and Robotics*, **1**(2), 021002.

[95] Joshi, S. A., & Tsai, L. W. (2002). Jacobian analysis of limited-DOF parallel manipulators. *Transactions-American Society of Mechanical Engineers Journal of Mechanical Design*, **124**(2), 254-258.

[96] Cutkosky, M. R., & Howe, R. D. (1990). Human grasp choice and robotic grasp analysis. In *Dextrous robot hands* (pp. 5-31). Springer New York.

[97] Ma, R. R., & Dollar, A. M. (2011, June). On dexterity and dexterous manipulation. In *Advanced Robotics (ICAR), 2011 15th International Conference on* (pp. 1-7). IEEE.

[98] Doty, K. L., Melchiorri, C., Schwartz, E. M., & Bonivento, C. (1995). Robot manipulability. *IEEE Transactions on Robotics and Automation*, **11**(3), 462-468.

[99] Bicchi, A. (2000). Hands for dexterous manipulation and robust grasping: A difficult road toward simplicity. *IEEE Transactions on robotics and automation*, **16**(6), 652-662.

[100] Roberts, R. G. (2001). The dexterity and singularities of an underactuated robot. *Journal of Field Robotics*, 18(4), 159-169.

[101] Merlet, J. P. (2006). Jacobian, manipulability, condition number, and accuracy of parallel robots. *Journal of Mechanical Design*, **128**(1), 199-206.

[102] Borras, J., and Dollar, A. M. (2014). Framework comparison between a multifingered hand and a parallel manipulator. *In Computational Kinematics* (pp. 219-227). Springer Netherlands.

[103] Borràs, J., and Dollar, A. M. (2013). A parallel robot framework to study precision grasping and dexterous manipulation. *In Robotics and Automation (ICRA), 2013 IEEE International Conference on* (pp. 1595-1601). IEEE.

[104] Roth, L., and Semple, J. G. (1949). *Introduction to algebraic geometry*. Clarendon Press, Oxford.

Appendix A

Four coefficient matrices of bilinear forms below from (A.1) to (A.4) represent four second-order constraints of the derivative queer-square mechanism at the singularity configuration. The blank entry in these matrices are zeros. These expressions of constraints can be used to simplify the constraints of the mechanism and this was discussed in detail in Section 5.5.

$$\left[\begin{array}{cccc|cc|cc|cc|cc}
0 & & a+\frac{1}{2}b & a+\frac{1}{2}b & & & a+\frac{1}{2}b & a+\frac{1}{2}b & & & & \\
 & 0 & 2a+\frac{3}{2}b & 2a+\frac{3}{2}b & & & 2a+\frac{3}{2}b & 2a+\frac{3}{2}b & & & & \\
 & & 0 & a+b & & & -a+\frac{1}{2}b & \frac{3}{2}b & -b & -(a+2b) & & \\
 & & & 0 & & & -\left(2a+\frac{b}{2}\right) & -a+\frac{1}{2}b & -b & -(a+2b) & & \\
\hline
 & & & & 0 & & & & & & & \\
 & & & & & 0 & & & & & & \\
 & & & & & & 0 & a+b & -b & -(a+2b) & & \\
 & & & & & & & 0 & -b & -(a+2b) & & \\
\hline
 & & & & & & & & 0 & & & \\
 & & & & & & & & & 0 & & \\
 & & & & & & & & & & 0 & \\
 & & & & & & & & & & & 0
\end{array}\right] \tag{A.1}$$

$$\left[\begin{array}{cccc|cccc|cccc}
0 & & -1 & -1 & & & & & & & -1 & -1 \\
 & 0 & -1 & -1 & & & & & & & -1 & -1 \\
 & & 0 & & & & 1 & 1 & & & & \\
 & & & 0 & & & 1 & 1 & & & & \\
\hline
 & & & & 0 & & & & & & & \\
 & & & & & 0 & & & & & & \\
 & & & & & & 0 & & & & -1 & -1 \\
 & & & & & & & 0 & & & -1 & -1 \\
\hline
 & & & & & & & & 0 & & & \\
 & & & & & & & & & 0 & & \\
 & & & & & & & & & & 0 & \\
 & & & & & & & & & & & 0
\end{array}\right] \tag{A.2}$$

$$\left[\begin{array}{cccc|cc|ccc|cccc}
0 & & & & & & & & & & & \\
 & 0 & & & & & & & & & & \\
 & & 0 & a+b & -(a+2b) & -b & & & & & & \\
 & & & 0 & -b & a & & & & & & \\
\hline
 & & & & 0 & -(a+b) & & & & & & \\
 & & & & & 0 & & & & & & \\
 & & & & & & 0 & & & & & \\
 & & & & & & & 0 & & & & \\
\hline
 & & & & & & & & 0 & & & \\
 & & & & & & & & & 0 & & \\
 & & & & & & & & & & 0 & \\
 & & & & & & & & & & & 0
\end{array}\right] \tag{A.3}$$

$$
\left[\begin{array}{cccc|cccc|cc|cc}
0 & & & & & & & & & & & \\
 & 0 & & & & & & & & & & \\
 & & 0 & & & & & & & & & \\
 & & & 0 & & & & & & & & \\
\hline
 & & & & 0 & & & & & & & \\
 & & & & & 0 & & & & & & \\
 & & & & & & 0 & -(a+b) & a+2b & b & & \\
 & & & & & & & 0 & b & -a & & \\
\hline
 & & & & & & & & 0 & a+b & & \\
 & & & & & & & & & 0 & & \\
 & & & & & & & & & & 0 & \\
 & & & & & & & & & & & 0
\end{array}\right]
\tag{A.4}
$$

Appendix B

The Matlab program of a mathematical function to implement Lie bracket calculation and the Jacobian modelling are presented in the table below.

```
function [L] = LieProduct(S1,S2)

S1Pri=S1(:,1:3);
S1Sec=S1(:,4:6);
S2Pri=S2(:,1:3);
S2Sec=S2(:,4:6);

L=[cross(S1Pri,S2Pri) cross(S1Pri,S2Sec)+cross(S1Sec,S2Pri)]';

end


function ad_fng = liebracket(f,g,x,n)

ad_fng = sym(zeros(length(f),n+1));
ad_fng(:,1) = g;

if n>0
   for t = 2:n+1
      ad_fng(:,t) = jacobian(ad_fng(:,t-1) ,x)*f - jacobian(f,x)*ad_fng(:,t-1);
   end
end

ad_fng = expand(ad_fng);

end
```

The codes to implement the recursive algorithm of Lie bracket of screws discussed in Chapter 5 are presented in the table below.

```
clear all;
clc;

syms l1 l2 l3 k1 k2 k3 a b real;
syms w1 w2 w3 w4 w5 w6 w7 w8 w9 w10 w11 w12 real;
S1=[0 1 0 0 0 a+0.5*b]';
S2=[0 1 0 0 0 2*a+1.5*b]';
S3=[1 0 0 0 0 -a]';
S4=[1 0 0 0 0 -(2*a+b)]';
S6=[1 0 0 0 0 -(a+b)]';
S5=[1 0 0 0 0 -2*(a+b)]';
S7=[0 1 0 0 0 a+2*b]';
S8=[0 1 0 0 0 b]';
S10=[0 1 0 0 0 a+b]';
S9=[0 1 0 0 0 0]';
S11=[1 0 0 0 0 -(a+1.5*b)]';
S12=[1 0 0 0 0 -0.5*b]';

W=[w1 w2 w3 w4 w5 w6 w7 w8 w9 w10 w11 w12]';

JLoop1=[S1 S2 S3 S4 S7 S8 S11 S12];
WLoop1=[w1 w2 w3 w4 w7 w8 w11 w12];
n1=size(JLoop1,2);
k1=1;

for i = 1:(n1-1)
   for j = (i+1):n1

LieLoop1(:,k1)=WLoop1(i)*WLoop1(j)*LieProduct((JLoop1(:,i))',(JLoop1(:,j))');
      k1=k1+1;
   end
end
LieLoop1;
size(LieLoop1,2);
Loop1=sum(LieLoop1,2)


JLoop2=[-S3 -S4 S5 S6];
WLoop2=[w3 w4 w5 w6];
n2=size(JLoop2,2);
k2=1;
```

```
for i = 1:(n2-1)
   for j = (i+1):n2

LieLoop2(:,k2)=WLoop2(i)*WLoop2(j)*LieProduct((JLoop2(:,i))',(JLoop2(:,j))');
      k2=k2+1;
   end
end
LieLoop2;
size(LieLoop2,2);
Loop2=sum(LieLoop2,2)


JLoop3=[-S7 -S8 S9 S10];
WLoop3=[w7 w8 w9 w10];
n3=size(JLoop3,2);
k3=1;

for i = 1:(n3-1)
   for j = (i+1):n3

LieLoop3(:,k3)=WLoop3(i)*WLoop3(j)*LieProduct((JLoop3(:,i))',(JLoop3(:,j))');
      k3=k3+1;
   end
end
LieLoop3;
size(LieLoop3,2);
Loop3=sum(LieLoop3,2)
```

The codes to solve the equation system of the first-order and second-order constraints are presented in the table below.

```
clear all;
clc;

syms w1 w2 w3 w4 w5 w6 w7 w8 w9 w10 w11 w12 a b real;

B1=w3+w4+w11+w12;
```

```
B2=w1+w2+w7+w8;
B3=b*w8-a*w3-(b*w12)/2+w1*(a + b/2)-w4*(2*a+b)+w7*(a+2*b)-
w11*(a+(3*b)/2)+w2*(2*a+(3*b)/2);
B4=w5-w4-w3+w6;
B5=a*w3+w4*(2*a+b)-w5*(2*a+2*b)-w6*(a+b);
B6=-w7-w8+w9+w10;
B7=b*w10-w7*(a+2*b)-w8*(a+b);

Loop14=(a+b)*(w1*w2-w7*w8)+(a*w3+(2*a+b)*w4-(a+1.5*b)*w11-
0.5*b*w12)*(w7+w8);
Loop15=(a+b)*(w3*w4-w11*w12)+(0.5*b*w3+(-
a+0.5*b)*w4+(a+2*b)*w7+b*w8)*(w11+w12)-
((a+2*b)*w7+b*w8+(a+b)*w12)*(w3+w4);

Loop2=(a+b)*(w3*w4-w5*w6)-b*w3*(w5+w6)+a*(w4*w6-w3*w5)-
b*w5*(w3+w4)
Loop3=(a+b)*(w9*w10-w7*w8)+b*w7*(w9+w10)+a*(w7*w9-
w8*w10)+b*w9*(w7+w8)

[w2,w3,w4,w5,w6,w7,w8,w9,w10,w11,w12]=solve(Loop14==0,w3*w4-
w11*w12==0,w3+w4==0,Loop3==0,B1==0,B2==0,B3==0,B4==0,B5==0,B6==0,
B7==0,w2,w3,w4,w5,w6,w7,w8,w9,w10,w11,w12)
```